

UNIVERSITY OF SOUTHERN QUEENSLAND
FACULTY OF ENGINEERING AND SURVEYING

Supercritical Carbon Dioxide Geothermal Energy System Analysis

A dissertation submitted by

Mr Patrick Taylor

In fulfillment of requirements of

Bachelor of Engineering (Mechanical)

October 2014

ABSTRACT

There has been considerable interest in the possibility of using supercritical carbon dioxide (SCCO₂) as a geothermal heat mining fluid instead of water. Some favourable fluid transport properties may prove to give an advantage in some circumstances. The low viscosity to density ratio suggests higher mass flow rates and better suitability to low permeability reservoirs may be possible. Higher frictional losses in the wellbores may degrade that advantage.

It has been shown that SCCO₂ has the potential to utilise buoyancy effects such that a thermosiphon circulates the geothermal fluid without the need for a pump. In addition, it has been proposed that SCCO₂ could be used to drive a turbine directly rather than a conventional binary heat exchange system. This could dramatically reduce surface plant complexity and cost.

This study details the creation of a Matlab model of the subsurface circuit of geothermal fluid. After establishing a reference case to study general fluid and system behaviour, the model is used to test and compare the effects of wellbore diameter variation, reservoir depth, permeability and temperature on the net exergy and thermal efficiency using each of water and SCCO₂.

For the specific test cases, SCCO₂ was shown to perform significantly better than water with increased well bore diameter, low permeability and low temperature reservoirs. The performance was found to degrade with shallower reservoirs; although this leads to observations that the SCCO₂ system operates on a narrow band of efficiency which could make the system less robust than comparable water based system.

DISCLAIMER

University of Southern Queensland

Faculty of Health, Engineering and Sciences

ENG4111/ENG4112 Research Project

Limitations of Use

The Council of the University of Southern Queensland, its Faculty of Health, Engineering & Sciences, and the staff of the University of Southern Queensland, do not accept any responsibility for the truth, accuracy or completeness of material contained within or associated with this dissertation.

Persons using all or any part of this material do so at their own risk, and not at the risk of the Council of the University of Southern Queensland, its Faculty of Health, Engineering & Sciences or the staff of the University of Southern Queensland.

This dissertation reports an educational exercise and has no purpose or validity beyond this exercise. The sole purpose of the course pair entitled “Research Project” is to contribute to the overall education within the student’s chosen degree program. This document, the associated hardware, software, drawings, and other material set out in the associated appendices should not be used for any other purpose: if they are so used, it is entirely at the risk of the user.

CANDIDATES CERTIFICATION

I certify that the ideas, designs and experimental work, results, analyses and conclusions set out in this dissertation are entirely my own effort, except where otherwise indicated and acknowledged.

I further certify that the work is original and has not been previously submitted for assessment in any other course or institution, except where specifically stated.

Patrick Taylor

Student Number: 0019522109

Signature

ACKNOWLEDGEMENTS

I would like to thank...

- Dr Ruth Mossad for her valuable input and guidance on this project.
- Dr David Fletcher for his patient and valuable advice on the CFD modelling.
- Most of all I am grateful to my eternally patient wife Arna, my two protégé's Joel and Nyah who have endured the ups and downs of 8 years study with grace and understanding.
- And to my extended family, friends and colleagues who have patiently understood that our respective relationships have often been paused but never forgotten during this time.

TABLE OF CONTENTS

Abstract.....	i
Disclaimer.....	ii
Candidates Certification.....	iii
Acknowledgements.....	iv
Table of Contents.....	v
List of Figures.....	viii
List of Tables.....	x
Glossary and Acronyms.....	xi
1 Introduction.....	1
1.1 Background.....	1
1.2 Geothermal Energy Overview.....	2
1.2.1 Types of Geothermal Energy Utilisation.....	3
1.2.2 Geothermal Electricity Production Cycles.....	5
1.2.3 Well Drilling.....	7
1.2.4 Geothermal Resources.....	8
1.3 Research Objectives.....	10
2 Literature Review.....	11
2.1 Supercritical CO ₂ System Operation Overview.....	11
2.1.1 System Overview.....	11
2.1.2 Supercritical Carbon Dioxide.....	13
2.2 Previous Studies on SCCO ₂ EGS.....	14
3 Research Design and Methodology.....	17
3.1 Introduction.....	17
3.2 Methodology.....	17
3.3 Assumptions.....	18
3.4 Parametric Study Design.....	19
3.4.1 Reference Case.....	20
3.4.2 Parametric Investigation.....	24
3.5 System Mathematical Model.....	26
3.5.1 Model Overview.....	26
3.5.2 Matlab Program Structure.....	27

- 3.5.3 CO₂ Property Model29
- 3.5.4 Water Property Model35
- 3.5.5 Preliminary System Estimates – CO₂.....35
- 3.5.6 Preliminary System Estimates - Water.....37
- 3.5.7 Wellbore Pressure Gradient.....39
- 3.5.8 Wellbore Heat Transfer.....40
- 3.5.9 Reservoir Fluid State42
- 3.5.10 Turbine Power Output (CO₂).....43
- 3.5.11 Cooling Tower Heat Extraction (CO₂).....43
- 3.5.12 Heat Exchanger Energy Extraction (Water)43
- 3.5.13 Pumping Power Input (Water).....43
- 3.5.14 Energy Balance43
- 3.6 Performance Comparison44
 - 3.6.1 Exergy44
 - 3.6.2 Thermal Efficiency.....45
- 3.7 CFD Analysis46
 - 3.7.1 CFD Model Geometry.....47
 - 3.7.2 CFD Model Mesh.....47
 - 3.7.3 CFD Model Analysis Settings.....49
- 4 Results and Discussion52
 - 4.1 Fluid Property Behaviour52
 - 4.2 Reference Case.....57
 - 4.2.1 Carbon Dioxide Single Loop – Thermosiphon Limited57
 - 4.2.2 Carbon Dioxide Single Loop – Friction Limited60
 - 4.2.3 Water Based Binary – Friction Limited62
 - 4.2.4 Carbon Dioxide Reference Case Final64
 - 4.2.5 Water Based Binary – Reference Case Final65
 - 4.3 Effect of Wellbore Diameter Variation66
 - 4.4 Effect of Reservoir Depth Variation69
 - 4.5 Effect of Reservoir Permeability Variation.....72
 - 4.6 Effect of Reservoir Temperature Variation.....74
- 5 Conclusions76

5.1	Overall Findings.....	76
5.1.1	Model Uncertainty	76
5.1.2	Parametric Test Outcomes.....	76
5.1.3	CFD Analysis Outcomes.....	77
5.2	Further Work.....	78
	Appendix A – Project Specification	79
	Appendix B – Reference Case Parameter Sources.....	81
	Appendix C – Matlab Script.....	83
	Geothermal_Main.....	83
	Geothermal_CO2.m	86
	CO2_Prop.m	93
	Geothermal_Water.m.....	97
	XSteam.m	103
	References.....	104

LIST OF FIGURES

Figure 1-1 - Global Carbon Cycle Components (U.S. Department of Energy Genomic Science 2008).....	1
Figure 1-2 - Diagram of the earth's structure	2
Figure 1-3 - Home Heating With a Geothermal Heat Pump System (GeoExchange 2011)	4
Figure 1-4 - Indicative thermal gradient at shallow depths (Solarpraxis 2014)	4
Figure 1-5 - Geothermal Power plant Basic Schematic (EPA 2013).....	5
Figure 1-6 - Representative geothermal well design (Gurgenci 2011)	7
Figure 1-7 - EGS System Diagram (Dorminey 2012).....	9
Figure 2-1 - Concept for geothermal plant designs. (Atrens, Gurgenci & Rudolph 2008).....	11
Figure 2-2 - Carbon dioxide pressure-temperature phase diagram	14
Figure 3-1 - Matlab Script Hierarchy	27
Figure 3-2 - CFD Model Geometry	47
Figure 3-3 - CFD Model Mesh - Overview	48
Figure 3-4 - CFD Model Mesh - Reservoir Inlet Region.....	48
Figure 3-5 - CFD Model Mesh - Injection well inflation and domain interface.	49
Figure 3-6 - Trial CFD model fluid flow - CO ₂ into the reservoir	50
Figure 3-7 - Trial CFD model fluid flow - CO ₂ into the reservoir	50
Figure 3-8 - Trial CFD model fluid flow - CO ₂ into the reservoir	51
Figure 4-1 - CO ₂ system injection well – typical fluid property variation	53
Figure 4-2 - CO ₂ system reservoir – typical fluid property variation	53
Figure 4-3 - CO ₂ system production well – typical fluid property variation	54
Figure 4-4 - Specific heat capacity vs temperature non-linearity.....	55
Figure 4-5 – Water system injection well fluid – typical property variation	56
Figure 4-6 – Water system reservoir fluid – typical property variation	56
Figure 4-7 – Water system production well – typical fluid property variation	57
Figure 4-8 – Mass flow rate vs injection pressure - limited by energy balanced thermosiphon (no pump).....	58
Figure 4-9 - Exergy vs injection pressure - limited by energy balanced thermosiphon (no pump).....	58
Figure 4-10 - Thermal efficiency vs injection pressure - limited by energy balanced thermosiphon (no pump).....	59
Figure 4-11 – Maximum mass flow rate vs injection pressure - limited by system impedance (pumped flow - production well minimum pressure constraint).....	60

Figure 4-12 - Thermal efficiency vs mass flow rate limited by system impedance (pumped flow - production well minimum pressure constraint).....	61
Figure 4-13 - Exergy vs mass flow rate limited by system impedance (pumped flow - production well minimum pressure constraint).....	61
Figure 4-14 – Maximum mass flow rate vs injection pressure - limited by system impedance (pumped flow - production well minimum pressure constraint).....	62
Figure 4-15 - Thermal efficiency vs mass flow rate limited by system impedance (pumped flow - production well minimum pressure constraint).....	63
Figure 4-16 - Exergy vs mass flow rate limited by system impedance (pumped flow - production well minimum pressure constraint).....	63
Figure 4-17 - Exergy vs mass flow rate for the reference case injection pressure of 10 MPa.....	66
Figure 4-18 – Mass flow rate vs pipe diameter for water and SCCO ₂ systems.....	66
Figure 4-19 – Net exergy vs pipe diameter for water and SCCO ₂ systems.....	67
Figure 4-20 – Thermal efficiency vs pipe diameter for water and SCCO ₂ systems.....	67
Figure 4-21 – Power loss from friction vs pipe diameter for water and SCCO ₂ systems.....	68
Figure 4-22 – Mass flow rate vs reservoir depth for water and SCCO ₂ systems.....	69
Figure 4-23 – Net exergy vs reservoir depth for water and SCCO ₂ systems.....	69
Figure 4-24 – Thermal efficiency vs reservoir depth for water and SCCO ₂ systems.....	70
Figure 4-25 – Pressure at production well head vs reservoir depth for water and SCCO ₂ systems.....	70
Figure 4-26 – Mass flow rate vs reservoir permeability for water and SCCO ₂ systems.....	72
Figure 4-27 – Net exergy vs reservoir permeability for water and SCCO ₂ systems.....	73
Figure 4-28 – Thermal efficiency vs reservoir permeability for water and SCCO ₂ systems.....	73
Figure 4-29 – Mass flow rate vs reservoir temperature for water and SCCO ₂ systems.....	74
Figure 4-30 – Net exergy vs reservoir temperature for water and SCCO ₂ systems.....	75
Figure 4-31 – Thermal efficiency vs reservoir temperature for water and SCCO ₂ systems.....	75

LIST OF TABLES

Table 3-1 - Matlab Script File Functional Descriptions	28
Table 4-1 - Reference Case Data – SCCO ₂	64
Table 4-2 - Reference Case Data – Binary Water System	65
Table B-1 - System Parameter Values and Source Reference	81

GLOSSARY AND ACRONYMS

CFD	Computational Fluid Dynamics
EGS	Enhanced (or Engineered) Geothermal System – refers to a system with an artificially stimulated reservoir.
EOS	Equation of State
Exergy (net exergy)	Defined as usable energy or available energy. Interchangeably used in terms of power. In this study, net exergy refers to the exergy measured in terms of fluid state potential minus the parasitic pumping power.
Flashing	The changing of phase from liquid to steam in a well bore.
Geothermal Fluid	The fluid which is pumped underground to transport heat energy to the surface for conversion to useful power.
GHP	Geothermal Heat Pump
HDR	Hot Dry Rock – refers to deep impervious granite geothermal reserves (typically >4km under the surface)
Injection well	The drilled and lined well through which the geothermal fluid flows from the surface to the reservoir.
Production well	The drilled and lined well through which the heated geothermal fluid flows from the reservoir to the surface.
Reservoir	The geological formation underground which contains the heat energy to be mined.
SCCO ₂	Supercritical Carbon Dioxide
Stimulation	The act of injecting high pressure fluid into impervious or low porosity rock to create or increase fractures so that flow of the geothermal fluid is optimised.
Surface plant	The collective name for all energy conversion equipment required at the surface to extract heat from the geothermal fluid and convert it to useful power.
Thermosiphon	The circulation of fluid and transfer of heat due to natural convection without pumping.

1 INTRODUCTION

1.1 Background

It is almost universally acknowledged that humankind's current dependence on the combustion of carbon based fuel for energy is not sustainable. This is most obviously due to the finite fossil fuel resources available; the rate of natural production of fossil fuels is many orders of magnitude slower than the rate of human consumption. Therefore, alternate, renewable energy sources need to be developed to replace fossil fuels which will eventually expire.

In addition, the effects of burning fossil fuels on the environment are becoming apparent and measurable. Carbon dioxide (CO₂) is a primary product of combustion. It is a known greenhouse gas; i.e. helps trap heat in the earth's atmosphere which is essential to life as we know it. The current scientific position (again, almost universally) is that the amount of carbon dioxide directly or indirectly released by human activity is affecting the natural carbon system balance. Figure 1-1 shows this schematically. In simple terms, the result of this imbalance is an increase in atmospheric CO₂ concentration and therefore an increase in the natural "greenhouse effect" and average surface temperature over time. This global temperature increase is enough to have adverse effects on the balance of many natural systems.

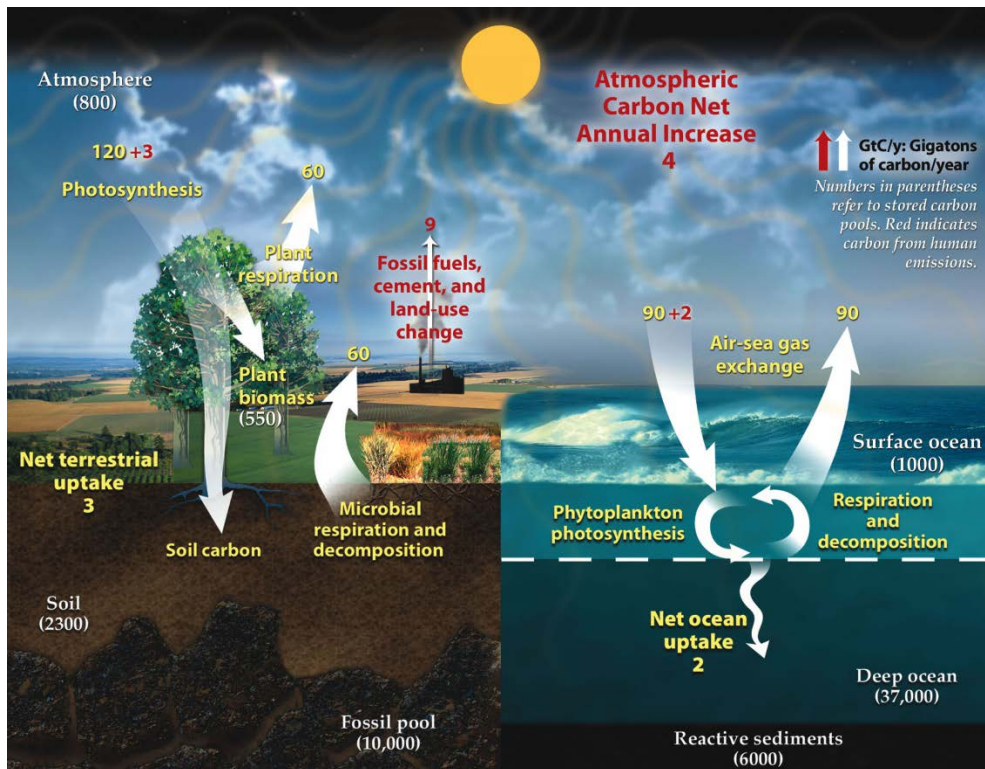


Figure 1-1 - Global Carbon Cycle Components (U.S. Department of Energy Genomic Science 2008)

There is a wide body of readily available scientific literature, for example IPCC (2014), on global warming and the role of fossil fuel combustion. For the purpose of this project, it is taken as accepted knowledge that global warming is occurring and to some extent caused by human activity. This is important in so far that it is the fundamental principle driving the research and development of alternative, sustainable energy sources such as wind, solar and hydropower. Geothermal energy is also a sustainable resource with large but yet to be realised potential.

1.2 Geothermal Energy Overview

Geothermal energy is heat from the earth itself. This heat energy can be used either directly heating water or buildings or indirectly to generate electricity. It is considered to be in under the umbrella of renewable resources although, strictly speaking, due to the scale of this energy (the heat of the earth itself) is so large that it can be considered infinite (rather than having a capability to be renewed). Yusaf, Goh and Borserio (2011) agree with this perspective. A partial exception to this is in the case of utilising “hot dry rock” technology where the heat in deep granite is regenerated by radioactive decomposition of elements such as uranium, thorium and potassium isotopes. The rate of heat regeneration is still slow compared to the rate of heat extraction.

DiPippo (2012) makes the comparison between the thickness of the earth’s crust and the shell of an egg. Proportionally, the thickness of an eggshell is three times that of the lithosphere (the earth’s crust). Considering the next region, the asthenosphere, is a semi molten layer averaging about 80km below the earth’s surface, one can expect there is a natural thermal gradient through the lithosphere and that the deeper we go, the hotter the rocks. Figure 1-2 shows the structure of the earth’s crust.

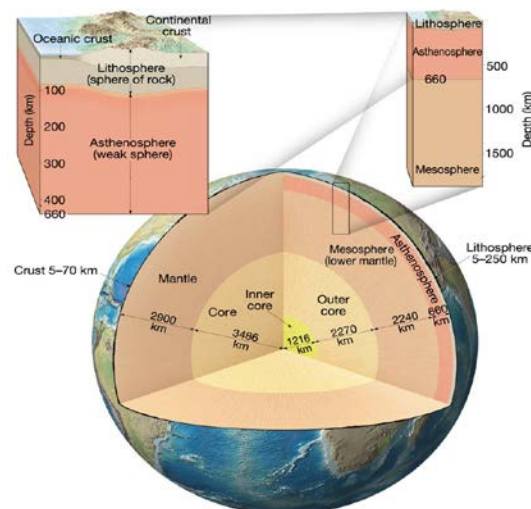


Figure 1-2 - Diagram of the earth's structure

1.2.1 Types of Geothermal Energy Utilisation

Renewable Energy World (2014) and the Geothermal Energy Association (2014) provides a layman's overview of the types of geothermal energy utilisation which are briefly presented here for contextual reference.

1.2.1.a Geothermal Direct Use

Regions which are near the earth's plate boundaries or other volcanic activity often have shallow access to hot regions due to a naturally thin region of crust and fractures at plate boundaries. The historic utilisation of geothermal energy has been by direct use of hot water and/or rocks in these geologically active regions. For thousands of years, water from hot springs and surrounding heated rock has been used for cooking, heating and bathing. In more recent times, the heat has been used directly for industrial processes, heating buildings and many similar applications where low grade heat can be utilised directly. Accessing this energy resource can be very cheap and with a low impact on the environment however it is inherently restricted to geologically active regions. In addition, near surface regions are usually a low enthalpy resource – i.e. the temperature difference between the accessible resource and the surface is generally low. Considering that in any thermodynamic system the rate of heat (energy) transfer is proportional to the difference in absolute temperature, this is an important detail which directly impacts the viability of generating electricity.

1.2.1.b Geothermal Heat Pumps

Geothermal energy can also be utilised through Geothermal Heat Pump (GHP) systems. GHP's take advantage of the fact that, at approximately 3 to 100 metres below the surface, at almost any location on earth, the temperature is almost constant (Geothermal Energy Association 2014). In winter the below surface earth temperature will tend to be warmer than ambient surface temperature. During summer the below surface earth temperature will tend to be cooler than the surface temperature. Water can be pumped through pipes buried in the earth (or ground water) at these relatively shallow depths to either bring the heat energy to the surface in colder months or conversely, use the earth (or ground water) as a heat sink in the cooler months. Figure 1-3 (GeoExchange 2011) shows a schematic of the layout. Figure 1-4 shows an indicative temperature gradient at the typical depths of a GHP system related to the weather seasons.

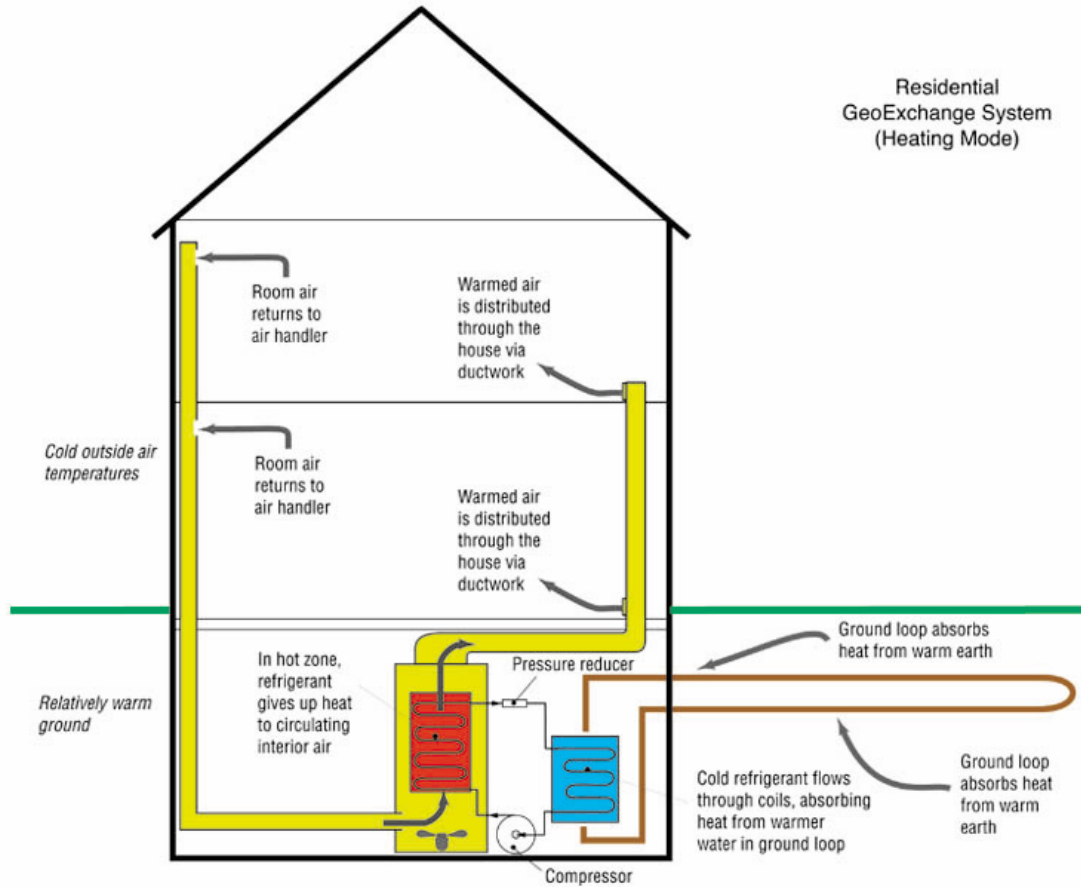


Figure 1-3 - Home Heating With a Geothermal Heat Pump System (GeoExchange 2011)

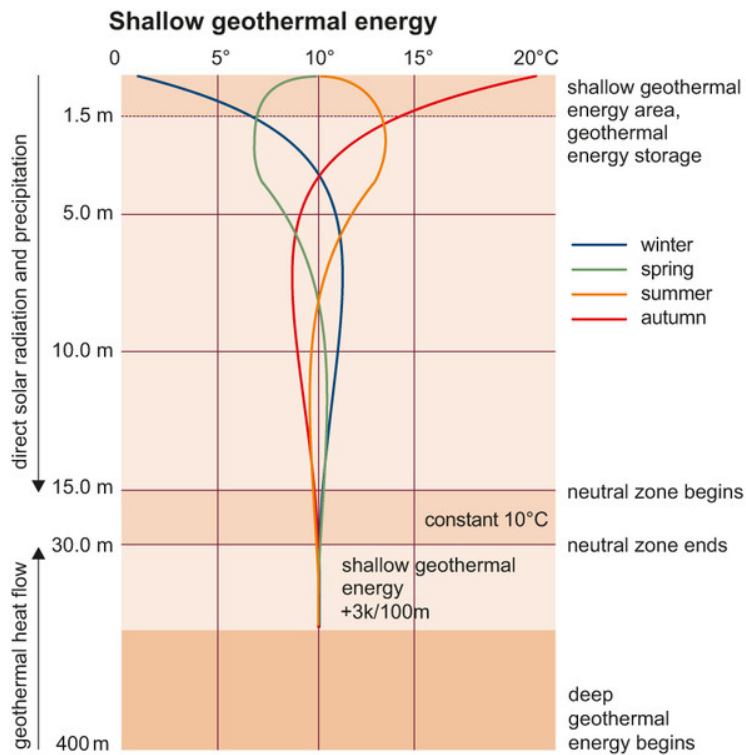


Figure 1-4 - Indicative thermal gradient at shallow depths (Solarpraxis 2014)

A GHP system can be more financially efficient in heating or cooling a building space than an equivalent electric or gas system because the heat energy comes from the ground. The only energy input is the pumping of the geothermal fluid and the compression of the vapour cycle gas. GHP systems are classified as low enthalpy due to the relatively low operating temperature of the resource being utilised.

1.2.1.c Geothermal Electricity Production

The geothermal systems that are designed to be of a scale to generate base load power (i.e. the heat energy is used explicitly to generate electricity) are the systems of interest in this project. There are several different types of plant system; all of which share the same desired output of a high pressure gas (or fluid) to drive a turbine. The turbine drives a generator to produce useable electricity to either feed into a power grid, or for direct use by industry (especially in remote locations). Figure 1-5 shows an extremely basic overview of a geothermal power plant. This will be expanded on significantly in following sections.

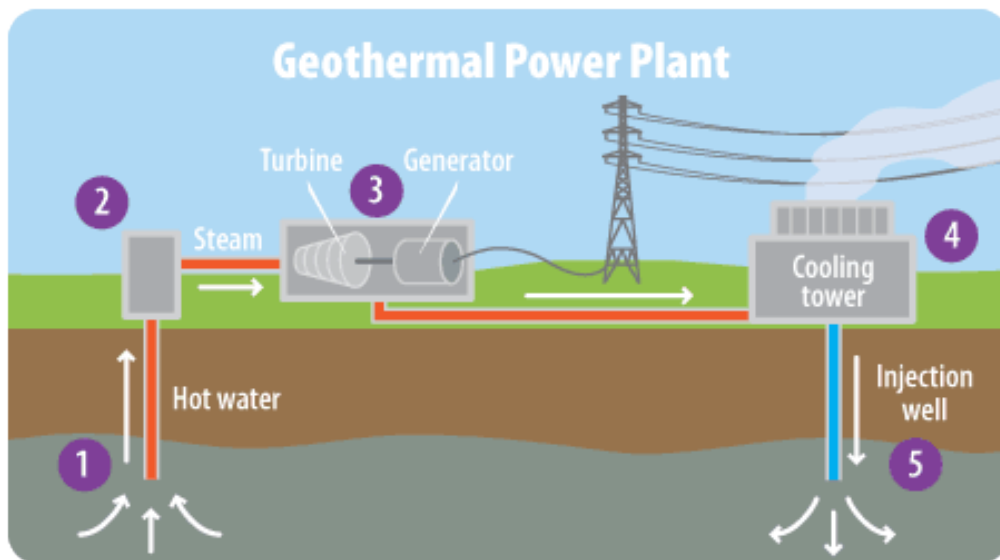


Figure 1-5 - Geothermal Power plant Basic Schematic (EPA 2013)

1.2.2 Geothermal Electricity Production Cycles

Some commonly used nomenclature for all these systems are introduced here;

- **Production well** - is the passageway (usually drilled) out of which the heated geothermal fluid flows.
- **Injection well** – is the passageway (usually drilled) through which the geothermal fluid is reinjected into the geothermal reservoir after the heat has been extracted.
- **Flash steam** – refers to a system where high temperature pressure geothermal fluid experiences a pressure drop and partially turns to steam. The pressure drop may be introduced specifically via an engineered device

or by natural reduction of pressure head as the fluid nears the surface. The flash steam is the “useful” component for electricity generation.

- **Brine** – refers to the fluid component of the geothermal fluid after the flash steam is removed.

The type of plant selected to achieve this depends on the type of geothermal resource being utilised. Briefly, there are four main types of commercial power plant. Renewable Energy World (2014) lists three:

- a) Flash power plants,
- b) Dry steam power plants,
- c) Binary cycle power plants

and Geothermal Energy Association (2014) includes a fourth combination:

- d) Flash/binary combined.

1.2.2.a Flash Power Plants

Flash power plants are the most common systems used in geothermally active regions. Hot water flows up through the production well and “flashes” at some point to become a mixture of hot water (brine) and flash steam. The flash steam is separated from the brine and used to drive a turbine. The brine (and condensate from the used flash steam) is reinjected to the geothermal reservoir. Fluid temperatures of above 180°C are generally required for flash systems (Renewable Energy World 2014).

1.2.2.b Dry Steam Power Plants

Dry steam power plants can be used if the geothermal resource produces steam directly from the production well. The system is schematically very simple as the steam directly drives a turbine to generate electricity. This type of system is rare in practice due to the limited available resource quality. For example Renewable Energy World (2014) say that there are only two known underground resources capable of producing dry steam in the United States, one of which is Yellowstone National Park and is protected from development.

1.2.2.c Binary Cycle Power Plants

Binary cycle power plants are a more recent development which uses an Organic Rankine Cycle to permit energy extraction from much lower temperature geothermal resources. Renewable Energy World (2014) make a reference to a usable geothermal fluid temperature range of 107° to 182°C where Geothermal Energy Association (2014) mention resources lower than 150°C can be exploited. The system works by pumping the geothermal fluid through a heat exchanger to transmit the heat energy to a secondary fluid. This secondary fluid is selected to

have a lower boiling point than water – often an organic fluid such as isobutane or pentafluoropropane (Geothermal Energy Association 2014). As such, the “flashing” of the secondary fluid can be used to drive a turbine and generate power in the same way as steam, but at a lower temperature.

1.2.3 Well Drilling

The art and science of well drilling is not directly relevant to the scope of this project. However, since an arbitrary well geometry will form part of the system analysis model, it is important to note the shape of a deep well (up to 5km depth for an HDR EGS) may not be perfectly cylindrical. It is made up of a series of reducing pipe diameters as shown schematically in Figure 1-6.

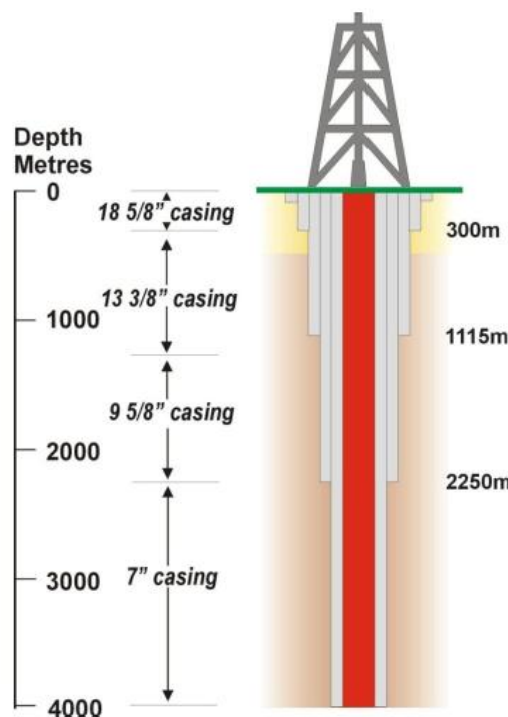


Figure 1-6 - Representative geothermal well design (Gurgenci 2011)

Some additional well nomenclature;

- **Casing** – the surface lining of the drilled hole – usually concrete. Casing diameter is the effective flow cross-sectional area at a given point.
- **String** – refers to a length of section of the same diameter. Referring to Figure 1-6, there are 5 “strings”, the largest diameter at the top and the smallest diameter at the bottom.

Note that the values in Figure 1-6 are indicative of scale only; an actual well design, depth, diameter, casing detail, number and length of strings are all highly dependent on local factors. These factors might include rock properties, formation fluids, well control considerations or regulatory controls. Typical geothermal

production casing diameters may be 200mm to 340mm (Finger & Blankenship 2010).

1.2.4 Geothermal Resources

1.2.4.a Traditional Hydrothermal Geothermal Resources

Traditional geothermal systems rely heavily on a naturally occurring set of phenomena which are required in combination to create a useful source of geothermal energy. DiPippo (2012) describes the conditions required for a given region to be considered useful in a hydrothermal geothermal energy generation capacity as:

- a) A large heat source,
- b) a permeable reservoir,
- c) a supply of water,
- d) an overlying layer of impervious rock,
- e) a reliable recharge mechanism.

This is reasonably intuitive when considering the basic schematic shown in Figure 1-5. It can be seen that a geothermal energy system fundamentally operates by forcing a working fluid through a permeable layer of hot underground rock and extracting that heat at the surface for power generation. The quality of the heat source (temperature and overall heat capacity) directly affects the system performance.

The permeability of the geothermal reservoir must be such that the working fluid can pass through with a minimal pressure drop, but with enough time and mixing so that heat energy is fully absorbed by the fluid. To an extent, the permeability of an underground region can be improved by hydraulic fracturing. This is achieved by the injection of high pressure fluid into a region to increase the size of natural fractures.

An overlying layer of impervious rock is a requirement to provide some directional control for the geothermal fluid. Without this, the water/steam would dissipate slowly over an area rather than being channelled through a passage with a pressure and flow-rate that is useful.

A supply of naturally available water is usually requirement to provide a heat transfer medium to the surface and must be able to be replenished to account for losses in what will always be a non-sealed system (DiPippo 2012). A focus of this project is to consider supercritical carbon dioxide (SCCO₂) as an alternative working fluid instead of the water. However for current commercial operations, a water source is a fundamental requirement.

Traditionally, this set of conditions has significantly reduced the regions which could be considered to have geothermal energy production potential to those readily identified by observing natural hot springs, geysers and other surface activity.

1.2.4.b Enhanced Geothermal Systems (EGS) – Hot Dry Rock (HDR)

In areas which do not have a permeable pathway or readily available underground aquifers, a Hot Dry Rock (HDR) Enhanced Geothermal System (EGS) is a relatively new way of exploiting heat energy from the earth. This system concept is central to the focus of this project. Referring to the five conditions of a traditionally viable geothermal resource (in 1.2.4.a preceding), it can be seen that conditions (a) and (d) are a fundamental requirement. Condition (b), a permeable layer, can be man-made and this is the basis of an EGS system.

Figure 1-7 (Dorminey 2012) shows the basic layout of an EGS system. It is virtually identical to the traditional system shown in Figure 1-5; the critical difference is the hot granite being used as the heat source. This is important as granite is not permeable other than for some small fractures and discontinuities. For an EGS system to operate, the natural fractures must be “enhanced” with hydraulic fracturing techniques. This usually entails forcing water into the reservoir at high pressure in an incremental manner until the desired permeability and fracture field is achieved.

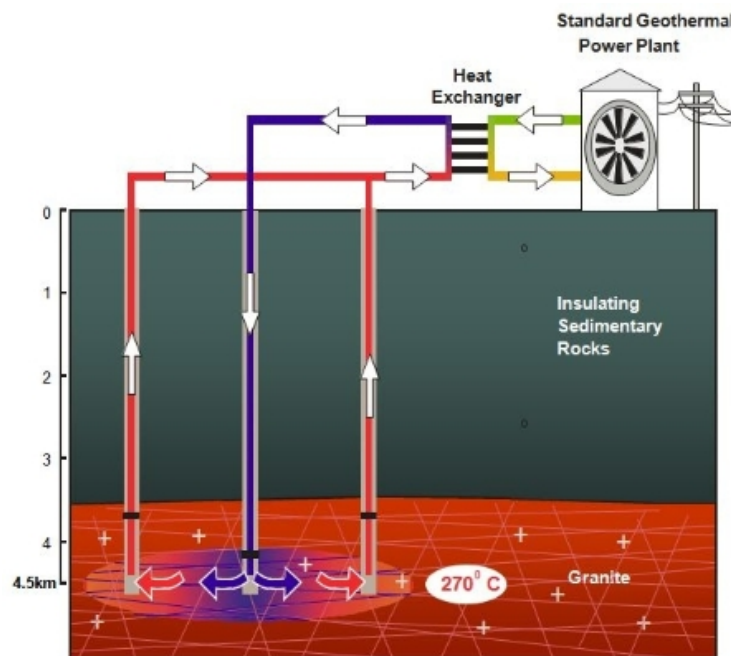


Figure 1-7 - EGS System Diagram (Dorminey 2012)

At the time of writing, there are no commercial scale instances of an EGS system (although there are several planned or operating at pilot scale). More recently,

mostly due to development in deep drilling capability, EGS is been considered to have increasing commercial viability (Bahadori, Zendehboudi & Zahedi 2013).

Engineered Geothermal Systems (EGS) are the sole focus of this study; most specifically, analysis of the supercritical carbon dioxide (SCCO₂) geothermal fluid concept. At the time of writing there have been no working instances of an SCCO₂ EGS trialled; even at pilot scale.

1.3 Research Objectives

Following from the background information, the objectives of this project are to:

1. Investigate the feasibility of using SCCO₂ as a geothermal heat mining fluid in a deep granite EGS.
2. Create a mathematical model of the wellbore and geothermal reservoir and compare SCCO₂ with water as a geothermal heat mining fluid.
3. Develop a Matlab program using the mathematical model to investigate the parameters that affect its performance.
4. Validate the model with a CFD analysis of system components.

The methodology used to achieve these objectives is detailed in Chapter 3. Some studies have been performed on this concept by others and the intent is to validate their results and develop a Matlab program that can be used for future analysis. Chapter 2 provides a background on existing literature related to this concept.

2 LITERATURE REVIEW

2.1 Supercritical CO₂ System Operation Overview

2.1.1 System Overview

The concept of using SCCO₂ as a geothermal working fluid was first proposed by Brown (2000) in the paper "A Hot Dry Rock Geothermal Energy Concept Utilising Supercritical CO₂ Instead of Water" presented to the Twenty-Fifth Workshop on Geothermal Reservoir Engineering at Stanford University, California. His paper is the foundation stone for this project and much previous work by others to investigate the feasibility of using SCCO₂ as a geothermal heat mining fluid. Figure 2-1 (Atrens, Gurgenci & Rudolph 2008) shows a side by side comparison of a conventional water based binary EGS and a proposed SCCO₂ thermosiphon design.

- Traditional water-based binary plant design with associated organic Rankine cycle. Fluid flow from reference point 1 → 2 indicate injection well, 2 → 3 the reservoir, 3 → 4 the production well, 4 → 5 the heat extraction, and 5 → 1 the water pump for compression to injection pressure.
- CO₂ thermosiphon design. Fluid flow from reference point 1 → 2 indicate injection well, 2 → 3 the reservoir, 3 → 4 the production well, 4 → 5 the turbine, and 5 → 1 the cooling system.

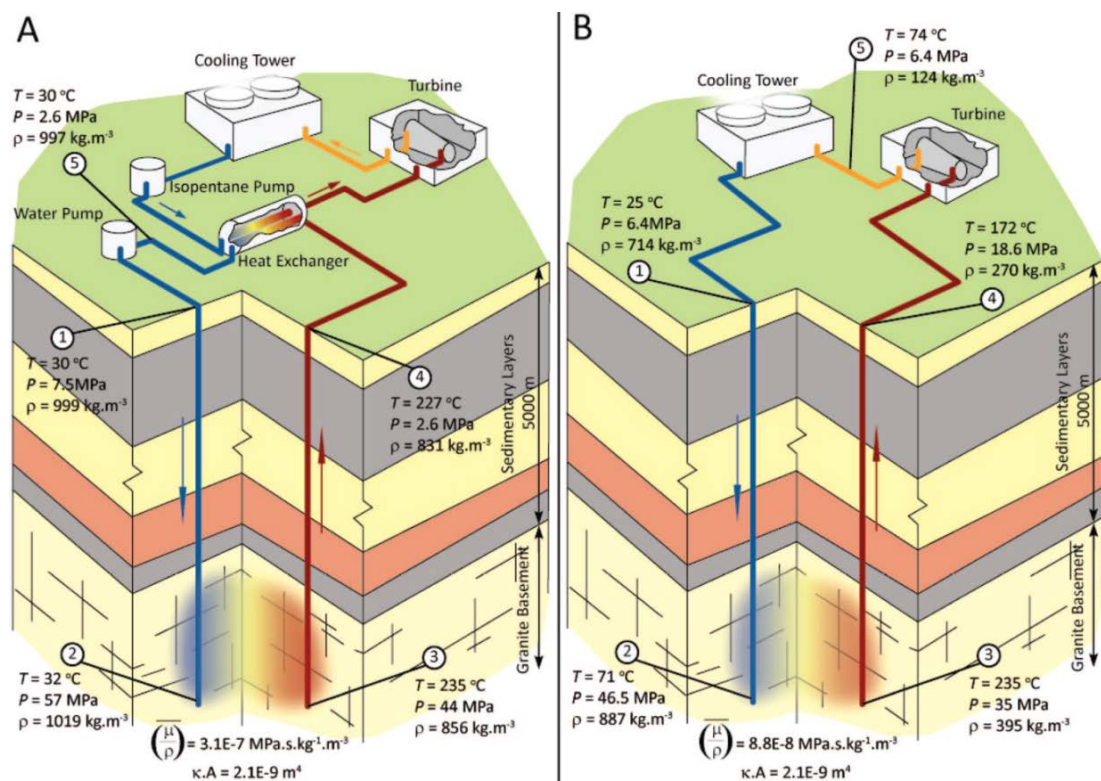


Figure 2-1 - Concept for geothermal plant designs. (Atrens, Gurgenci & Rudolph 2008)

With reference to Section 1.2.4.a and the list of conditions required for geothermal energy generation, the idea using of SCCO₂ as a geothermal fluid in an EGS was conceived to address the requirement for large volumes of water for both initial filling of the reservoir and ongoing replenishment of the inevitable losses during operation (Pruess 2006). Investigation of the concept has revealed several additional attractive features of SCCO₂ that justify further investigation and analysis.

Brown (2000), Pruess (2006) and Atrens, Gurgenci and Rudolph (2008) all agree on the following attractive features of the concept which include:

1. The reduced requirement for large volumes of water – especially attractive where HDR regions are far from water supplies (e.g. the Cooper Basin in Australia); making almost any location a potential site for geothermal plant. The requirement for large volumes of water in both initial filling of a reservoir and ongoing replenishment of the inevitable losses during operation can be a significant problem (Pruess 2006). Atrens, Gurgenci and Rudolph (2008) refer to potential steady losses in the order of 10%. Brown (2000) notes that SCCO₂ can be used as the hydraulic fracturing fluid during reservoir.
2. The properties of a supercritical fluid (discussed in detail in later sections) lead to a large pressure difference between the injection well and the production well. The difference is of a magnitude such that the system can operate on buoyant forces alone (a thermosiphon) – the potential is that no pumping is required (Atrens, Gurgenci & Rudolph 2010; Brown 2000; Pruess 2006) as shown schematically in Figure 2-1.
3. The rapidly expanding SCCO₂ can be used to drive a turbine directly, much like dry steam in a conventional system. This could lead to significantly reduced plant complexity and cost. In addition, a source of energy transmission loss, at the heat exchanger of a binary system, is removed.
4. The viscosity to density ratio of SCCO₂ is lower than water allowing for a larger mass flow rate for a given reservoir. This is offset somewhat by a lower specific heat capacity; however it is estimated to result in roughly equivalent energy generation capacity between water and SCCO₂.
5. SCCO₂ does not readily dissolve minerals. This is a major issue in geothermal systems with water resulting in scaling and deposits, reducing the efficiency of pipes, heat exchangers and other related plant.
6. A secondary benefit is the potential for geological sequestration of carbon. It is noted that this is most certainly a secondary consideration. In the context of reducing man-made atmospheric carbon, it is the move to sustainable energy and removal of fossil fuel combustion that leads to the majority of the net benefits. At the very least, if carbon offsets become a

commodity in the future, the value of the carbon sequestration may help reduce the cost per MW and increase the attractiveness of the investment (Pruess & Azaroual 2006)

There have been some drawbacks identified with the SCCO₂ concept. Most of the earlier studies (identified by the author as prior to 2009) have significant simplifying assumptions. None appear to be unreasonable in the context of the respective papers; however, neglecting friction losses was a common feature. Atrens, Gurgenci and Rudolph (2009) found in their paper that the frictional losses in the pipe were a dominant factor in an exergy analysis. They found large gains linked to increasing the well bore diameter in an SCCO₂ EGS model (the effect of which is reducing the ratio of frictional losses at the boundary region). This is an easy adjustment from an academic perspective, however considering the drilling costs associated with an increased well bore diameter and the fact that the wellbores form the majority of construction cost (DiPippo 2008), this may not be a practical approach when cost analysis is inevitably applied.

The major and less tangible drawback is uncertainty. No such system has yet been constructed even at a pilot scale.

2.1.2 Supercritical Carbon Dioxide

A supercritical fluid is any substance held above a critical temperature and pressure at which it exists in a “4th state” (solid, liquid and gas being the traditionally recognised three). The supercritical state can be thought of as partway between liquid and gas, behaving in a homogenous way, but more like one or the other depending on the temperature and pressure. Some defining properties include:

- Supercritical fluid is compressible – changes in pressure or temperature result in large changes in density. It expands to fill its container like a gas.
- In general, the density of the supercritical fluid is close to that of a liquid.
- Supercritical fluid can dissolve materials like a liquid.
- It can diffuse through solids like a gas.
- There is no surface tension since there is no liquid/gas boundary.

Figure 2-2 shows the phase diagram for carbon dioxide. It can be seen that the critical point for carbon dioxide occurs at 304.25 K and 73.9 bar (7.39 MPa).

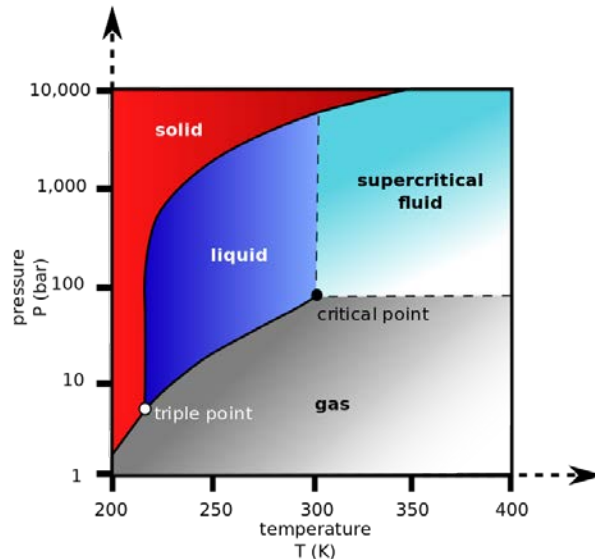


Figure 2-2 - Carbon dioxide pressure-temperature phase diagram

The physical and thermodynamic properties of SCCO₂ can be calculated by various equations of state (EOS) with differing accuracies and levels of computational complexity. Heidaryan and Jarrahan (2013) explains that the van der Waals equation of state was developed in 1873 to improve the accuracy of the ideal gas law. Redlich and Kwong developed an improved equation of state by introducing temperature dependence. Peng and Robinson (1976) proposed additional modifications for more accuracy. Various improvements to these EOS have been developed to improve accuracy in certain areas of interest – for example behaviour close to the critical point. The Peng Robinson EOS and its derivatives are widely used in industry and are less computationally complex than its successors.

Span and Wagner (1996) proposed a new EOS for carbon dioxide; it is a modified version of the Helmholtz energy functions. Critical transport and thermodynamic properties specifically for CO₂ have been calculated from the equations of state and published on isobaric tables in their paper “*A New Equation of State for Carbon Dioxide*” (1996). The tables are very easy to use for simple calculations however the equations from which they are derived contain in the region of 50 terms. This makes coding of the Span and Wagner EOS cumbersome at best. The Peng Robinson EOS is significantly more straightforward with similar levels of accuracy in the context of this project.

2.2 Previous Studies on SCCO₂ EGS

There have been a succession of analyses conducted on the SCCO₂ EGS concept proposed by Brown (2000). Studies by Pruess and Azaroual (2006), Pruess (2006), Pruess (2007) and Pruess (2008) performed basic calculations on likely system performance and found the following generally encouraging conclusions:

- Confirmed the possibility of the SCCO₂ system generating sufficient buoyant forces to circulate without a pump.
- Temperature increase due to compression of SCCO₂ is likely to increase the temperature of the fluid by about 25°C; reducing thermal efficiency and buoyant forces. An increase in temperature at the injection well reduces the capacity to mine heat from the reservoir.
- For a given total pressure drop between injection and production wells, SCCO₂ will generate approximately four times the mass flow and 50% larger net heat extraction than water.
- The advantages of SCCO₂ over water for energy extraction become more pronounced with reduced temperature.

It is noted that frictional and inertial pressure gradients are neglected in these analyses.

Gurgenci et al. (2008) in the paper "*Challenges for Geothermal Energy Utilisation*" propose that an SCCO₂ EGS could operate on either a Rankine cycle or a Brayton cycle. In the case of the former, the CO₂ is cooled through a condenser to below sub-critical state before reinjection. The Brayton cycle maintains the CO₂ in supercritical state throughout the circuit. Gurgenci et al. calculate the thermal efficiency of the Rankine cycle to be 29.5% and the Brayton to be 23.5%. However, it is noted that the Rankine cycle is not feasible for CO₂ where ambient temperatures rise above the supercritical point of 31°.

Atrens, Gurgenci and Rudolph (2008) conducted a similar analysis to Pruess (et al.) using Matlab to compare a SCCO₂ thermosiphon and equivalent water based system (refer to Figure 2-1). It is noted that frictional and inertial pressure gradients are neglected in these analyses. And the results are summarised as:

- SCCO₂ and water systems produced approximately the same net power output; 17MW vs 18MW respectively, based on the arbitrary parameters selected for the study.
- The slightly lower production of the SCCO₂ system is somewhat offset by a significant reduction in complexity of surface plant requirements. SCCO₂ systems do not require pumping equipment or any secondary heat exchange system.
- In addition, the turbine is likely to be approximately half the size (and cost) of an isopentane turbine and approximately equal to a steam turbine.

An exergy analysis of a CO₂ thermosiphon was carried out by Atrens, Gurgenci and Rudolph (2009). This study is noted to account for frictional losses in the production well; this has been a simplifying exclusion from previous studies. Friction loss is

found to be a more of a critical factor than previously assumed. The study does explain that the comparison is assuming equal well bore geometry. An increase in the production wellbore diameter can overcome the frictional losses to the point of being equivalent with water based system. This is a point worth considering in that the studies to date have assumed direct replacement of the working fluid (and required plant) only rather than a specifically designed SCCO₂ replacement system. Also noted in this study, SCCO₂ systems perform equally as well as water in conditions of lower temperature, permeability or shallower reservoirs. The findings detailed here are given in Atrens, Gurgenci and Rudolph (2010).

Haghshenas Fard, Hooman and Chua (2010) presented a paper on a numerical simulation of a CO₂ thermosiphon. This paper is closely aligned in method to the intended work for this project. The paper does not include much detail on the CFD model used. Interestingly, this study also concludes that due to the increased pressure drop found in the injection well using SCCO₂, it is better suited to shallow reservoirs.

Bıyıkoğlu and Yalçınkaya (2013) presented a parametric study "*Effects of different reservoir conditions on carbon-dioxide power cycle*". This is effectively a feasibility study for a proposed SCCO₂ EGS in the geothermal district of Ömerbeyli near the city of Aydın in Turkey. The study considers 22 sets of operating parameters to produce a range of expected possible outputs. The reader is referred directly to this paper to review the extensive results however it can be concluded that, for the conditions of the study, the first law efficiency of the system (useful energy out divided by total energy in) was found to be in the range of 0.19 and 0.25.

Zhang, Jiang and Xu (2013) have expanded on the previously detailed system analysis and extended to focus on the entire cycle (including the subsurface heat transfer and flow and the above-ground energy conversion systems) performance comparison between water EGS and SCCO₂ EGS in terms of the net power output, thermal efficiency and exergy efficiency. The method of analysis is algebraic using the NIST REFPROP code resulting in the following (relevant) findings:

- CO₂ is more appropriate for smaller reservoirs while water performs better for larger reservoirs for a given well diameter. This is due to the increased friction with high mass flow rates with CO₂ becoming a dominant factor.
- Ambient temperature has a significant effect on the efficiency of CO₂ EGS. This is due to two factors:
 - the critical temperature for CO₂ (31°C) is very close to a typical ambient temperature
 - the compressible nature of the fluid results in large pressure and density variation with temperature change.

3 RESEARCH DESIGN AND METHODOLOGY

3.1 Introduction

Atrens, Gurgenci and Rudolph (2010) and Zhang, Jiang and Xu (2013) refer to wellbore friction and reservoir flow being dominant factor when comparing SCCO₂ and water in an EGS. These studies use Darcy friction factor equations to model the frictional losses. It was therefore considered valuable by the author to develop a mathematical model (in the form of a Matlab script) which models the system and allows for parametric analysis of some system variables. In addition, the intent was to validate the mathematical model with comparison to similar studies and also with a CFD analysis to study the frictional losses in the circuit of a SCCO₂ EGS.

The primary deliverable of this project is a mathematical model of the EGS. In a parametric study, some conditions for selecting either SCCO₂ over water (or vice versa) as a geothermal heat mining fluid are identified. The parameters investigated extend to reservoir conditions (temperature, depth, and permeability), well diameters and other factors affecting the efficiency of the system.

The comparative measure of system performance is net exergy. For the SCCO₂ system, this is measured between the entry and exit of the turbine. For the water system, exergy is measured between the entry and exit of the heat exchanger with the pumping power requirements subtracted. Section 3.6.1 contains further detail on exergy as a performance measure.

In addition to exergy, the first law thermal efficiency is also measured for both systems. This is detailed further in Section 3.6.2.

3.2 Methodology

At the time of writing, no physical SCCO₂ EGS had been constructed or tested. As a theoretical system, some parameters have to be assumed as a baseline for comparison. Some parameters have been determined using reference values from previous studies done by others (these are referenced as such throughout). For this project, the beginning point was selected as the desired system output. An arbitrary output of 5MW was chosen and used in the preliminary estimations of system scaling and fluid properties. Further refinement resulting from the analysis models highlights the areas of comparison between water and SCCO₂.

The methodology used for the investigation followed the steps outlined below:

1. Determination of system parameters for which it was reasonable to use assumed values, find and validate referenced values or those that require calculation.

2. Design a parametric study to compare the systems to guide subsequent development of computer code.
3. Estimation of fluid state properties at each of the significant points 1, 4 and 5 shown in Figure 2-1
4. Estimation of the system mass flow rate to generate 5MW. This was done using base parameters from the analysis done by Atrens, Gurgenci and Rudolph (2008) and Atrens, Gurgenci and Rudolph (2010)
5. Estimation of the Reynolds number for flow in wellbores. This was to confirm the assumed wellbore diameter was appropriate and allow selection of appropriate fluid transport and heat transfer equations for the model.
6. Development of a Matlab code (written as a function file) that calculates thermodynamic and transport properties of supercritical carbon dioxide as a function of pressure and temperature.
7. Development of Matlab code to model the flow through the system making allowance for variable equations of state to be called as functions.
8. Development of a Matlab code to run a series of iterative test cases in the parametric study.
9. Construction of a scaled CFD model of the system to validate pressure drop in the system.
10. Repetition of points 1 to 9 using water based binary system.
11. Comparison of results resulting from critical parameter changes.

3.3 Assumptions

The most fundamental assumption for comparison of the two geothermal fluid systems is that the wellbore size and construction, geothermal reservoir and atmospheric conditions are the same for each. This is unlikely to be the case in a real system which would be designed to be optimised for the chosen fluid. The study varies one critical parameter through a range of values but holds the remaining parameters constant. This introduces a possibility that a system may not be optimised to benefit from the parameter change. It was decided that it was more valuable to investigate change by varying a single component per test case. The only exception is mass flow rate, which is calculated as a function of the system rather than being specified. This is explained in more detail in the next section.

The wellbores are assumed to be of uniform diameter, without mineral scaling or other imperfections above the level of uniform surface roughness. Heat transfer is modelled in the well bore using a fixed heat flux. This was chosen after investigation showed the heat flux is not dominated by the capacity or heat transfer coefficient of the fluid. Section 3.5.8 expands the reasoning behind this choice.

The geothermal reservoir is assumed to be sealed and modelled as a porous region of an assumed length and depth providing a linear temperature gain to the fluid along its length. It is assumed that the fluid reaches the full temperature of the reservoir. It is acknowledged that the validity of this assumption is dependent on the reservoir design. Parameters that affect this over time include heat capacity and conductivity of the rock as well as fracture geometry. Considering this study is focussed only on fluid performance, it is reasonable to assume that a real reservoir system would be designed to allow full utilisation of the fluid heat capacity.

The system efficiency factors are assumed values derived from referenced sources but are very much open to variation from case to case. Measured values for system efficiencies do not exist for the SCCO₂ system. Efficiencies for the water based binary system can vary significantly dependant on more parameters than can be reasonably be modelled for this project. Section 3.4.1.b provides detail on the efficiency factors selected. Considering the purpose of this study is more oriented to the “shape of the curve” and general system behaviour rather than a specific case design, the use of assumed values is considered reasonable.

The costs of implementing the parameter changes are not considered. There is no attempt to justify system parameters variation and their respective performance effect based on cost.

The mass flow rate for the SCCO₂ thermosiphon is estimated using energy balance methods. This is considered reasonable for the sub-surface circuit but makes no allowance for surface plant restrictions to flow.

For both circuits, it is assumed there is no phase change. This is reasonable for the SCCO₂ system as part of the cycle design. For the water based binary system, it is an opportunity for refinement of this work. It is quite possible that a surface system could be designed as a flash plant, and may affect the overall system efficiency. Since flashing typically occurs in the upper section of the production well (the end of the circuit studied here), it was considered reasonable to exclude phase change from the analysis of the fluid flow and heat transport capacity.

Expansion through the turbine in the SCCO₂ system is calculated as isentropic, with a general efficiency correction applied to the power output. This assumption does allow for any correction to the fluid state at reference point 5.

3.4 Parametric Study Design

It has been discussed that there are fundamental differences between the two systems being considered. The common factors are the sub-surface element; well bores and reservoir. Following this it was decided that these be the focus of the detailed study. Determination of the available energy (exergy) and application of

factors to allow for surface plant conversion efficiency would provide a reasonable comparison.

A reference case is determined to provide a baseline and also a comparison between previous studies. The parameters selected that have an effect on the system efficiency are detailed below:

1. Reference case
2. Well bore diameter variation
3. Reservoir depth variation
4. Reservoir permeability variation
5. Reservoir temperature variation

Other parameters were considered; turbine exit pressure and injection pressure both have significant effect on the thermal efficiency of each system but can be regarded as system design parameter rather than a differentiating condition that may favour SCCO₂ or water as a heat mining fluid. As such, both systems were initially investigated to develop a reference case that optimised their performance.

3.4.1 Reference Case

In the first instance, the design of the reference case to compare the two systems was based on previous similar studies in order to allow a natural comparison and/or expansion of their findings. Literature review of typical parameters found either by experience, experiment or reasonable assumption by experts in the field. Appendix B – Reference Case Parameter Sources contains a full list of basic system parameter values and their respective sources for the reader's reference.

Some of the base parameters were refined after iteration of the initial case. This is especially true for mass flow rate. Interestingly, none of the literature containing similar studies was explicit on the method used to specify a mass flow rate for the SCCO₂ thermosiphon system. For this study, the mass flow rate was derived as a product of the initial model testing and interpretation of results. The reasoning is detailed further in the following section and the results shown in Chapter 4.

3.4.1.a Carbon Dioxide Single Loop Mass Flow Rate

The mathematical (and CFD) model for the system requires a mass flow rate to be specified as an input. However, the mass flow rate is a function of the system parameters and as such; iteration from an initial guess was required. It was identified that there were two primary governing conditions that would determine the mass flow rate of the SCCO₂ system. Firstly, the natural limitation of the thermosiphon's driving force and secondly, the resistance to flow from friction, reservoir impedance and surface plant reaching a critical point as fluid velocity increases.

The SCCO₂ system chosen for comparison is that with no pump. It relies on a natural thermosiphon to drive the flow. In a thermosiphon system, the mass flow rate is not directly controlled. It is a product of the geometry, heat flux, and fluid properties among other things. Ultimately, the motive force is generated by connected fluid columns containing fluid of different density (the production and injection well bores).

There must also be an energy balance in the system. The equations for this energy balance are detailed in Section 3.5. The method for finding the mass flow rate of the thermosiphon system in a balanced state is through identifying the point at which all the energy in and out of the system is in equilibrium. The mathematical model solves for the mass flow rate at which there is an energy balance with no pump power input.

The second limitation is friction which increases by the square of fluid velocity, resulting in a functional limit on the system flow rate. In a pumped system, a pump can be selected to overcome the overall impedance of the system; mass flow rate can generally be specified up to the limits of practicality. At some stage, energy losses due to the parasitic pumping power will outweigh the useful energy gained. The resistance to flow generated by friction in the well bores and impedance in the fractured rock reservoir causes a pressure drop through the system. In this study, a Brayton cycle is assumed, with the SCCO₂ directly expanding through the turbine. For isentropic expansion through a turbine, the useful energy is a function of the pressure drop between the inlet and outlet of the turbine (refer to Section 0). As such, the pressure at reference point 4 cannot be lower than the pressure at reference point 1. This consideration forms the secondary limit on mass flow rate in the SCCO₂ circuit.

It can be seen that there are two separate considerations for determining the mass flow rate for the SCCO₂ system, thermosiphon driving potential and practical limits from friction effects. Both are investigated in each parametric study to determine which proved to be the overriding factor in each instance.

3.4.1.b Surface Plant Efficiency

For fair comparison, some allowance must be made for the different power generation potential and losses associated with the different systems' surface plant. It is acknowledged that the values selected are very rough estimations. The actual efficiency factors will be highly case specific and dependant on more factors that could be reasonably explored during this project. Refinement of the values could form an entire study in their own right and are easily adjusted as model inputs for further refinement.

For the SCCO₂ system, since most of the system is include directly in the model, it is only the efficiency of the turbine that is assumed. This has been set at:

$$\eta_{turbine} = 0.8$$

Previous studies have referenced values of between 0.8 and 0.85. As such, the lower value was selected to partially allow for surface piping losses, pressure drop through the cooling tower (which was calculated as isobaric) and other ancillary losses in the surface plant. All reasonable sub-surface losses are built into the mathematical model. Note that the waste heat energy dispersed by the cooling tower is modelled in the system and accounted for directly.

For the water based system, there is a conversion efficiency associated with the heat exchanger as well as the pump. Further to this, the secondary isopentane circuit driving the turbine has energy loss associated with pumping power, turbine efficiency and waste heat dumped by the cooling tower. The secondary isopentane circuit is not explicitly modelled in the Matlab script, rather it is factored with an overall rate of useful heat energy conversion which has been calculated as follows:

$$\eta_{watersys} = \eta_{exchange} \times \eta_{coolingtower} \quad \mathbf{3-1}$$

Where DiPippo (2008) estimates

$$\eta_{exchange} = 0.9 \quad \text{(Heat exchange loss factor)}$$

$$\eta_{coolingtower} = 0.151 \quad \text{(The proportion of turbine work to total energy in – accounting for waste heat out of the cooling tower).}$$

Leading to:

$$\eta_{watersys} = 0.136$$

The value $\eta_{watersys}$ is applied as an overall factor to the entire water based binary system and treated as a proportion of mined heat energy that can be converted to useful turbine work.

The efficiency of the geothermal water pump is applied directly to the calculated power requirements and included separately in the model.

$$\eta_{pump} = 0.9$$

In summary, these adjustment factors are indicative only for the purpose of normalising the mathematical model outputs for this study. They could vary significantly depending on a large range of case specific factors.

3.4.1.c Water Based Binary Mass Flow Rate

With reference to the preceding section, the same constraints apply to the water based binary system. The mass flow rate specification is considerably less complicated as it can be specified with a pumping power input. Once again, it is governed mainly by practicality of pumping energy requirements.

In contrast to the direct drive SCCO₂ circuit, the surface plant of a binary circuit extracts the useful energy through a heat exchanger. This is an important point as it means the output is largely a function of temperature difference rather than pressure. In theory, the circuit can suffer pressure drop before the primary useful energy conversion rate is greatly affected. It was theorised that a higher mass flow rate, combined with lower heat loss through the production well bore (from the higher fluid velocity) should result in an optimised state for the water system.

A phenomenon that was also taken into account is flashing. Inspection of the system diagram from Atrens, Gurgenci and Rudolph (2008) shown in Figure 2-1 shows the fluid at reference point 4 has undergone flashing; it is below saturation pressure and has changed phase to steam. Analysis of a multi-phase circuit is more complex than the scope of work for this study. As a result, a constraint for this study was to identify the mass flow rate at which the pressure drop in the production well bore is such that flashing occurs. Section 1.2.2 outlines some different surface plant arrangements that design flashing into the system. However, as a simplifying assumption, flashing does not occur in the production well bore. This condition is used as the flag the upper boundary for mass flow in the water based system. Assuming the fluid temperature is close to the reservoir temperature, the saturation pressure at which flashing begins to occurs is about 3 MPa. During iteration of the mass flow rate, the mathematical model treats 5 MPa as the lowest allowable pressure.

The selection of mass flow rate for the water based study was a function of the output from the SCCO₂ test case. The purpose was to match projected power output such that the systems are compared using functionally similar requirements; power out from a given reservoir. As such, the water based system was first tested for the mass flow rate practical limits, where pumping to overcome friction and reservoir impedance outweighs the net output. The system was subsequently tested and chosen to match the net power output of the SCCO₂ reference case.

3.4.2 Parametric Investigation

The parametric case studies each followed these steps:

1. All base parameters set to be the same as the reference case except mass flow rate and the parameter under investigation.
2. Setting the variable parameter (eg well bore diameter) to its minimum value to be investigated.
3. Setting a low initial value for mass flow rate – 5 kg/s for each.
4. Running and looping of the SCCO₂ model, increasing the mass flow rate iteratively until the criteria of energy balance is met.
5. Writing results for the SCCO₂ model for that case.
6. Running and looping of the water model, increasing the mass flow rate iteratively until the criteria of the production well exit pressure dropping below 5 MPa.
7. Writing results for the water model for that case.
8. Looping back to step 3 with the variable parameter increased iteratively until the full range of the variable parameter has been tested and recorded.
9. Production of comparative plots showing trends and magnitude for mass flow rate, net exergy and thermal efficiency in each case.

Note that the preceding steps are the underpinning method written into the Matlab model (discussed in Section 3.5).

3.4.2.a Well bore diameter

It has been theorised that the frictional effects of SCCO₂ in the well bores is a dominant factor in that systems efficiency. Increasing the diameter reduces the ratio of wall surface area to bulk fluid volume. This has the dual benefit of increasing the volume of fluid that can flow and also reducing the proportion of fluid subject to boundary layer friction.

The reference case well bore diameter was 0.2 metres. The study investigates the effect of doubling the diameter to 0.4 metres and at 0.05 metre increments between.

3.4.2.b Reservoir depth

It is theorised that SCCO₂ systems may perform better where a reservoir is at a reduced depth. This concept follows from the preceding; if frictional effects dominate the behaviour of a SCCO₂ circuit more than water, a reduced well bore length may reduce the gap in performance (if one exists).

The reference case reservoir depth is set at 5000m. This study investigates the effect of reducing the depth to 3000m and at 250m increments between.

3.4.2.c Reservoir permeability

SCCO₂ has a much lower viscosity to density ratio than water which suggests it could be superior for reservoirs with lower permeability. It has also been noted that the heat carrying capacity of water is much greater. As such, both the mass flow rate and net exergy are of interest in this case.

The reference case permeability (k_A) is set at $2.1 \times 10^{-9} \text{ m}^4$. This study investigates the range of $0.5 \times 10^{-9} \text{ m}^4$ through to $8.5 \times 10^{-9} \text{ m}^4$ at intervals of $1 \times 10^{-9} \text{ m}^4$. This represents a range of four times lower permeability to four times higher than the reference case.

3.4.2.d Reservoir temperature

It is reasonably predictable that the effect of reservoir temperature reduction will be a similar reduction in the heat energy that can be mined with either fluid. This case seeks to investigate the system behaviour under reduced reservoir temperature and identify if either SCCO₂ or water prove to favour such conditions.

The reference case sets the reservoir temperature at 510K. This study investigates the effect of reservoir temperature on the systems down to 460K at intervals of 10K.

3.5 System Mathematical Model

3.5.1 Model Overview

The system model takes the form of a Matlab script file that calculates the change of fluid state iteratively along the fluid flow path. With reference to Figure 2-1 (Atrens, Gurgenci & Rudolph 2008), in each case it is the fluid flow from point 1 through to point 4 that is modelled. The fluid state at reference point 5 is calculated as a function of the respective energy extraction method - isentropic expansion through a turbine for SCCO₂ and isobaric heat exchange for the water system. The difference between fluid state properties at points 4 and 5 is used to estimate the exergy available from the respective systems with overall system efficiency corrections applied to give a net exergy result.

With reference to the key system reference points shown in Figure 2-1, the mathematical model progresses in distinct stages and feeds back results in a loop to converge on a final answer;

1. The fixed parameters are set and an initial guess value given for the mass flow rate (5 kg/s).
2. Iterative calculation of fluid state down the injection well (reference point 1 through to 2) making allowance for pressure gain due to gravity, pressure loss due to friction and heat flux through the well bore wall.
3. Iterative calculation of the fluid state through the fractured granite geothermal reservoir (reference point 2 through to 3) making allowance for pressure drop through the porous media, and temperature gain.
4. Iterative calculation of fluid state up the production well (reference point 3 through to 4) making allowance for heat flux through the well bore wall in addition to pressure loss due to gravity and friction.
5. For the SCCO₂ system only, calculation of the temperature at point 5 after isentropic expansion of the fluid through the turbine (reference point 4 through to 5). For the water system, power extraction is thorough isobaric heat extraction; the pressure and temperature at reference point 5 are the same as the preceding and succeeding reference points respectively.
6. For the SCCO₂ system, an energy balance calculation is performed. As long as the energy balance is positive, the code loops back to step 2 above with a new higher mass flow rate. At the point the energy balance is achieved (± 1 kg/s), this is determined to be the result for the case being tested. For the water system, if the pressure a reference point 4 is greater than 5 MPa, the code loops back to step 2 above with a higher mass flow rate until the condition is satisfied.

The preceding model forms the basis for the mathematical approach to the problem.

3.5.2 Matlab Program Structure

As an overview before outlining mathematical methods, Figure 3-1 shows the hierarchy of Matlab script and function files to carry out the calculations. Table 3-1 lists the files with a functional description for each. Note that the mathematical methods for each will be described in detail in succeeding sections.

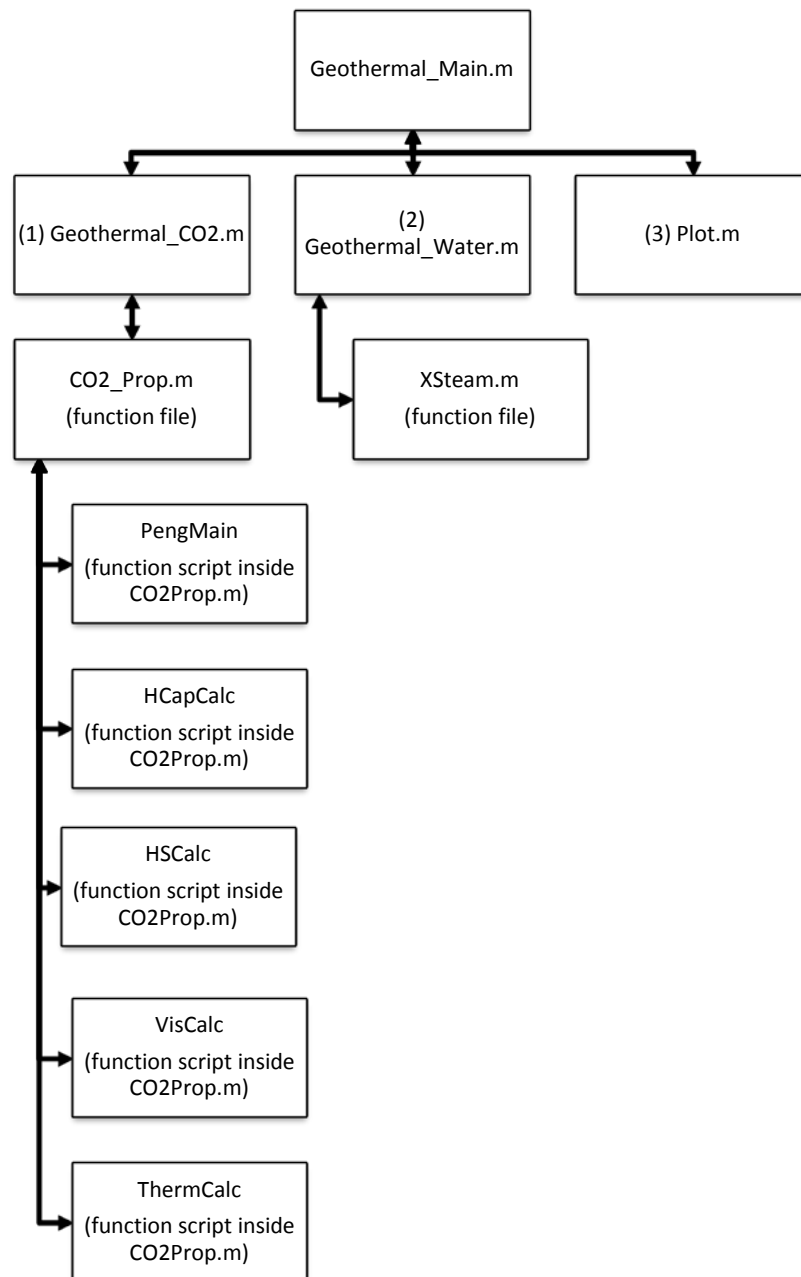


Figure 3-1 - Matlab Script Hierarchy

Table 3-1 - Matlab Script File Functional Descriptions

Script Name	Description
Geothermal_Main.m	<ul style="list-style-type: none"> • Sets shared parameters • Initiates the respective geothermal scripts. • Loops through the analysis scripts until all test results are converged and complete for each of the systems and varied parameters. • Calls the results and plotting scripts.
Geothermal_CO2.m	<ul style="list-style-type: none"> • Contains all fluid transport and thermodynamic equations for the CO2 system. • Iterates along the fluid path from reference point 1 through to reference point 4. • Calls '<i>CO2_Prop.m</i>' at each iteration to calculate fluid state properties • Constructs a matrix of fluid state properties at each differential point through the circuit for each of the injection well, reservoir and production well (3 in total).
Geothermal_Water.m	<ul style="list-style-type: none"> • Contains all fluid transport and thermodynamic equations for the water system. • Iterates along the fluid path from reference point 1 through to reference point 4. • Calls '<i>XSteam.m</i>' at each iteration to calculate fluid state properties • Constructs a matrix of fluid state properties at each differential point through the circuit for each of the injection well, reservoir and production well (3 in total).
CO2Prop.m (function file) Written by the author specifically for this project	<ul style="list-style-type: none"> • [density,h,s,cp,cv,mu,kf] = CO2_Prop(T,P) • Outputs thermodynamic and transport properties based on the Peng Robinson equations of state and related departure functions. Input required is pressure and temperature • Specific to supercritical carbon dioxide. • Sub-functions called up in same file will be detailed in following sections (PengMain, HCapCalc, HSCalc, VisCalc, ThermCalc).
XSteam.m (function file)	<ul style="list-style-type: none"> • Written by Magnus Holmgren, www.x-eng.com • Water and steam properties according to IAPWS IF-97 calculated with pressure and temperature input. • (Holmgren 2007)
Plot.m	<ul style="list-style-type: none"> • File containing graph plotting scripts only.

3.5.3 CO₂ Property Model

In order to model the fluid flow and heat transport of the CO₂ system, a Matlab script was required to allow the properties of supercritical carbon dioxide to be calculated at differential points around the circuit. Carbon dioxide in the supercritical state is compressible like a gas but it exhibits significant variation from simple ideal gas property relations. In addition, all the critical transport and thermodynamic properties are interdependent and are not necessarily linear. The Peng Robinson equations of state (1976) and associated departure functions were used.

The following subsections detail the underlying equations used in the Matlab system model written as the primary analysis tool for the project.

3.5.3.a Peng Robinson Equations of State

The model of the system calculates the fluid properties along the respective section. SCCO₂ is compressible therefore the density change due to gravity is not linear. All critical fluid properties are functions of temperature and pressure. The Peng Robinson equations of state were selected for two reasons:

- Ansys CFX (the software used for the CFD work) has these equations built into the fluid library. Using the same equations of state for both the CFD and manual calculation was desirable.
- The Peng Robinson equations are very commonly used in industry calculation. The fit of data is reported to be very close to measured data and covers the range of temperature and pressure covered in this study.

The equations (3-2, 3-3 and subsequent coefficients) are repeated here directly as sourced from Peng and Robinson (1976) with the input p = pressure [Pa] and T = temperature [K]:

$$p = \frac{RT}{v - b} - \frac{a(T)}{v(v + b) + b(v - b)} \quad 3-2$$

Which can be rearranged and written as:

$$Z^3 - (1 - B)Z^2 + (A - 3B^2 - 2B)Z - (AB - B^2 - B^3) = 0 \quad 3-3$$

Where:

$$A = \frac{ap}{R^2T^2}$$

$$B = \frac{bp}{RT}$$

$$Z = \frac{pv}{RT}$$

$$a = \left(0.45724 \frac{R^2 T_c^2}{p_c} \right) \alpha$$

$$\alpha = \left(1 + k \left(1 - T_r^{1/2} \right) \right)^2$$

$$k = 0.37464 + 1.54226\omega - 0.26995\omega^2$$

$$b = 0.07780 \frac{RT_c}{p_c}$$

$R = 8.314$ [J/mol.K] = gas constant

T_c = critical temperature

p_c = critical pressure

$$T_r = \frac{T}{T_c}$$

ω = acentric factor

Note that "Z" is commonly known as the compressibility factor.

The Peng Robinson EOS is written into a function file (PengMain – contained in CO2Prop.m) which is called up during iteration. Practical use of the equation requires solving the cubic equation and finding the real roots. For a gas, Z is the lowest real root. For a liquid, it is the highest real root. Density is found by the equation:

$$\rho = \frac{(p)(MW)}{ZRT} \quad \text{3-4}$$

MW = Molecular weight

These are the equation sets that are used in the Matlab code. The function file output was tested across a large range of pressure and temperature combinations and checked for correlation with the tabulated values given in Span and Wagner (1996). A very good correlation was found. *Note – this is a comment on correct scripting of formula rather than a comparison between EOS methods.*

3.5.3.b Specific Heat Capacity

Poling (2001) details an empirical correlation equation to estimate the specific heat capacity c_p or c_v [J/kg.K] of a liquid or gas;

$$C_p^0 = R(a_0 + a_1T + a_2T^2 + a_3T^3 + a_4T^4) \quad 3-5$$

Where for carbon dioxide, the coefficients are;

$$\begin{aligned} a_0 &= 3.259 \\ a_1 &= 1.356 \times 10^{-3} \\ a_2 &= 1.502 \times 10^{-5} \\ a_3 &= -2.374 \times 10^{-8} \\ a_4 &= 1.056 \times 10^{-11} \end{aligned}$$

The Peng Robinson departure functions are as follows (Shmakov 2012);

$$C_p = a''(T) \frac{T}{2\sqrt{2}b} \ln \left[\frac{Z + (\sqrt{2} + 1)}{Z - (\sqrt{2} - 1)} \right] + \left[\frac{R(M - N)^2}{M^2 - 2A(Z + B)} - R \right] + C_p^0 \quad 3-6$$

$$C_v = \frac{R(M - N)^2}{2A(Z + B) - M^2} + C_p \quad 3-7$$

Where;

$$M = \frac{Z^2 + 2BZ - B^2}{Z - B}$$

$$N = a'(T) \frac{B}{bR}$$

$$a'(T) = \kappa a_c \left[\frac{\kappa}{T_c} - \frac{1 + \kappa}{\sqrt{TT_c}} \right]$$

$$a''(T) = \frac{\kappa a_c (1 + \kappa)}{2\sqrt{T^3 T_c}}$$

The remaining terms are as defined in the Peng Robinson Equations of State preceding. These are the equation sets that are used in the model. Specifically, they are contained in the function HCapCalc (contained in CO2Prop.m). The function file output was tested across a large range of pressure and temperature combinations and checked for correlation with the tabulated values given in Span and Wagner (1996). A very good correlation was found. *Note – this is a comment on correct scripting of formula rather than a comparison between methods.*

3.5.3.c Entropy and Enthalpy

The specific entropy s [J/kg.K] and enthalpy h [J/kg] are of particular interest since it is from these values that the energy flow and capacity in the fluid is determined. These properties are commonly stated as a property change from a reference state. The value for specific entropy and enthalpy are set to zero at the reference state. The reference state used in this study is:

$$p_{ref} = 101325 \text{ Pa}$$

$$T_{ref} = 298 \text{ K}$$

The method for calculation of specific enthalpy and entropy is as follows:

$$h(T, p) = -h_{dep}(T_{ref}, p_{ref}) + h_{ideal}(T_{sys}, p_{sys}) + h_{dep}(T_{sys}, p_{sys}) \quad 3-8$$

$$s(T, p) = -s_{dep}(T_{ref}, p_{ref}) + s_{ideal}(T_{sys}, p_{sys}) + s_{dep}(T_{sys}, p_{sys}) \quad 3-9$$

Where the Peng Robinson departure functions for entropy and enthalpy are as follows (Shmakov 2012):

$$h_{dep}(T, p) = RT_c \left[T_r(Z - 1) - 2.078(1 + \kappa)\sqrt{\alpha} \ln \left(\frac{Z + (\sqrt{2} + 1)B}{Z - (\sqrt{2} - 1)B} \right) \right] \quad 3-10$$

$$s_{dep}(T, p) = R \left[\ln(Z - B) - 2.078\kappa \left(\frac{1 + \kappa}{\sqrt{T_r}} - \kappa \right) \ln \left(\frac{Z + (\sqrt{2} + 1)B}{Z - (\sqrt{2} - 1)B} \right) \right] \quad 3-11$$

The coefficients Z , B , T_c , T_r , κ and α are the same as previously defined in the Peng Robinson EOS.

The ideal gas components of equation 3-10 and 3-11 are calculated using a modified relationship from Poling (2001) for specific heat capacity. The coefficients (a_0, \dots, a_4) are the same as referenced in the previous

Specific Heat Capacity section:

$$h_{ideal}(T, p) = \left[a_0(T - T_{ref}) + \frac{a_1}{2}(T^2 - T_{ref}^2) + \frac{a_2}{3}(T^3 - T_{ref}^3) + \frac{a_3}{4}(T^4 - T_{ref}^4) + \frac{a_4}{5}(T^5 - T_{ref}^5) \right] \frac{R}{MW} \quad 3-12$$

$$s_{ideal}(T, p) = \left[a_0 \ln\left(\frac{T}{T_{ref}}\right) + a_1(T - T_{ref}) + \frac{a_2}{2}(T^2 - T_{ref}^2) + \frac{a_3}{3}(T^3 - T_{ref}^3) + \frac{a_4}{4}(T^4 - T_{ref}^4) - \ln\left(\frac{p}{p_{ref}}\right) \right] \frac{R}{MW} \quad 3-13$$

These are the equation sets that are used in the model. Specifically, the calculations for s_{ideal} and h_{ideal} are contained in the function HCapCalc (contained in CO2Prop.m). The departure functions for s_{dep} and h_{dep} are contained in the function HSCalc (contained in CO2Prop.m). The function file output was tested across a large range of pressure and temperature combinations and checked for correlation with the tabulated values given in Span and Wagner (1996). A very good correlation was found. *Note – this is a comment on correct scripting of formula rather than a comparison between methods.*

3.5.3.d Viscosity

A method for calculating viscosity μ [cp] of supercritical carbon dioxide was detailed by Heidaryan et al. (2011) and used in this analysis:

$$\mu(T, p) = \frac{A_1 + A_2 p + A_3 p^2 + A_4 \ln(T) + A_5 (\ln(T))^2 + A_6 (\ln(T))^3}{1 + A_7 p + A_8 \ln(T) + A_9 (\ln(T))^2} \quad 3-14$$

The units of temperature are in [K] and pressure in [bar] (0.1MPa). The coefficients are as below;

$$\begin{aligned} A_1 &= -1.146067 \times 10^{-1} \\ A_2 &= 6.978380 \times 10^{-7} \\ A_3 &= 3.976765 \times 10^{-10} \\ A_4 &= 6.336120 \times 10^{-2} \\ A_5 &= -1.166119 \times 10^{-2} \end{aligned}$$

$$\begin{aligned}
A_6 &= 7.142596 \times 10^{-4} \\
A_7 &= 6.519333 \times 10^{-6} \\
A_8 &= -3.567559 \times 10^{-1} \\
A_9 &= 3.180473 \times 10^{-2}
\end{aligned}$$

These are the equation sets that are used in the model with the inputs and outputs converted from (and to) SI units. The calculations for μ are contained in the function VisCalc (contained in CO2Prop.m). The function file output was tested across a large range of pressure and temperature combinations and checked for correlation with the published values given in Heidaryan et al. (2011). A very good correlation was found. *Note – this is a comment on correct scripting of formula rather than a comparison between methods.*

3.5.3.e Thermal Conductivity

A method for calculating thermal conductivity k_f [$\text{mWm}^{-1}\text{K}^{-1}$] of supercritical carbon dioxide was detailed by Jarrahan and Heidaryan (2012) and used in this analysis;

$$k_f(T, p) = \frac{A_1 + A_2p + A_3p^2 + A_4 \ln(T) + A_5(\ln(T))^2}{1 + A_6p + A_7 \ln(T) + A_8(\ln(T))^2 + A_9(\ln(T))^3} \quad \mathbf{3-15}$$

The units of temperature are [K] and pressure [MPa]. The coefficients are reproduced in full as below;

$$\begin{aligned}
A_1 &= 1.49288267457998 \times 10^1 \\
A_2 &= 2.62541191235261 \times 10^{-3} \\
A_3 &= 8.77804659311418 \times 10^{-6} \\
A_4 &= -5.11424687832727 \times 10^0 \\
A_5 &= 4.37710973783525 \times 10^{-1} \\
A_6 &= 2.11405159581654 \times 10^{-5} \\
A_7 &= -4.73035713531117 \times 10^{-1} \\
A_8 &= 7.36635804311043 \times 10^{-2} \\
A_9 &= -3.76339975139314 \times 10^{-3}
\end{aligned}$$

These are the equation sets that are used in the model with the inputs and outputs converted from (and to) SI units. The calculations for k_f are contained in the function VisCalc (contained in CO2Prop.m). The function file output was tested across a large range of pressure and temperature combinations and checked for correlation with the published values given in Jarrahan and Heidaryan (2012). A very good correlation was found. *Note – this is a comment on correct scripting of formula rather than a comparison between methods.*

3.5.4 Water Property Model

For most applications, water can be treated as incompressible with reasonably constant transport and thermodynamic properties. In the case of a geothermal application, there is a large pressure and temperature range found in the system. With reference to Figure 2-1, it can be seen that density varies by around 15 to 20 percent. Following this, the requirements for a reliable mathematical model for water transport and thermodynamic properties was recognised.

The requirement was conveniently filled with an externally sourced Matlab model with full credit owed to Marcus Holmgren (2007). XSteam.m models steam and water properties using Matlab based on the "International Association for Properties of Water and Steam Industrial Formulation 1997" (IAPWS IF-97). It is a full implementation of the IF-97 standard that provides very accurate steam and water properties in ranges from 0-1000 bar and 0-2000°C (Holmgren 2007). Due to the size and complexity of the program, it was impractical for the author to thoroughly review the program for total accuracy and methodology. For the purpose of this study, confidence was achieved with extensive positive peer reviews at the download source.

3.5.5 Preliminary System Estimates – CO₂

In order to select appropriate empirical models for friction and heat transfer in the well bores, some initial estimates were made based on indicative pressure and temperature references from previous studies. The initial fixed parameter assumed is the required output from the turbine. Using the output P_{out} and an assumed pressure drop from the system diagram found in Atrens, Gurgenci and Rudolph (2008).

Refer to Figure 2-1 for positions of reference points and to Appendix B – Reference Case Parameter Sources for further information on selected values.

3.5.5.a Initial Estimate - Mass Flow Rate

Known or Assumed Values

$$P_{out} = 5 \text{ MW (basic output target for sizing purpose only)}$$

$$\eta_{turbine} = 0.8 \text{ (assumed)}$$

$$p_1 = 8 \text{ MPa (assumed as start point above critical pressure)}$$

$$T_1 = 315 \text{ K (assumed as start point above critical temperature)}$$

$$p_4 = 20 \text{ MPa}$$

$$T_4 = 445 \text{ K}$$

$$p_5 = p_1 = 8 \text{ MPa}$$

Point 4 – Properties

The fluid properties at reference point 4 – read from tables (Span & Wagner 1996)

$$\rho_4 = 292.065 \text{ kg/m}^3$$

$$c_{v4} = 0.874515 \text{ kJ/kg.K}$$

$$s_4 = -0.78088 \text{ kJ/K}$$

Point 5 – Properties

The fluid properties at reference point 5 are calculated by assuming isentropic and adiabatic expansion through the turbine. p_5 is known since it is the assumed injection pressure. Where:

$$s_4 = s_5 \text{ (Isentropic process)}$$

$$T_5 = 360 \text{ K (read from equation of state tables (Span & Wagner 1996) at}$$

$$s_4 = s_5$$

$$\rho_5 = 152.93 \text{ kg/m}^3$$

$$c_{v5} = 0.82137 \text{ kJ/kg.K}$$

Finding the average specific heat capacity:

$$\begin{aligned} c_{vavg}(4-5) &= \frac{0.874515 + 0.82137}{2} \\ &= 0.84769 \\ &= 847.69 \text{ J/kg.K} \end{aligned}$$

Solving for required mass flow rate estimate:

$$P_{out} = \eta_{turbine} \cdot c_{vavg} \cdot \Delta T \cdot \dot{m} \quad \text{3-16}$$

$$\dot{m} = \frac{P_{out}}{\eta_{turbine} \cdot c_{vavg} \cdot \Delta T} \quad \text{3-17}$$

Solving for the CO₂ circuit:

$$\dot{m} = \frac{5 \times 10^6}{0.8 \cdot 847.69 \cdot (445 - 360)} = 86.715 \text{ kg/s}$$

3.5.5.b Initial Estimate - Reynolds Number

Finger and Blankenship (2010) indicate that a typical geothermal well bore will have a diameter of between 200mm and 340mm. Since the system power output assumed is relatively small, an initial value of 200mm has been selected giving a cross-sectional area of:

$$A_p = \frac{\pi D^2}{4} = 0.03142 \text{ m}^2 \quad 3-18$$

The approximate Reynolds number is required to estimate the pressure drop due to friction in the well bores. It is to be calculated at reference points 1, 2, 3 and 4 since density is a function of temperature and pressure in the SCCO₂.

$$Re = \frac{\rho VL}{\mu} = \frac{VL}{\nu} \quad 3-19$$

At reference Point 1:

$$\rho_1 = 261.29 \text{ kg/m}^3 \text{ - read from EOS tables (Span \& Wagner 1996)}$$

$$\mu = 24.508 \times 10^{-6} \text{ Pa.s}$$

$$V = \frac{\dot{m}}{\rho A_p} = \frac{86.741}{(261.29)(0.031416)} = 10.567 \text{ m/s}$$

The Reynolds number for the pipe flow at Ref point 1 is:

$$Re = \frac{\rho VL}{\mu} = \frac{261.29 \times 10.56 \times 0.2}{24.508 \times 10^{-6}} = 22.5 \times 10^6$$

It is therefore expected that the flow at reference point 1 is turbulent. The Reynolds number is calculated iteratively through the system as density, velocity and viscosity vary.

3.5.6 Preliminary System Estimates - Water

In the same fashion as the SCCO₂ system, for selection of appropriate empirical models for friction and heat transfer in the well bores, some initial estimates were made based on indicative pressure and temperature references from previous studies. The initial fixed parameter assumed is the required output from the heat exchanger (between reference point 4 and 5). Using the output P_{out} and an assumed isobaric temperature drop through the heat exchanger from the system diagram found in Atrens, Gurgenci and Rudolph (2008).

3.5.6.a Initial Estimate - Mass Flow Rate

Known or Assumed Values

Refer to Figure 2-1 for positions of reference points and to Appendix B – Reference Case Parameter Sources for further information on selected values.

$$P_{out} = 5 \text{ MW (basic output target for sizing purpose only)}$$

$$\eta_{binary} = 0.136$$

$$p_1 = 7.5 \text{ MPa}$$

$$T_1 = 305 \text{ K}$$

$$p_4 = 2.6 \text{ MPa}$$

$$T_4 = 500 \text{ K}$$

$$p_5 = p_1 = 7.5 \text{ MPa}$$

Point 4 – Properties

The fluid properties at reference point 4 (p_4 and T_4) - specific heat capacity read from steam tables:

$$c_{p4} = 4160 \text{ kJ/kg.K}$$

Point 5 – Properties

The state properties at point 5 (p_5 and T_5) are known - specific heat capacity read from steam tables:

$$c_{p5} = 3401 \text{ kJ/kg.K}$$

Solving for required mass flow rate using Equation 3-17:

$$\dot{m} = \frac{5 \times 10^6}{0.136 \cdot \left(\frac{4160 + 3781}{2} \right) \cdot (500 - 305)} = 47.48 \text{ kg/s}$$

3.5.6.b Initial Estimate - Reynolds Number

In this study, the wellbore geometry is the same as outlined in the SCCO₂ section preceding.

At reference Point 1:

$$\rho_1 = 995 \text{ kg/m}^3$$

$$V = \frac{\dot{m}}{\rho A} = \frac{47.48}{(995)(0.031416)} = 1.52 \text{ m/s}$$

From steam tables

$$\mu = 630.3 \times 10^{-6} \text{ Pa} \cdot \text{s}$$

The Reynolds number for the pipe flow at Ref point 1 is therefore (using equation 3-19):

$$Re = \frac{995 \times 0.43 \times 0.2}{630.3 \times 10^{-6}} = 480.1 \times 10^3$$

It is therefore expected that the flow at reference point 1 is turbulent. The Reynolds number is recalculated iteratively through the system as density, velocity and viscosity vary.

3.5.7 Wellbore Pressure Gradient

From point one at the entry to the injection well travelling down to point two at the base of the injection well, the fluid increases pressure due to gravity head. Since the SCCO_2 is compressible, the density, viscosity, heat capacity and other fluid properties change. The fluid properties are calculated from the pressure and temperature at any given point using the equations of state outlined by Peng and Robinson (1976). However, the pressure and temperature are functions of these fluid properties; for example friction loss at the wellbore walls causes pressure drop and is dependant of fluid viscosity. Also the increase in pressure from gravity is dependent on fluid density.

In order to calculate the gradient of fluid property changes and ultimately the fluid state at point 4 of the system, the fluid state is calculated at each interval Δz . The governing equation for the path down the injection well is:

$$p_{z+dz} = p_z + \Delta p_g - \Delta p_f - \Delta p_v \quad \text{3-20}$$

Where:

$$\Delta p_g = \text{pressure change due to pressure head (gravity)} = \rho g \Delta z$$

$$\Delta p_f = \text{pressure drop from friction (refer to the following section)}$$

$$\Delta p_v = \text{pressure change from fluid velocity} = \frac{1}{2} \rho (v_1^2 - v_0^2)$$

Travelling up the production well is the same except the sign of Δp_g is reversed.

3.5.7.a Wellbore Friction

The wellbore friction factor is estimated using the equation given by Fox, Pritchard and McDonald (2009):

$$\frac{1}{\sqrt{f}} = -1.8 \log \left[\left(\frac{e/D}{3.7} \right)^{1.11} + \frac{6.9}{Re} \right] \quad 3-21$$

Solving for f :

$$f = \left[-1.8 \log \left[\left(\frac{e/D}{3.7} \right)^{1.11} + \frac{6.9}{Re} \right] \right]^{-2} \quad 3-22$$

The wellbore roughness (ϵ) is estimated at 0.0004m for concrete (Atrens, Gurgenci & Rudolph 2009) (Fox, Pritchard & McDonald 2009). At reference point 1 for the SCCO₂ system, the friction factor is:

$$f = \left[-1.8 \log \left[\left(\frac{0.0004/0.2}{3.7} \right)^{1.11} + \frac{6.9}{2.4E7} \right] \right]^{-2} = 0.023474$$

This correlates with the Moody friction factor charts in Fox, Pritchard and McDonald (2009, p. 331). Note that the friction factor is calculated iteratively in the Matlab script to account for the changing Reynolds number.

The pressure drop due to friction is given by;

$$dp_f = f \times \frac{dz}{D} \times \frac{1}{2} \rho v^2 \quad 3-23$$

This is also calculated at each differential point along the pipe.

3.5.8 Wellbore Heat Transfer

There is a temperature difference between the wellbore wall and the geothermal fluid which will drive a heat flow q [Watts] between the two. The with the contact area constant, quantity of heat flow is dependant of two primary factors:

1. The heat transfer coefficient h_c [W/m²K] between the fluid and wellbore wall.
2. The thermal capacity and conductivity of the surrounding rock.

The heat flow is limited by the lesser of these two factors. The first can be calculated and, assuming a constant wall temperature, is dependant only on the fluid properties. The wall temperature down the well bore has been modelled as a linear gradient between the ambient surface temperature at the top of the well and

the temperature of the reservoir at the bottom of the well. This is a reasonable assumption for the purpose of this study

The governing equation is:

$$q = h_c A_{wall} (T_{wall} - T_{fluid_avg}) = \dot{m} c_p (T_{fluid_out} - T_{fluid_in}) \quad 3-24$$

This is simple energy balance where the middle term represents the heat flow through the wellbore wall and ΔT is the difference between the wall and bulk fluid temperatures. The final term represents the energy gained or lost by the fluid as a result – in this case ΔT is the increase or decrease of fluid temperature due to the heat energy change. Other terms in the equation include:

$$h_c = \frac{Nu_D k_f}{D} \quad 3-25$$

Where:

$$Nu_D = \frac{h_c D}{k_f} = 0.027 Re_D^{0.8} Pr^n \quad (\text{Kreith, Manglik \& Bohn 2011}) \quad 3-26$$

$$Pr = \frac{c_p \mu}{k_f} \quad 3-27$$

$n = 0.4$ for heating or

$n = 0.3$ for cooling

μ = viscosity at bulk temperature

k_f = variable ≈ 0.04 W/m·K

D = hydraulic diameter

It can be seen that the potential heat transfer rate (based on fluid only) is variable from one end of a well to the other. It was found that applying this method to the injection well of the SCCO₂ circuit produced a range of $q = 0$ [W/m²] at the top of the well (where the fluid temperature equals ambient) up to $q = 1900$ [W/m²] at the bottom of the injection well (where $h_c = 3100$ [W/m²K]).

The thermal capacity and conductivity of the surrounding geology is much harder to quantify as it is very much case specific. Zhang, Jiang and Xu (2013) found that an indicative heat loss /gain from a geothermal well bore were in the region of 75 Watts per linear meter [W/m] of depth for a wellbore with a diameter of 60mm. In this study, the base line wellbore diameter is 200mm so to extrapolate their findings based on the increased contact area:

$$q_{well} = \left(\frac{D}{D_{ref}} \right) q_{ref} = \left(\frac{200}{60} \right) 75 = 250 \quad [\text{W/m}] \quad \text{3-28}$$

It was clear that the heat transfer through 5000m wellbore could be significant and worthy of more detailed study outside the bounds of this study. For the purpose of initial modelling, it would appear the overall heat transfer potential is limited by the capacity and conductivity of the surrounding geology. As a result, it was decided to model the heat transfer as a linear increase as quantified in equation 3-28.

3.5.9 Reservoir Fluid State

The geothermal reservoir is by definition a complex and unknowable chain of geometry. The resistance to flow imparted by the reservoir is difficult to quantify – especially for an assumed case. As a result, in this study, it is defined mathematically by the product of a permeability (k) and cross sectional area (A) to produce a combination kA [m^4]. This value would normally be determined through testing of a geothermal field. For the purpose of this study, the value of was used from a previous similar study (Atrens, Gurgenci & Rudolph 2008) and considered as a constant to compare the two fluids:

$$kA = 2.1 \times 10^{-9} \text{m}^4$$

The pressure drop across the reservoir is modelled as Darcy flow and defined by:

$$\Delta P_r = \frac{\dot{m} \mu \Delta L}{\rho k A} \quad \text{3-29}$$

This is also calculated at differential points through the reservoir to account for the changing fluid properties.

The temperature gradient from reservoir entry to exit was assumed to increase at a linear rate; finishing with the fluid at the reservoir temperature at the exit point. This method was chosen for modelling simplicity. It is not an unreasonable assumption in the context of this study where design of the reservoir is outside the scope. It is assumed that the reservoir is of a size and capacity to raise the fluid to full reservoir temperature.

The Reynolds number is also estimated through the fractured rock. It is calculated using an arbitrary cross sectional area of 100m x 100m with a hydraulic diameter (assumed) set at an arbitrary crack width. Due to the assumption of linear temperature increase, and permeability modelled with Darcy flow, the Reynolds number in the reservoir is of little direct value to this study but left in the Matlab script to provide continuity of the calculated values.

3.5.10 Turbine Power Output (CO₂)

The turbine power output is calculated in the same way as the initial estimation to determine the mass flow rate. The pressure p_4 , pressure p_5 and temperature T_4 are known. The value for entropy at reference point 4 can be found in the tables from Span and Wagner (1996). After isentropic expansion through the turbine to the pressure at reference point 5, the value for T_5 can be read from the table; this is done by finding the equivalent value for entropy. The Matlab code finds the value of T_5 by iteration, to an accuracy of 1 degree Kelvin.

The power output can be calculated by:

$$P_{OutTurb} = c_{vavg} \cdot (T_4 - T_5) \cdot \dot{m} \quad 3-30$$

3.5.11 Cooling Tower Heat Extraction (CO₂)

The cooling tower is modelled as isobaric heat extraction. The quantity of power loss can be calculated from:

$$P_{OutCool} = c_{pavg} \cdot (T_5 - T_1) \cdot \dot{m} \quad 3-31$$

3.5.12 Heat Exchanger Energy Extraction (Water)

Note that the heat exchanger efficiency was accounted for as an overall factor applied to the system. The heat extraction rate [W] can be calculated from:

$$P_{HeatExch} = c_{pavg} \cdot (T_4 - T_5) \cdot \dot{m} \quad 3-32$$

3.5.13 Pumping Power Input (Water)

The pumping power required for reinjection of the water is given by:

$$P_{InPump} = \frac{\dot{m}\rho(p_5 - p_1)}{\eta_{pump}} \quad 3-33$$

3.5.14 Energy Balance

The system is balanced by the sum of all the inputs and outputs. System energy inflows are heat transfer into the injection well bore and reservoir and pumping power (water system). System energy outflows are frictional losses, heat loss through the production wellbore, useful power extraction and cooling tower heat extraction (SCCO₂ system).

The power flow P [Watts] due to heat addition in the reservoir is calculated incrementally by the Matlab code and defined as:

$$P_{ResHeat} = \sum \dot{m}c_{p(avg)}\Delta T \quad 3-34$$

The power flow P [Watts] due to heat energy transferred through the wellbores is calculated incrementally by the Matlab code and defined as:

$$P_{WellHeat} = q_{wall} = \sum h_c A_{wall} \Delta T \quad 3-35$$

The power flow P [Watts] lost to friction in the wellbores and reservoir is calculated incrementally by the Matlab code and defined as:

$$P_{OutFric} = \sum \frac{\dot{m}}{\rho} dp_f \quad 3-36$$

Where dp_f is the differential change in pressure caused by friction as defined in equation 3-23 for the well bores and 3-29 for the reservoir.

The combination of energy flows for the SCCO₂ system must equal zero:

$$\begin{aligned} \sum P = 0 = & P_{WellHeatInj} + P_{ResHeat} - P_{WellHeatProd} - P_{OutTurb} \\ & - P_{OutCool} - \sum P_{OutFric} \end{aligned} \quad 3-37$$

The combination of energy flows for the water system must equal zero:

$$\begin{aligned} \sum P = 0 = & P_{WellHeatInj} + P_{ResHeat} - P_{WellHeatProd} - P_{HeatExch} \\ & + P_{InPump} - \sum P_{OutFric} \end{aligned} \quad 3-38$$

3.6 Performance Comparison

The water based binary and CO₂ “direct drive” systems have fundamentally different surface plant and energy extraction methods. Exergy was selected as the primary measure of system performance potential, with the results normalised using assumed efficiency factors (as detailed in Section 3.4.1.b).

3.6.1 Exergy

Exergy was selected as the system independent measure of performance. Perrot (1998) defines the exergy of a system as “the maximum useful work possible during a process that brings the system into equilibrium with a heat reservoir”. It is represented by the following equation (exergy ψ in Watts):

$$\psi = \dot{m}[(h_4 - h_5) - T_0(s_4 - s_5)] \quad 3-39$$

Where:

T_0 = Temperature at the property reference state (298 K usually)

The first term represents the added heat energy, enthalpy (h), reduced by the irreversible entropy (s) gain due to friction and heat losses. In this case exergy is measured as a function of fluid properties compared between reference point 4 and 5 (as denoted by the '4' and '5' subscripts) and multiplied by the mass flow rate (\dot{m}) to give the energy available able to be used.

It was initially considered that the exergy could be measured between the entry of the injection well and exit of the production well in order to isolate the measurement from surface efficiency factors. It was realised that this approach did not accurately account for the energy conversion methods. For the water system, the heat extraction is largely a function of fluid temperature and therefore a function of reservoir temperature. For the SCCO₂ system, if no pressure difference exists between injection wellhead and the production wellhead, there is no potential to drive a turbine irrespective of the fluid temperature and heat capacity. The measure of exergy applied to the well heads of the SCCO₂ circuit says there is useful energy potential in the fluid where, practically, there is only heat to be discharged through the cooling tower as waste.

Therefore, considering the very different surface plant and energy extraction, the measure of net exergy is used to compare the two fluid systems. This is simply a product of exergy potential and the conversion efficiency with the parasitic pumping power subtracted (in the water system):

$$\psi_{net} = \eta_{turbine} \dot{m} [(h_4 - h_5) - T_0 (s_4 - s_5)] \quad \text{SCCO}_2 \quad \text{3-40}$$

$$\psi_{net} = \eta_{watersys} \dot{m} [(h_4 - h_5) - T_0 (s_4 - s_5)] - P_{InPump} \quad \text{Water} \quad \text{3-41}$$

This method normalises the results at least to the accuracy of the assumed efficiency factors. Exergy is the primary quantifier of useful output from the system.

3.6.2 Thermal Efficiency

The basic thermal efficiency of the SCCO₂ system can be calculated.

$$\eta_{th} = \eta_{turbine} \frac{P_{OutTurb}}{\sum P_{in}} \quad \text{3-42}$$

Where $\sum P_{in}$ is the sum of all energy inflows (reservoir and injection well heat addition).

The basic thermal efficiency of the water system can be calculated.

$$\eta_{th} = \eta_{turbine} \frac{P_{OutTurb} - P_{InPump}}{\sum P_{in}}$$

3-43

Where $\sum P_{in}$ is the sum of all energy inflows (pump power, reservoir and injection well heat addition).

3.7 CFD Analysis

The objective of using CFD analysis as a tool was to validate and visualise the calculated results from the mathematical model. Ansys CFX is a commercial package for simulating fluid flow and was the software package chosen for the task.

In construction of the CFD model, simplified geometry is used owing to the scale and complexity of the real system. It was recognised that the number of elements required to fill two 5km wellbore pipes and a fractured rock field approximately 1 km² would be computationally intensive and practically inefficient – especially considering the element size required to resolve boundary layer behaviour in the well bore. It was determined that a scaled model would be analysed with the scaling factors determined by similitude and dimensional analysis.

Further to physical scaling, the study of fluid flow through fractured rock is a complex field worthy of being a project in its own right. Ansys CFX has functionality to model a 3D geometry as a porous region and handle the fluid velocity and pressure change as loss functions applied to the general fluid momentum equations. In simple terms, this reduces computational effort by orders of magnitude compared to resolving fluid behaviour with a physical model of fractured rock.

Initially, it was decided to construct a model of a directly scaled system to familiarise with the program and test the set-up of the supercritical fluid models through the range of pressure and temperatures that were to be expected. As such, it was decided to model the system as two wellbores of a shorter length (50m) joined by a simple porous region with energy input. Carbon dioxide and water flow were tested.

Though this is explained further in the Chapter 5, the CFD component of this project was not successful. Despite expert assistance, it was found that trying to get even the simplified geometry to converge to a result was very difficult. In full knowledge that the true model was going to be more complex, and with consideration to the significant portion of project time already invested to get a trial running, it was decided the benefit of CFD to this study was not worth the time and resources estimated to achieve a result. Ultimately it was the tool and not the project. As such, the dimensional analysis and similitude calculations were not carried out. In

the interest of documenting the work done before this decision, the trial CFD models are presented in the following sections.

3.7.1 CFD Model Geometry

The base model consists of two 0.2m diameter pipes descending 50m into a porous rock region which is 10m x 10m cross-section and 50m long. The reservoir is set at 510K. The model was created with multiple bodies to enable different domains to be created in the model definition stage; i.e. the injection well, production well and porous reservoir are all separate entities. The bodies were combined into a multi-body part. This detail ensures continuity of the mesh at the domain interfaces. The model is split in half to take advantage the symmetry – halving the number of elements required.

Note the large additional bodies shown in the geometry model (Figure 3-2) are frozen bodies used as a body of influence for the reservoir mesh refinement in a later stage.

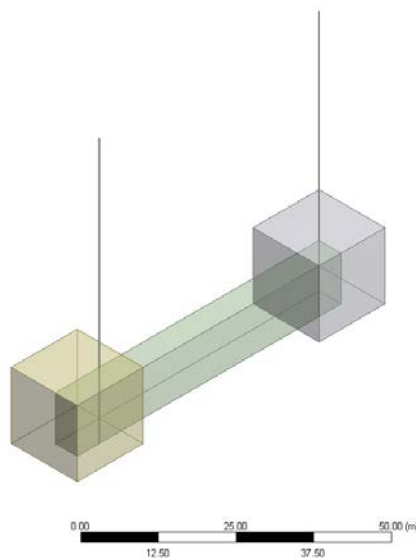


Figure 3-2 - CFD Model Geometry

3.7.2 CFD Model Mesh

The mesh was created using a sweep method for all bodies as shown in Figure 3-3 and Figure 3-4. The swept elements were inflated at the well bore walls to better resolve the boundary layer – this was a critical detail in order to correctly study the friction effects of flow in the pipe. This is shown in Figure 3-5. Also of note is the connection of elements between the multiple bodies at the domain interfaces. A body sizing was applied to the reservoir using the frozen bodies as a body of influence. This refines the mesh around the area of the well and reservoir interface.

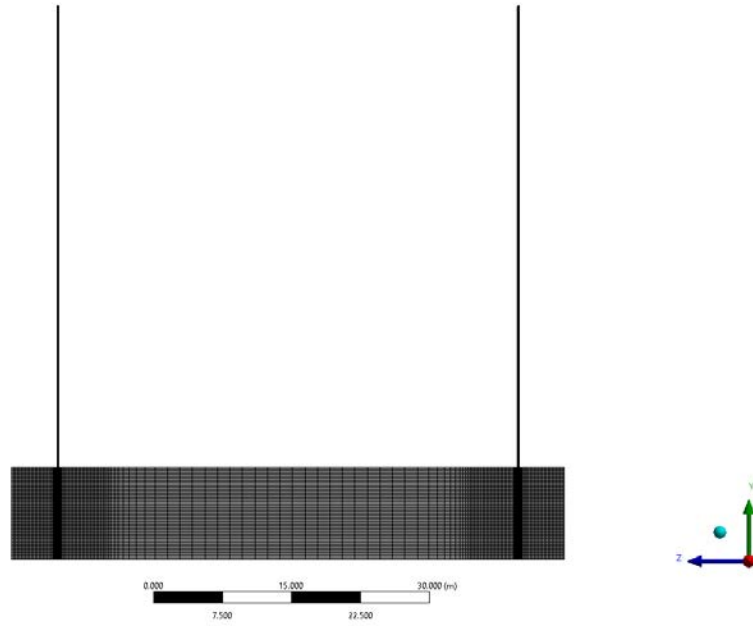


Figure 3-3 - CFD Model Mesh - Overview

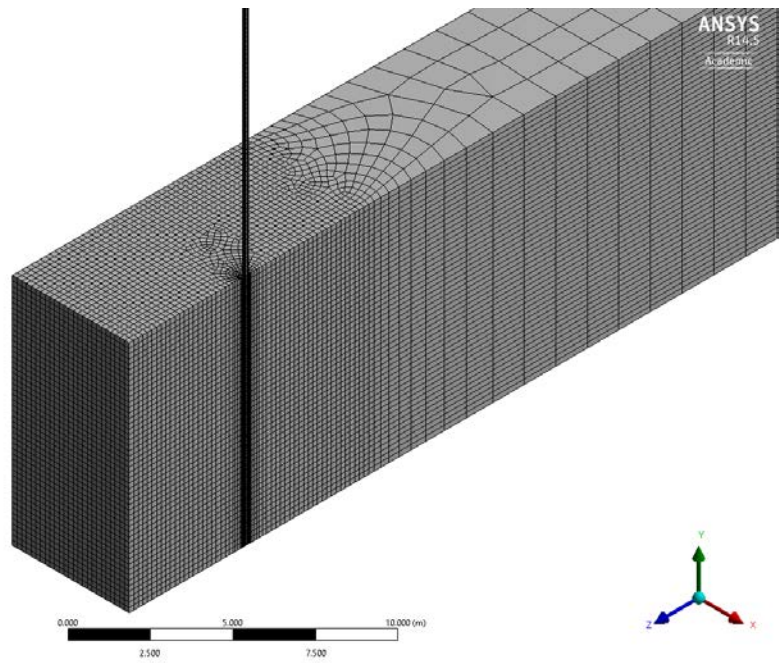


Figure 3-4 - CFD Model Mesh - Reservoir Inlet Region

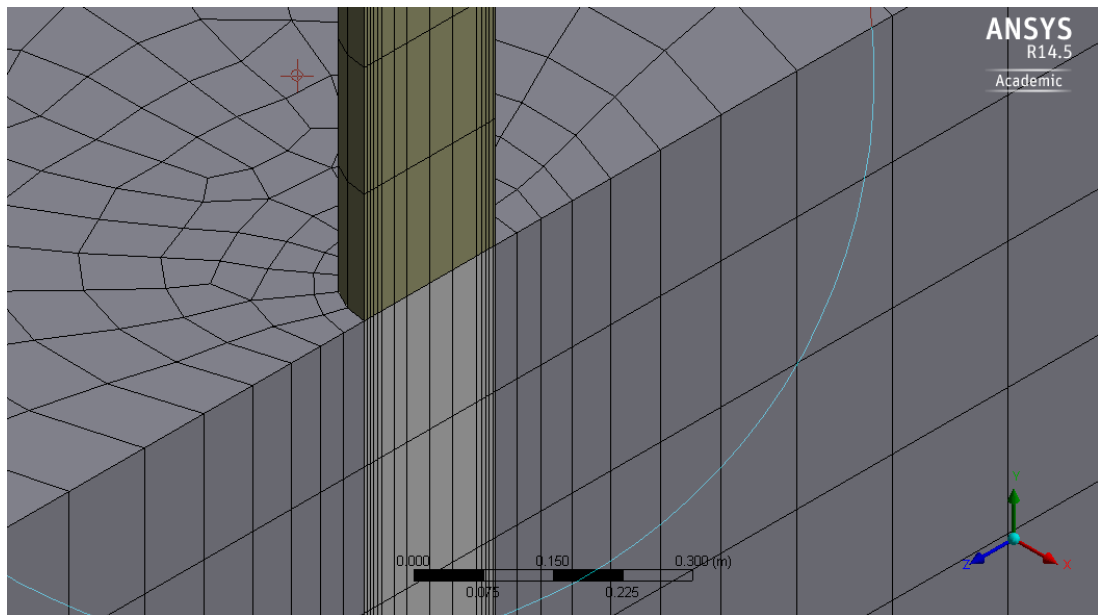


Figure 3-5 - CFD Model Mesh - Injection well inflation and domain interface.

The basic mesh statistics are:

- 232207 nodes
- 211212 elements
- Minimum orthogonal quality of 0.724

3.7.3 CFD Model Analysis Settings

Recalling that the model presented was created only to familiarise with the program suite and test the CO₂ fluid model in the supercritical region. Ansys has a built in library of fluids which includes CO₂ modelled with the Peng Robinson equations. This is the fluid selected at a reference pressure of 10 MPa.

The walls were modelled with a non-slip boundary condition. The inlet boundary condition was set to the relative pressure of 0 MPa (relative to the reference pressure of 10 MPa). The outlet boundary condition was set to the mass flow rate calculated in Section 3.5.5.a.

At this point, difficulties arose. It was found that the model would resolve and converge on a solution when the porous reservoir region was set to be fluid only. When either heat transfer or porosity were added to the model, no combination of boundary conditions, time step changes or otherwise would lead to a converged result. The only exception was by varying critical parameters (e.g setting porosity to 0.9 rather than 0.1) would get some results but were not helpful in achieving the project aims.

It became apparent that the difference in scales (small well bore diameter contrasted with long pipes and a large reservoir) meant that convergence was

difficult to achieve. Time step variation was thought to be the key. After expert help from the program vendor suggested a far more complex model may assist, it was clear that resolution required a commitment of time and resource that was beyond the capacity of the project. Some images of the trial model fluid flow are presented in Figure 3-6 and Figure 3-7.

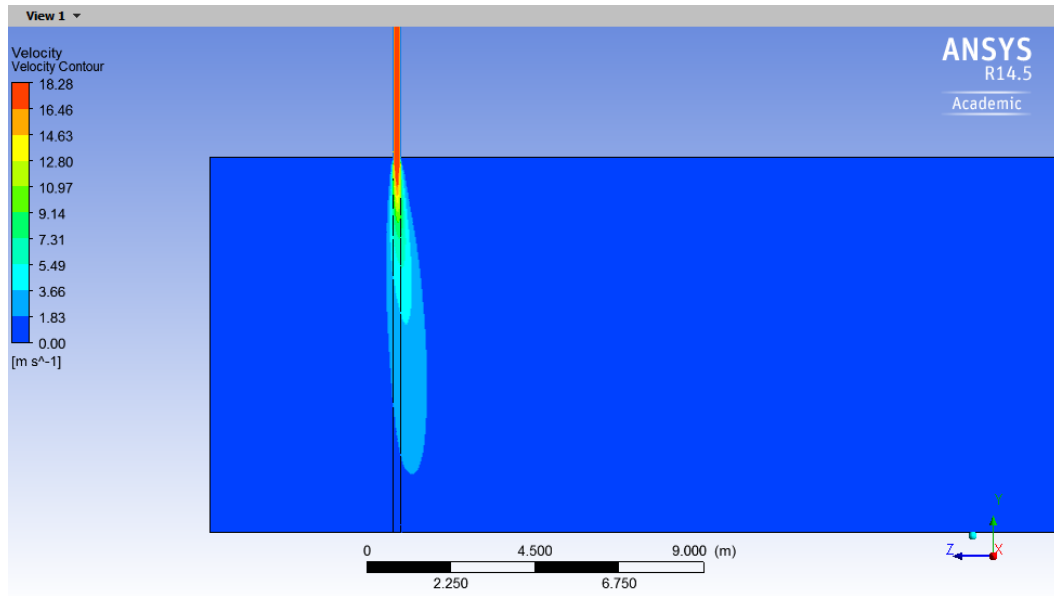


Figure 3-6 - Trial CFD model fluid flow - CO₂ into the reservoir

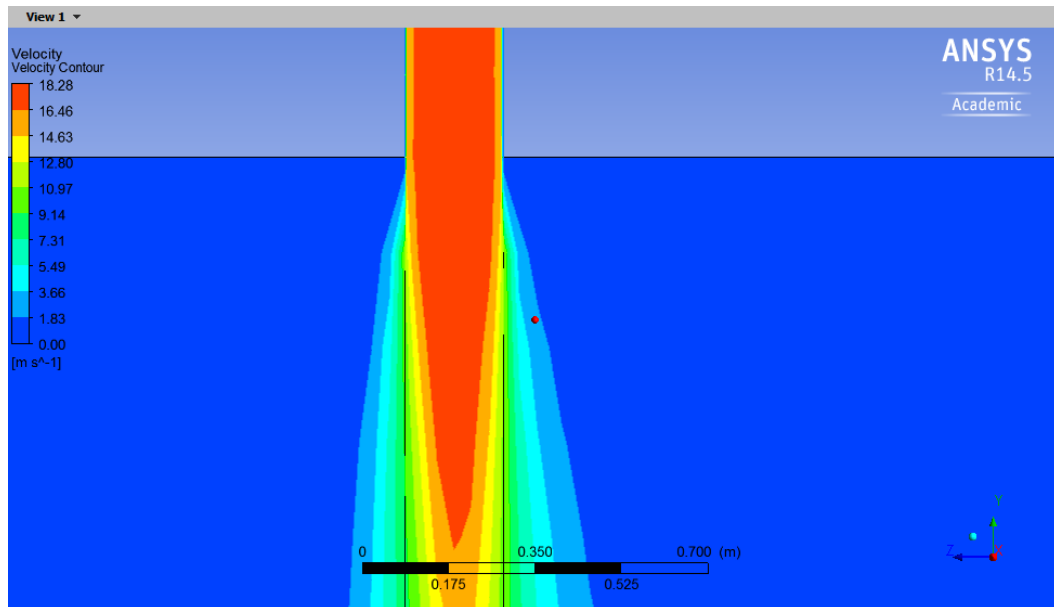


Figure 3-7 - Trial CFD model fluid flow - CO₂ into the reservoir

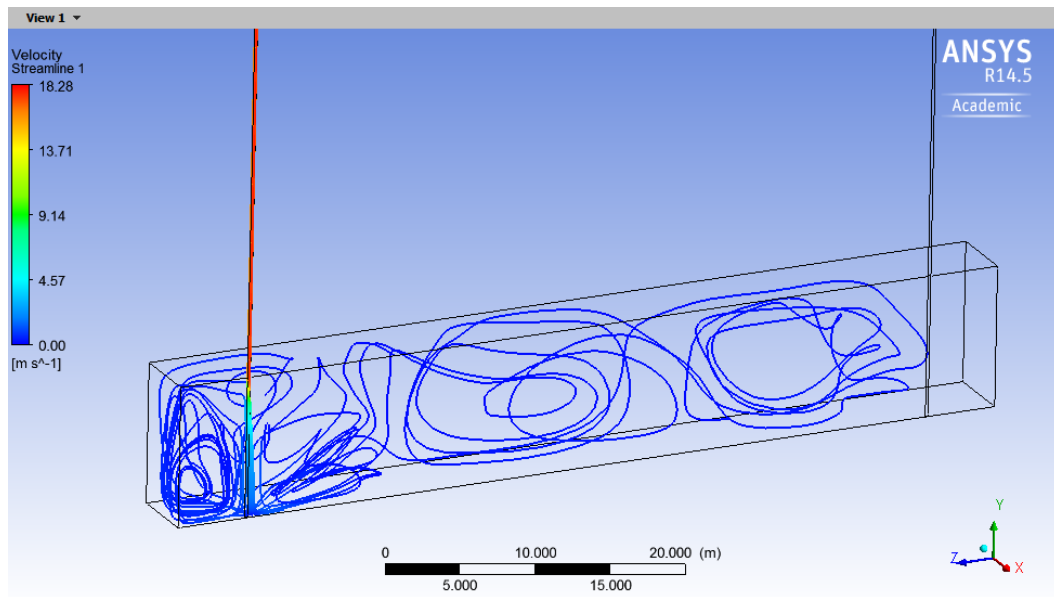


Figure 3-8 - Trial CFD model fluid flow - CO₂ into the reservoir

Figure 3-8 shows the streams lines of the fluid flow. Note that the solver has not resolved the streamlines out the production well.

It was determined that expansion of the CFD component of the project was unreasonable within the project specification. CFD did not add enough value to the results to neglect other components of the project in the first instance. As a result, the work presented was halted at this point and the focus turned to refining the mathematical model. Further discussion is included in Chapter 5.

4 RESULTS AND DISCUSSION

The mathematical model and methodology detailed in Chapter 3 was used to determine an appropriate reference case for fair comparison between the two geothermal fluids. A performance comparison is presented and discussed with respect to the following areas:

- Fluid property behaviour
- Reference case
- Well bore diameter
- Reservoir depth
- Reservoir permeability
- Reservoir temperature

4.1 Fluid Property Behaviour

To understand the different behaviour of the two systems being compared, an appreciation for the fluid property changes through the system is required. SCCO₂ is compressible and the fluid properties change dramatically with pressure and temperature. This is especially true near the critical region; Figure 2-2 shows the pressure and temperature phase diagram. The SCCO₂ EGS operates over a wide range of temperature and pressure with fluid at the surface operating very close to the critical point. Figure 4-1, Figure 4-2 and Figure 4-3 show the variation of some SCCO₂ properties through the length of the injection well, reservoir and production well respectively. These are shown for a reference case only where injection pressure is 9.5 MPa. Clearly, the pressure and temperature values will change with each specific case but the shapes of the curves demonstrate the non-linear nature of the fluid.

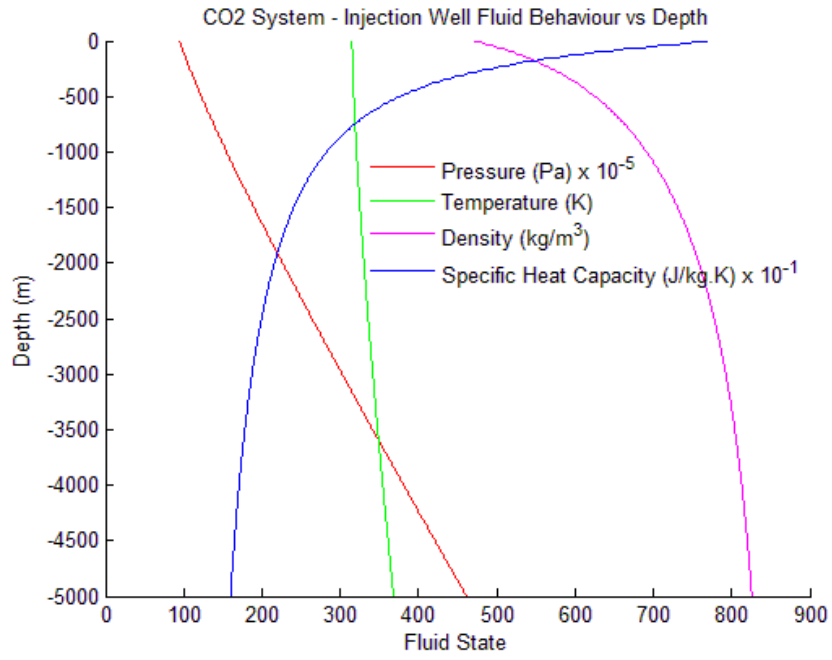


Figure 4-1 - CO₂ system injection well – typical fluid property variation

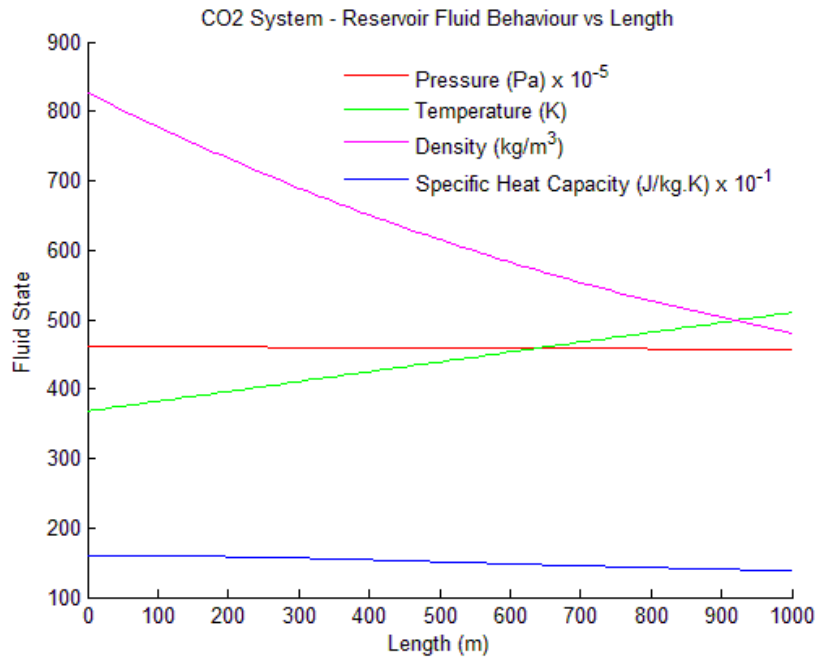


Figure 4-2 - CO₂ system reservoir – typical fluid property variation

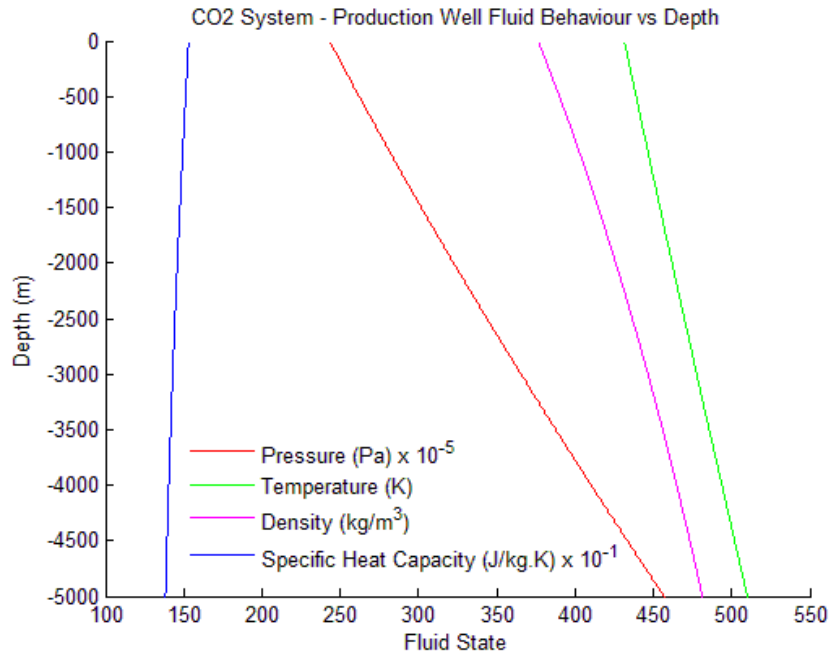


Figure 4-3 - CO₂ system production well – typical fluid property variation

Inspection of the density curve validates the need for an iterative approach to calculating fluid state properties. The fluid density curve is significantly different in comparison between the injection and production wells. To estimate transport or thermodynamic property variation as a linear gradient, between the entry and exit of the injection well particularly, would lead to erroneous results. This study uses a differential element length Δz of 10 meters which provides sufficient resolution of the curve for this purpose.

The most dramatic and directly relevant property non-linearity for SCCO₂ is specific heat capacity at constant pressure c_p . This is shown graphically in Figure 4-4 with a plot of c_p against temperature for a range of pressures near the fluid's critical region.

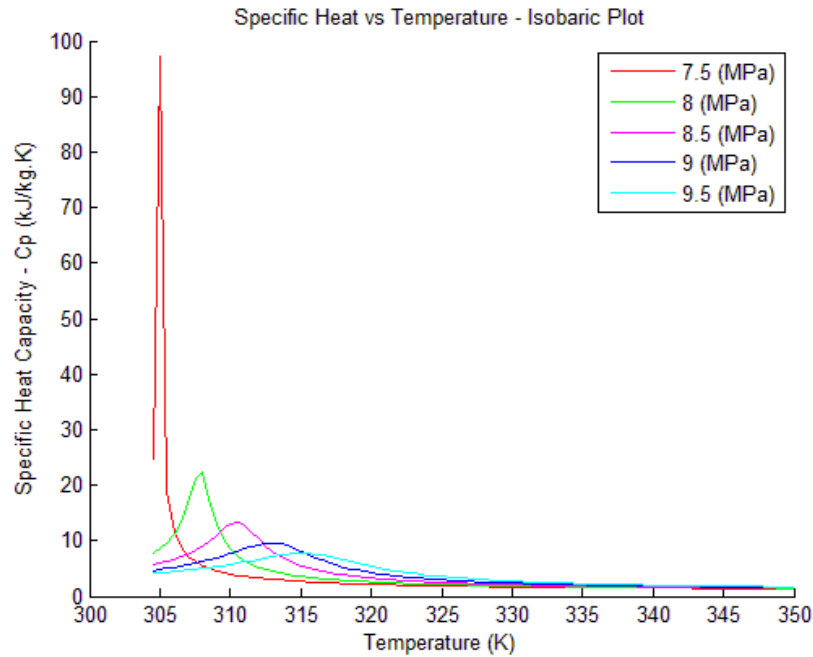


Figure 4-4 - Specific heat capacity vs temperature non-linearity

The plot presented is derived directly from the Peng Robinson EOS and correlates with Span and Wagner’s tabulated values; both of which are peer reviewed papers that have been validated with observations and measurements (by the original authors). The dramatic change in heat capacity would appear to be a departure that can be utilised favourably through system design. Noting the pressure and temperature range that experiences this dramatic change, it can be seen that it is the same as the pressure and temperature range seen at the surface region of the geothermal circuit where heat exchange is taking place. Determining the specification of the reference case in Section 4.2 expands more on this observation and its theoretical effect on system performance.

The nature of water is somewhat more intuitive being essentially incompressible and generally more linear in behaviour. The range of pressure and temperature observed in a geothermal system leads to reasonably significant changes in density, particularly seen through the reservoir and production well bore. Figure 4-5, Figure 4-6 and Figure 4-7 show typical property variation through the system.

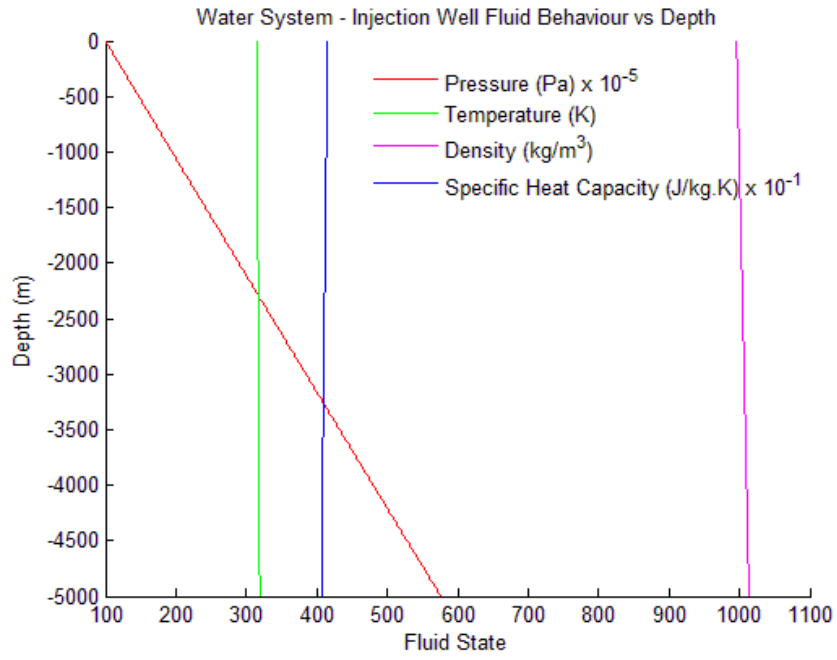


Figure 4-5 – Water system injection well fluid – typical property variation

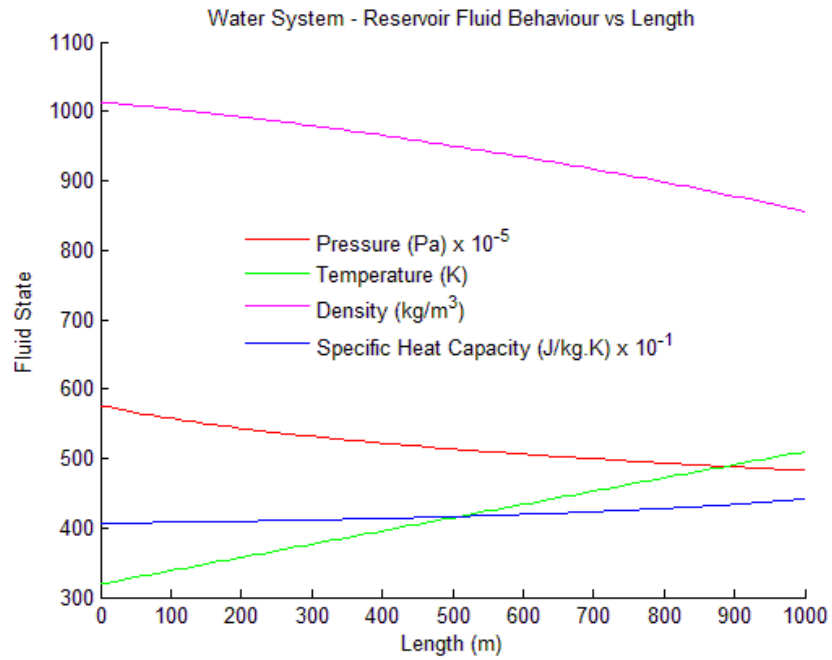


Figure 4-6 – Water system reservoir fluid – typical property variation

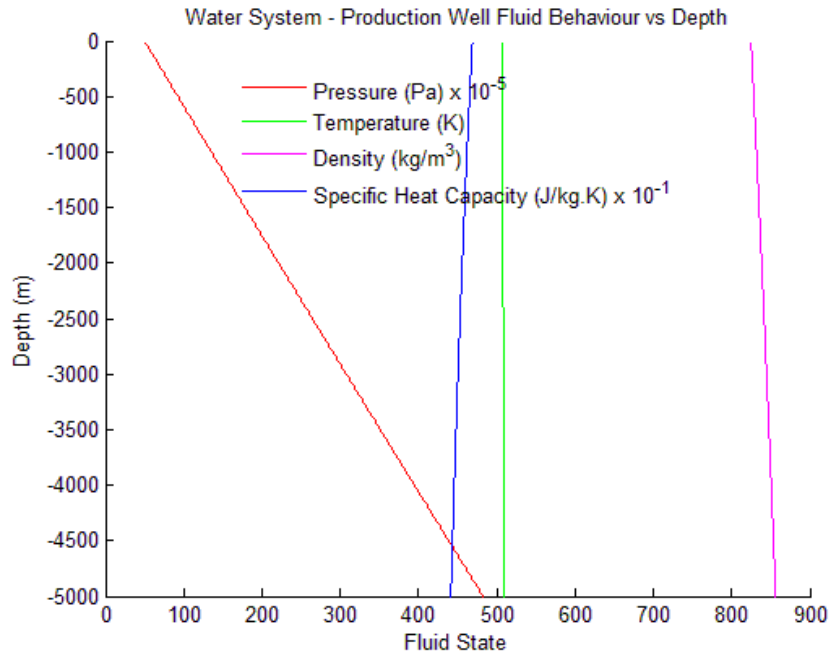


Figure 4-7 – Water system production well – typical fluid property variation

4.2 Reference Case

It was found that injection pressure has a significant effect on the performance of the SCCO₂ system. The best case for SCCO₂ thermosiphon was investigated and specified as a reference case. A reference case was then specified for the water system by finding the lowest injection pressure and corresponding mass flow rate at which the net exergy output matches the SCCO₂ system.

4.2.1 Carbon Dioxide Single Loop – Thermosiphon Limited

Two tests were run to determine an appropriate mass flow rate for the reference case. For reasons discussed in Section 3.4.1., the first test investigates the point at which energy balance is achieved such that no pumping power is required to circulate the fluid in steady state. The method used to determine this is to iteratively increase the mass flow rate for each in a series of specified injection pressures in the range of 7.5 MPa to 18 MPa. The Matlab code records the mass flow rate, exergy and thermal efficiency at energy balance. Figure 4-8 shows the mass flow rate that correlates to the balanced energy state for a series of different injection pressures.

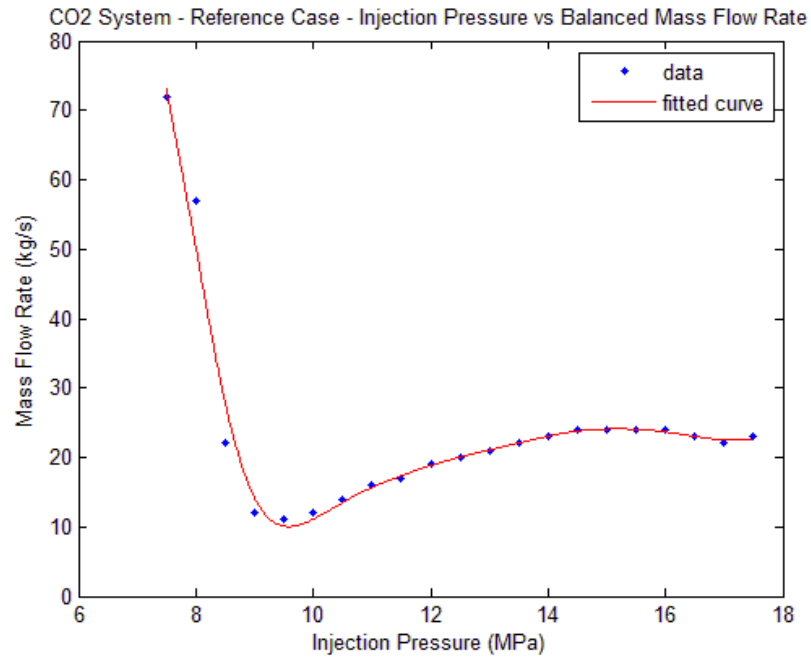


Figure 4-8 – Mass flow rate vs injection pressure - limited by energy balanced thermosiphon (no pump).

Figure 4-9 shows the exergy available between reference points 4 and 5 for the series of investigated injection pressures.

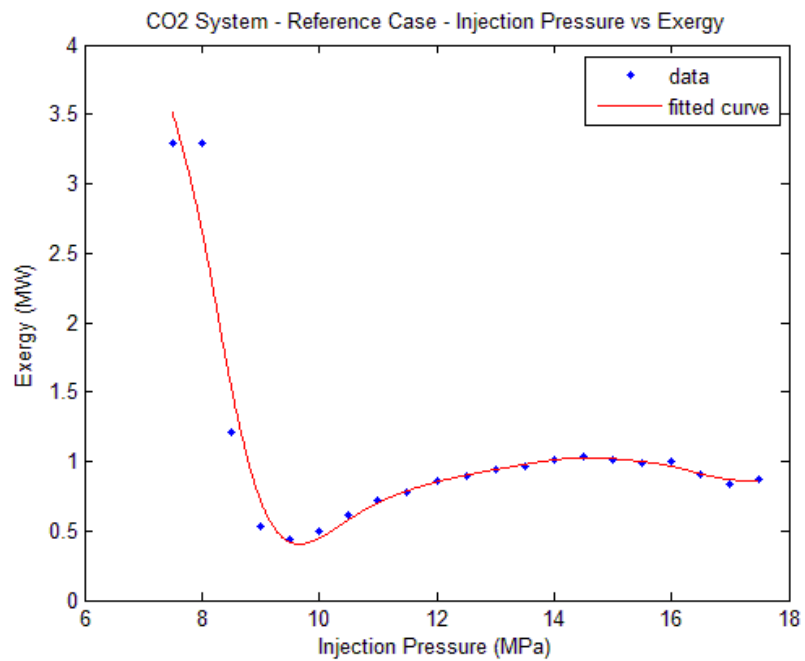


Figure 4-9 - Exergy vs injection pressure - limited by energy balanced thermosiphon (no pump).

Figure 4-10 shows the thermal efficiency of the system for the series of injection pressures.

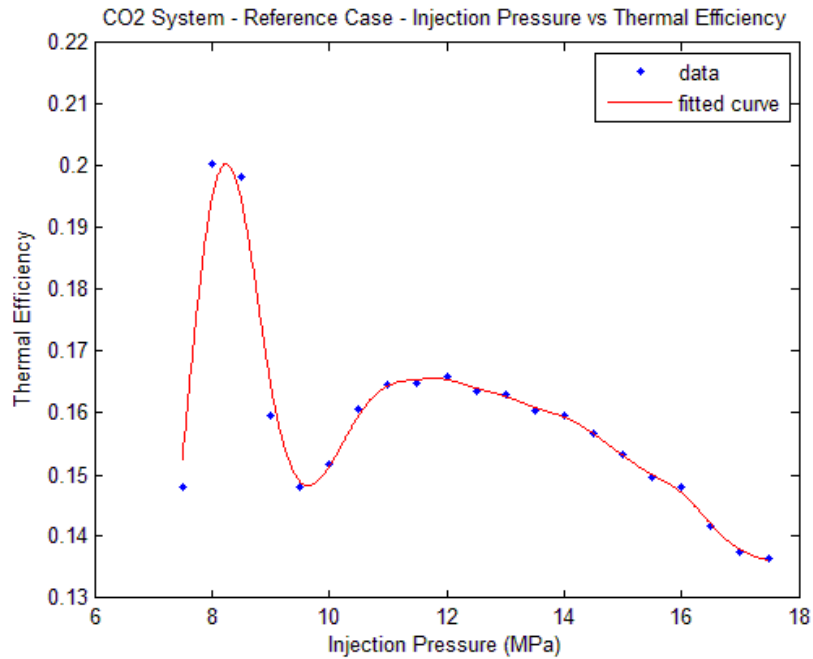


Figure 4-10 - Thermal efficiency vs injection pressure - limited by energy balanced thermosiphon (no pump).

The plots show significant deviation from linear behaviour. It is worth noting the reason behind this variation is due to dramatic fluid thermodynamic and transport property changes at the pressure and temperature seen at the surface. Recalling that the critical temperature and pressure for SCCO_2 is 304.25 K and 7.39 MPa respectively, and with an appreciation for the fluid property plots shown in Section 4.1, such a dramatic change in system potential over a small range of pressure variation is more easily understood.

It is clear from these plots that the injection pressure has a significant effect on the system’s useful output. There is a narrow band of high output, producing about 3 MW, before the theorised system output drops by a factor of 6 and then stabilises at an output of about 1 MW for higher injection pressure (approximately 14 MPa). It is expected that this discontinuity can be used to advantage however the narrow band of optimal behaviour introduces significant risk on a real systems performance compared to design expectations. Small variations at any part of the circuit which change the thermosiphon mass flow rate or surface pressure may see the system drop out of this “sweet spot” and suffer dramatic performance loss. Most significantly, if the balanced mass flow rate of the thermosiphon drops out of the narrow band, the ability of the thermosiphon to self-generate back to equilibrium in the higher performing zone deserves further investigation.

4.2.2 Carbon Dioxide Single Loop – Friction Limited

The case was investigated where mass flow rate is limited by the requirement for the production well head pressure to exceed the injection well head pressure such that there is a pressure difference that can be exploited by expansion through the turbine.

The mathematical approach to this test was to iteratively increase the mass flow rate for a range of injection pressures (7.5 MPa to 25 MPa) and record the mass flow rate at which frictional losses and impedance cause the exit pressure to approach the inlet pressure (for this study, within 1 MPa). This is the point at which no useful energy can be extracted by a turbine without the fluid needing to be compressed for reinjection. Figure 4-11 shows the results of this case. Note this reference case assumes a pumped flow but only such that system fluid flow potential can be investigated outside the limits of the thermosiphon flow rate.

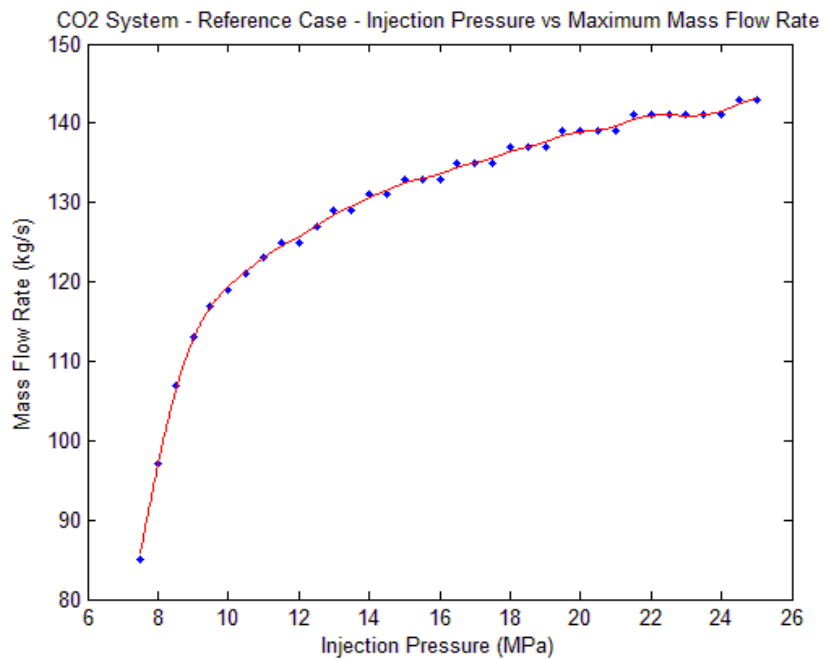


Figure 4-11 – Maximum mass flow rate vs injection pressure - limited by system impedance (pumped flow - production well minimum pressure constraint).

Figure 4-12 shows the thermal efficiency related to mass flow rate for the tested isobars.

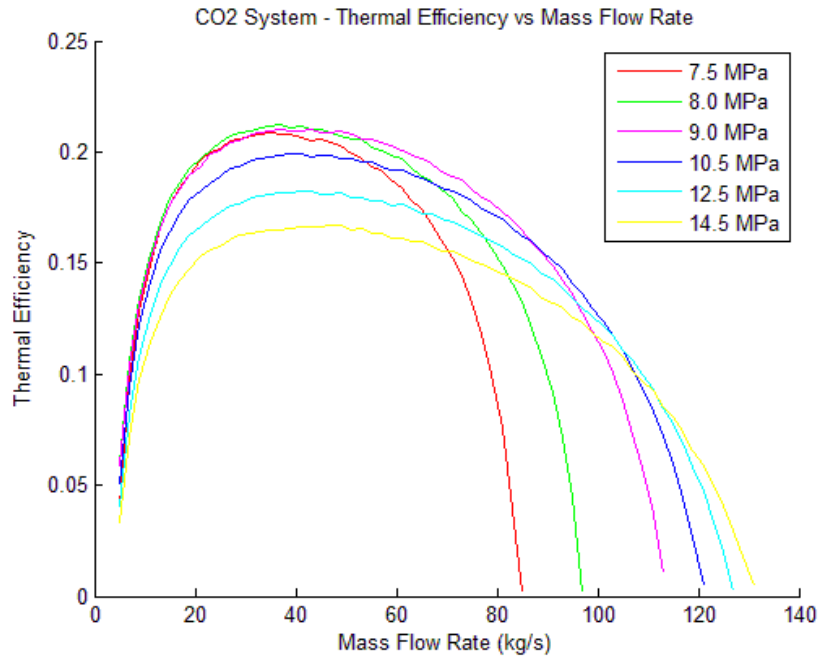


Figure 4-12 - Thermal efficiency vs mass flow rate limited by system impedance (pumped flow - production well minimum pressure constraint).

Figure 4-13 shows the exergy available between reference points 4 and 5, related to mass flow rate for the tested isobars.

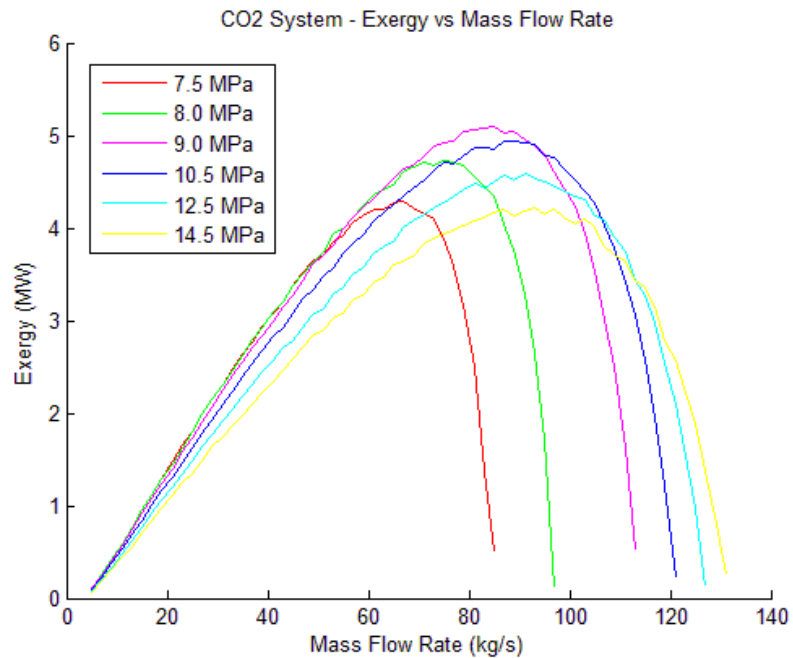


Figure 4-13 - Exergy vs mass flow rate limited by system impedance (pumped flow - production well minimum pressure constraint).

A sharp decline in performance is observed as the power lost from frictional effects overtakes the useful output. Also of note is that the exergy shows a peak at 9 MPa injection pressure with a mass flow rate of approximately 90 kg/s. This does not correlate to peak thermal efficiency.

Note that the results for the pumped flow case for SCCO₂ are not investigated further in this study, recalling the purpose of inclusion was to test the system behaviour past the point of thermosiphon flow rate as a reference point only.

4.2.3 Water Based Binary – Friction Limited

The initial test conducted on the water based binary system shares the same method and objective as the previous section. In this case, the practical limit is where friction and impedance cause a pressure drop in the circuit such that the fluid at the production well exit approaches the point of flashing. Figure 4-14, Figure 4-15 and Figure 4-16 show the results for this case.

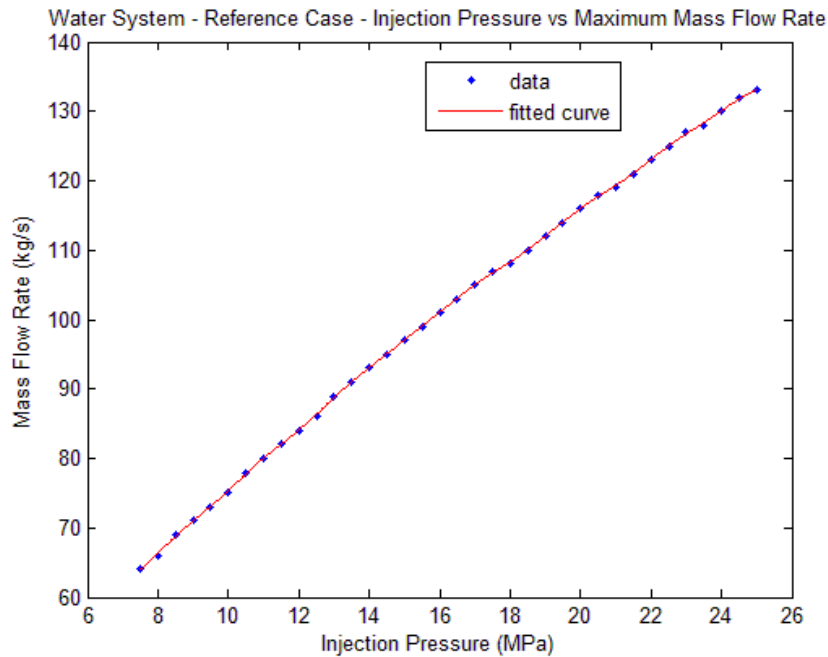


Figure 4-14 – Maximum mass flow rate vs injection pressure - limited by system impedance (pumped flow - production well minimum pressure constraint).

In comparison to the SCCO₂ pumped flow case, a far more linear behaviour is observed when comparing injection pressure to peak mass flow rate. Review of Figure 4-15 shows that outside a small range of low mass flow rate, the efficiency of the system is very much a function of surface energy conversion. The efficiency curve plateaus and converges to the fixed value assumed in Section 3.4.1.b. This observation is repeated throughout this study and lead to the recommendation that the method of determining overall system efficiency be refined in future work.

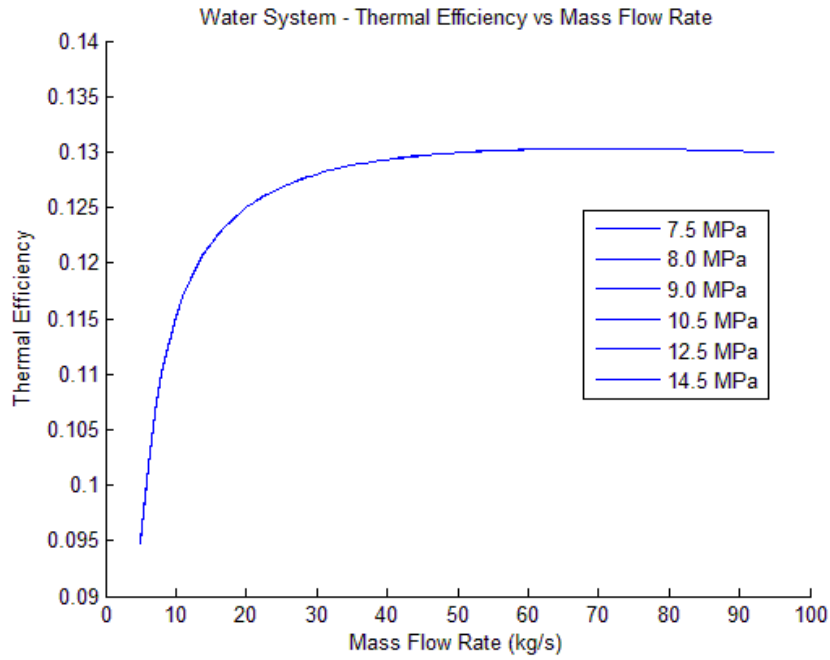


Figure 4-15 - Thermal efficiency vs mass flow rate limited by system impedance (pumped flow - production well minimum pressure constraint).

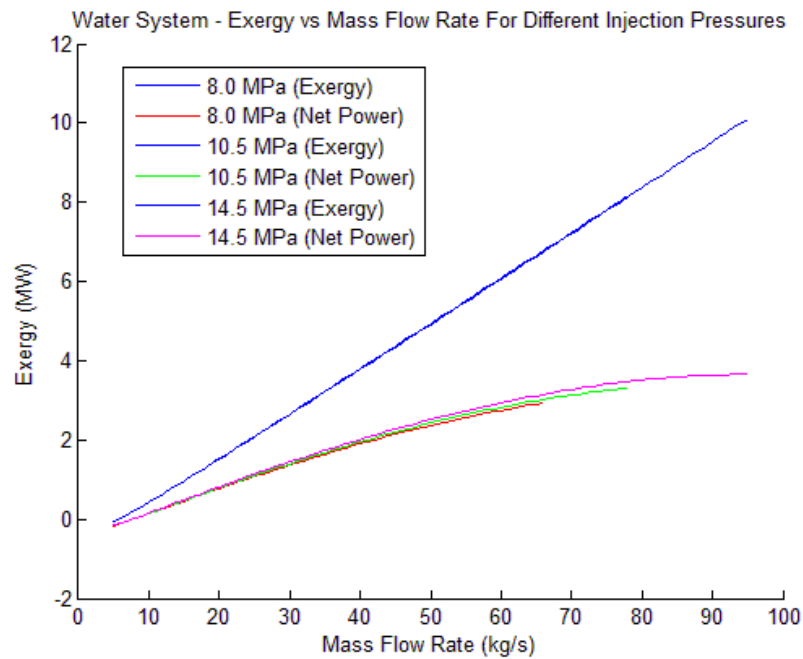


Figure 4-16 - Exergy vs mass flow rate limited by system impedance (pumped flow - production well minimum pressure constraint).

Review of Figure 4-16 shows the effect of pumping power requirements compared to mass flow. The plotted lines for exergy (ψ) show the fluid potential only as a function of the enthalpy and entropy measurements at reference points 4 and 5 and are shown to be linear. The plotted lines for net exergy (ψ_{net}) show the useful

power available once the parasitic pumping requirements are accounted for and demonstrate the increased pumping requirements as mass flow increases.

The important feature of this plot is that within the limits of the production well minimum pressure boundary condition, the net exergy does reach a maximum before the peak mass flow rate is achieved; i.e. the pumping power requirements do not reach the point where they rapidly increase with fluid velocity. Practically for this study this means selection of the reference case injection pressure can be done by choosing the injection pressure and corresponding peak mass flow that matches the SCCO₂ system for comparison.

4.2.4 Carbon Dioxide Reference Case Final

Based on the results from preceding sections, the reference case for SCCO₂ was selected such that it operates in the region of highest efficiency that occurs at an injection pressure of close to 8 MPa. The previous results indicate a reasonably narrow range of injection pressure that achieves significant increase in the exergy available for conversion to useful work. The key data relating to the SCCO₂ reference case is shown in Table 4-1 below:

Table 4-1 - Reference Case Data – SCCO₂

Reference Point Fluid State

	Pressure (MPa)	Temperature (K)
Ref Point 1 (input)	8	315
Ref Point 2	44.12	325
Ref Point 3	41.73	510
Ref Point 4	21.64	494
Ref Point 5	p5 = p1 = 8	395

Performance Measures

Mass Flow Rate (\dot{m})	57	kg/s
Thermal Efficiency (η)	0.2	
Net Exergy (adjusted with efficiency factors) (ψ)	3.29	MW

4.2.5 Water Based Binary – Reference Case Final

Based on the exergy values achieved for the SCCO₂ system of 3.29 MW, a test case was run to determine the mass flow rate that was required to achieve the same result.

This mass flow rate and associated parameters were regarded as the final reference case for the water based system. The key data is presented in Table 4-2:

Table 4-2 - Reference Case Data – Binary Water System

Reference Point Fluid State

	Pressure (MPa)	Temperature (K)
Ref Point 1 (input)	10	315
Ref Point 2	57.6	319
Ref Point 3	48.5	510
Ref Point 4	4.9	506
Ref Point 5	4.9	T5=T1=315

Performance Measures

Mass Flow Rate (\dot{m})	75	kg/s
Thermal Efficiency (η)	0.13	
Net Exergy (adjusted with efficiency factors) (ψ)	3.23	MW

The plot of mass flow rate compared to net exergy for the water system is presented in Figure 4-17 - Exergy vs mass flow rate for the reference case injection pressure of 10 MPa showing that peak power corresponds with peak mass flow under the conditions set for the study.

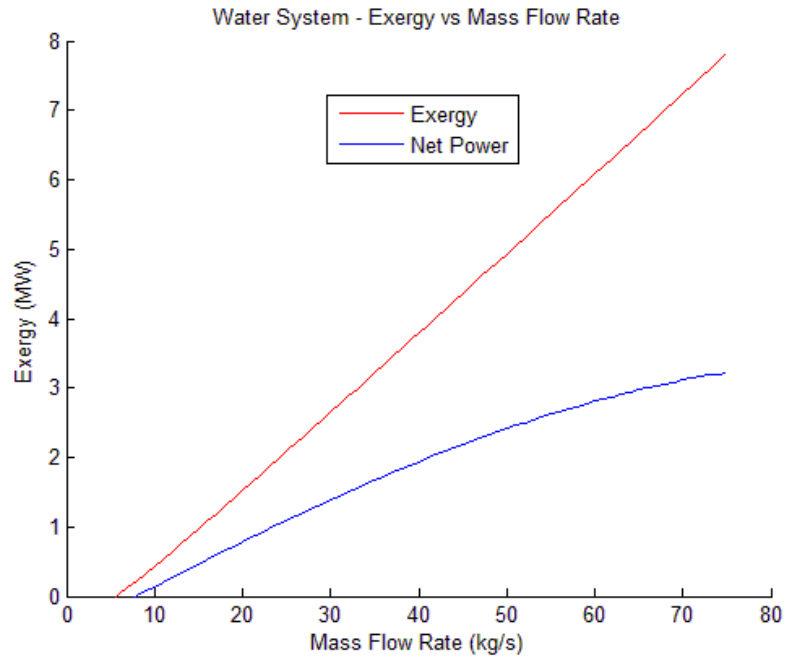


Figure 4-17 - Exergy vs mass flow rate for the reference case injection pressure of 10 MPa

4.3 Effect of Wellbore Diameter Variation

The results for the test case of well bore variation are presented in Figure 4-18, Figure 4-19 and Figure 4-20. The case for well bore diameters between 0.2 metres and 0.4 metres was tested at increments of 0.05 metres. Significantly different trends are apparent between the two fluids.

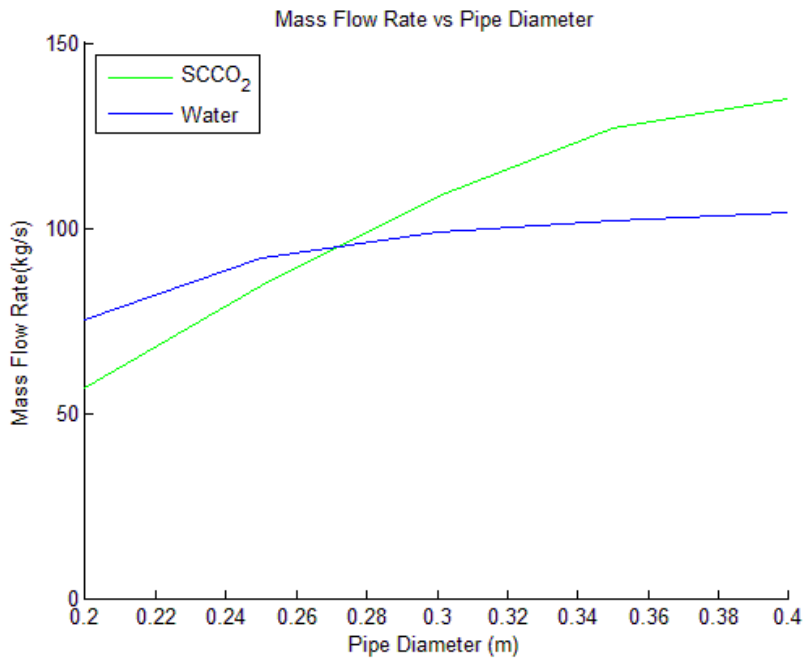


Figure 4-18 – Mass flow rate vs pipe diameter for water and SCCO₂ systems

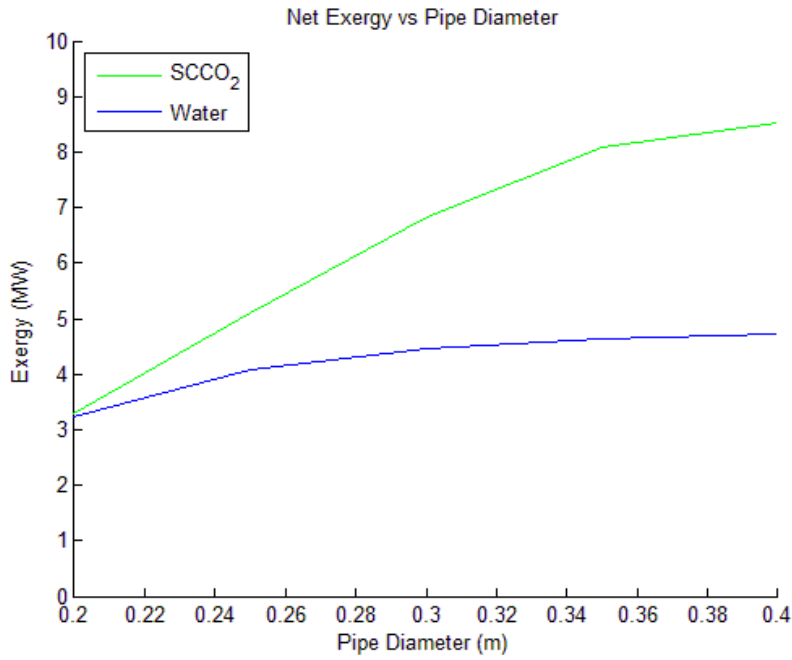


Figure 4-19 – Net exergy vs pipe diameter for water and SCCO₂ systems

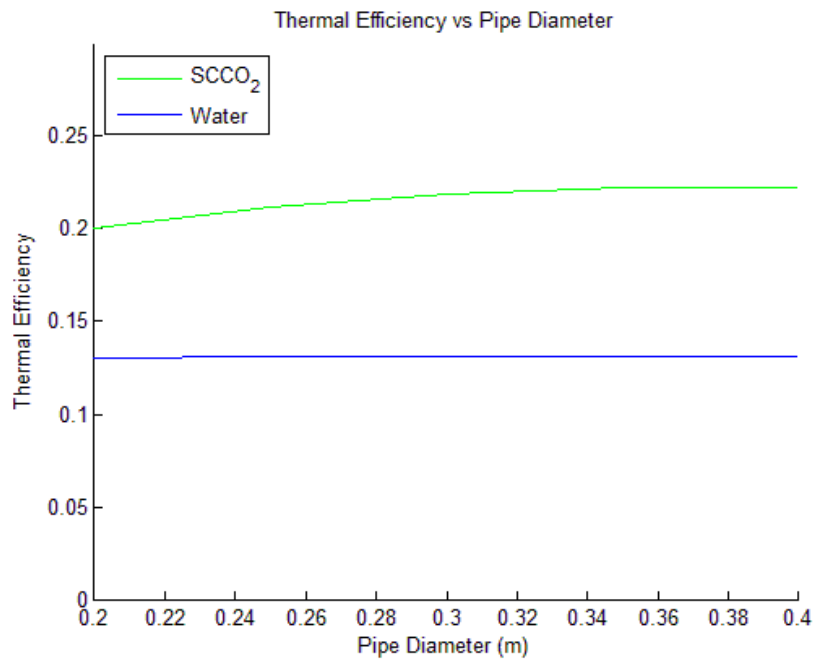


Figure 4-20 – Thermal efficiency vs pipe diameter for water and SCCO₂ systems

The SCCO₂ shows a marked improvement in thermosiphon flow rate and net exergy with diameter increase. The thermal efficiency shows a small improvement but the gain is clearly due to the increased ability to generate higher mass flow rate in the thermosiphon. The dramatic improvement gives strong weight to the theory that friction in the production well bore is a dominant factor in an SCCO₂ system. Data extracted from the mathematic model shows the power lost from friction for each

of the test cases and is presented in Figure 4-21. An increase in friction/ impedance through the reservoir is noted due to the increased mass flow rate. A decrease in the frictional power loss is seen in both injection well and production well. Overriding the specific loss or gains in each section, it is clear that the magnitude of loss due to friction becomes less significant compared to the exergy generated by the system.

The water system also shows improvement but the rate of improvement tends to decline. This suggests the well bore diameter is not the primary constraining parameter in this case. As discussed previously, the thermal efficiency converges towards the assumed surface plant factors applied.

A point worth considering is that this study assumes a constant diameter well bore where this is not usually the case. As shown in Section 1.2.3, a well bore is commonly made up of a series of reducing pipe diameters. This leads the author to believe that the constant diameter assumption may not be reasonable and unfairly penalise the case for SCCO₂ as a geothermal fluid.

The final and possibly most relevant point is that while it is academically easy to increase the well bore diameter, the cost of drilling can be up to 80% of the total system development investment. Any assertions about the gains from well bore diameter increase would need to be tested in a business case.

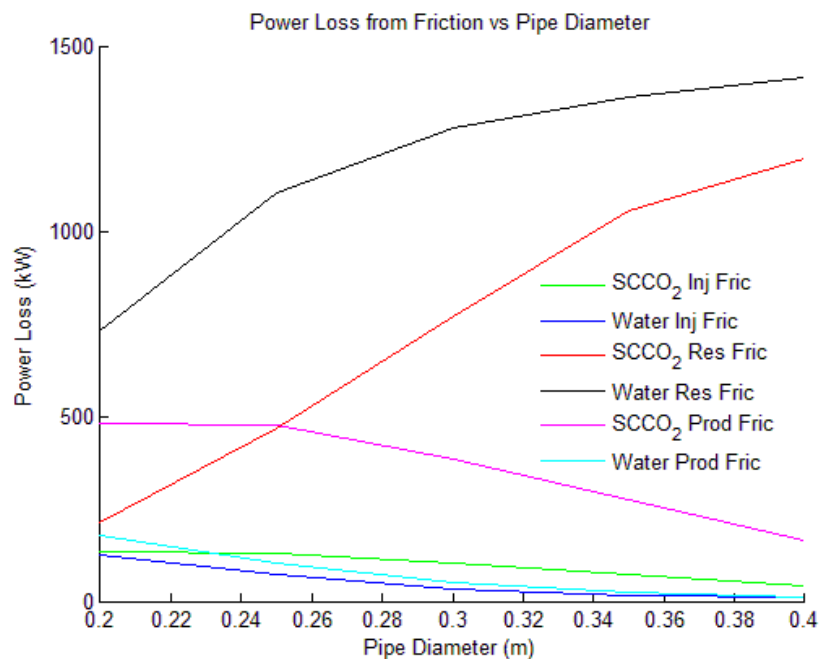


Figure 4-21 – Power loss from friction vs pipe diameter for water and SCCO₂ systems

4.4 Effect of Reservoir Depth Variation

The effect of reservoir depth variation was tested in a range from 3000 metres depth to 5000 metres depth at increments of 250 metres. The calculated performance criteria are given in Figure 4-22, Figure 4-23 and Figure 4-24.

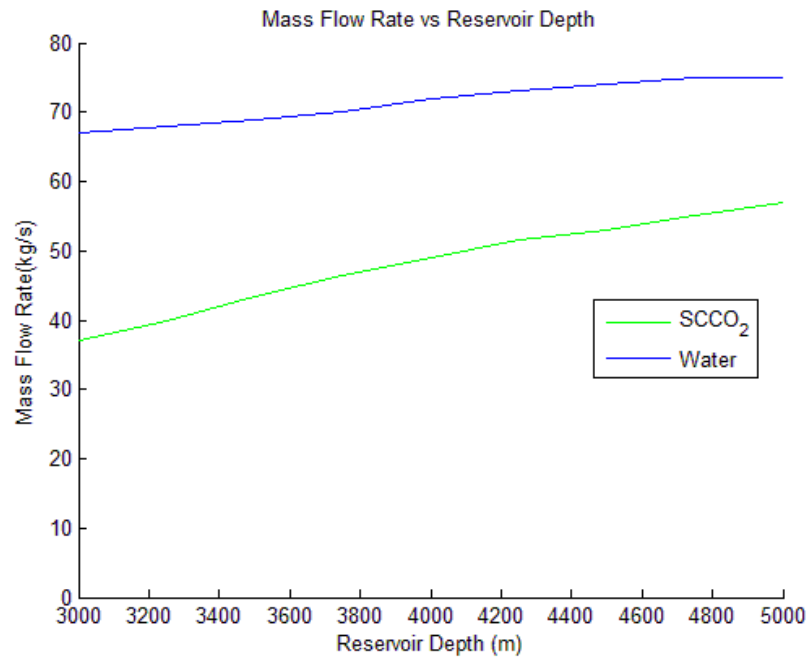


Figure 4-22 – Mass flow rate vs reservoir depth for water and SCCO₂ systems

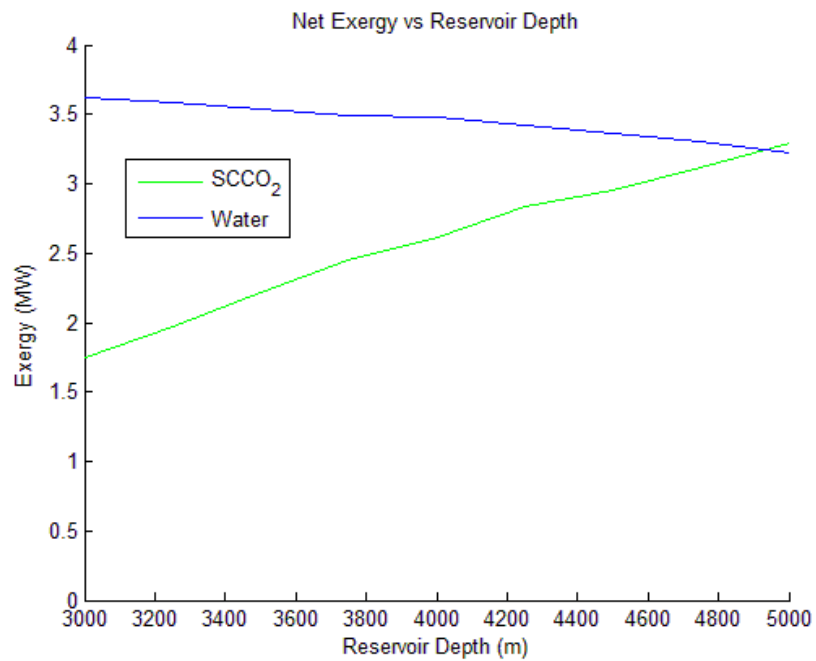


Figure 4-23 – Net exergy vs reservoir depth for water and SCCO₂ systems

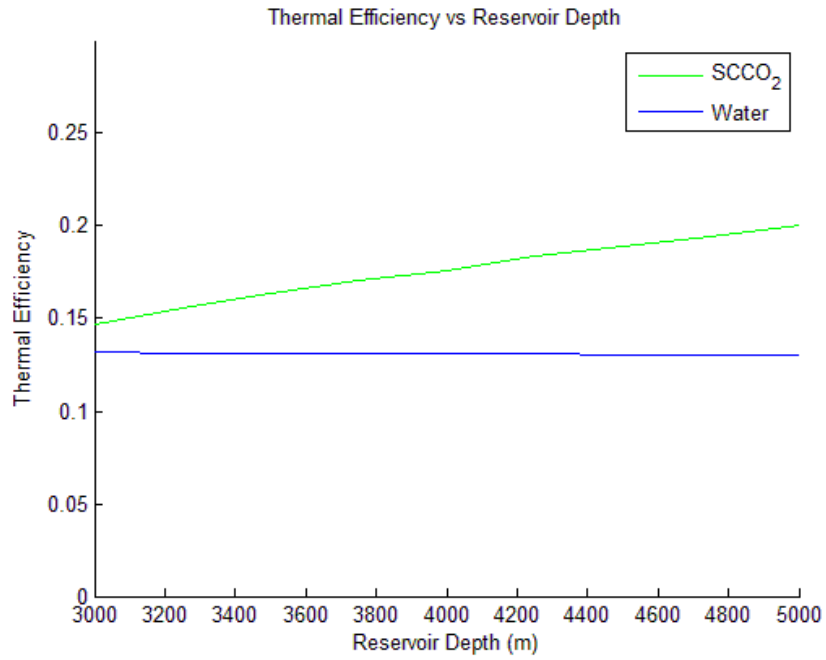


Figure 4-24 – Thermal efficiency vs reservoir depth for water and SCCO₂ systems

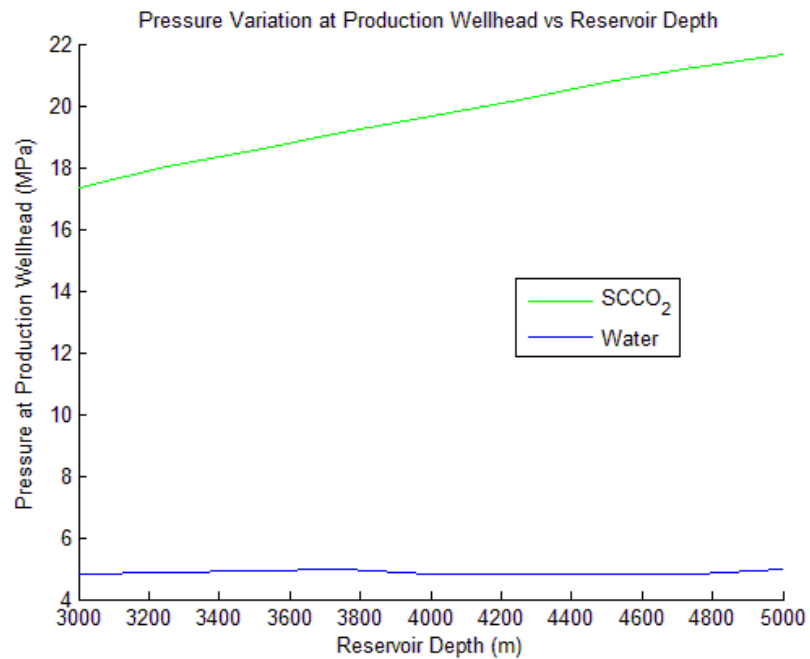


Figure 4-25 – Pressure at production well head vs reservoir depth for water and SCCO₂ systems

The results show trends that are not immediately intuitive. It was theorised that the SCCO₂ system in particular would show improvement in performance with a shorter well bore leading to reduced frictional losses. The water system behaves as expected however a significant reduction in exergy is shown in the SCCO₂ system.

Investigation of the results data showed a corresponding trend downwards in the production wellhead exit pressure as shown in Figure 4-25. As has been discussed,

this has a direct effect on power that can be extracted from the turbine. The effects on varying injection pressure were investigated for the reference case and it was found that at an injection pressure of 8 MPa, there is a narrow band of efficient operation, either side of which, a dramatic reduction in output is seen. In the case of a reduced depth for the well bore, it has been shown that the system needs to be optimised in a multi-dimensional approach. Linear change to a single parameter can have unintended results if it changes the ultimate fluid state in another region. Considering this study has no agenda to optimise for any particular case, the optimisation of a specific lower depth case has been left as an option for future work.

4.5 Effect of Reservoir Permeability Variation

The effect of reservoir permeability on the two fluid systems has been tested over the range of $kA = 0.5 \times 10^{-9} \text{ m}^4$ through to $8.5 \times 10^{-9} \text{ m}^4$ at intervals of $1 \times 10^{-9} \text{ m}^4$. This covers a range of variation from four times less to four times more permeability than the reference case. The simulation results are shown in Figure 4-26, Figure 4-27 and Figure 4-28.

The shape of the mass flow rate curves are the most descriptive of the fluid behaviour difference. The curve for SCCO_2 shows a distinct region of change (at about $1.5 \times 10^{-9} \text{ m}^4$ where the reservoir permeability becomes the dominant factor in the mass flow rate. If the permeability is above $1.5 \times 10^{-9} \text{ m}^4$, there is little improvement to system performance showing other factors govern the SCCO_2 fluid flow.

In the case of water, the curve shows continued improvement in mass flow as the impedance to flow is reduced. The higher specific heat capacity of water helps it to outperform the SCCO_2 as flow increases. The thermal efficiency of the systems is not dramatically affected by permeability.

In low permeability reservoirs, SCCO_2 is shown to outperform water up to a value of approximately $kA = 2 \times 10^{-9} \text{ m}^4$. In the case of an EGS, the permeability can be controlled or at least targeted during reservoir stimulation.

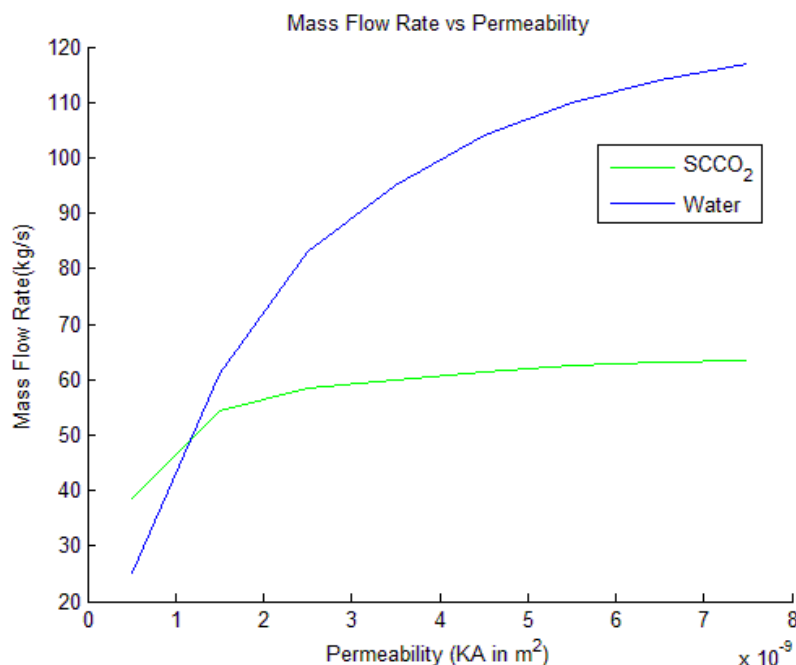


Figure 4-26 – Mass flow rate vs reservoir permeability for water and SCCO_2 systems

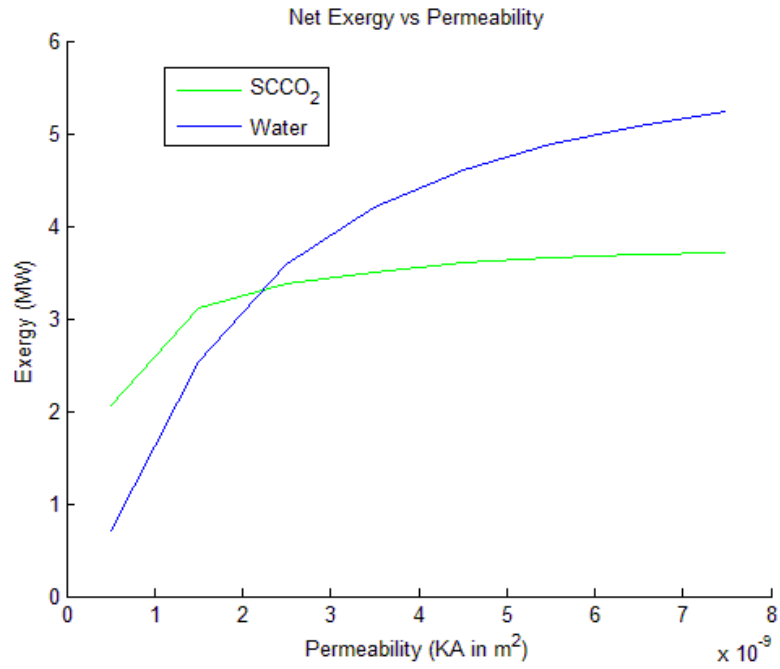


Figure 4-27 – Net exergy vs reservoir permeability for water and SCCO₂ systems

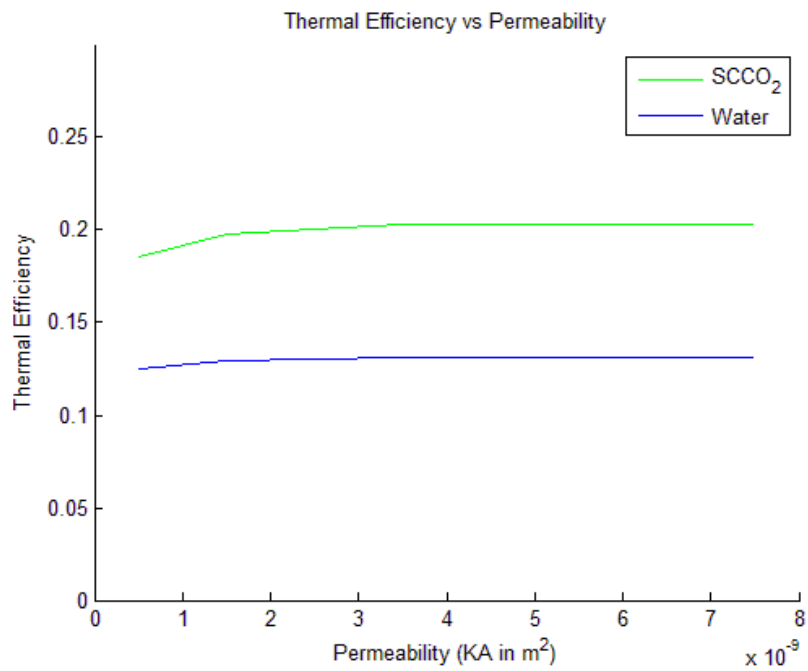


Figure 4-28 – Thermal efficiency vs reservoir permeability for water and SCCO₂ systems

4.6 Effect of Reservoir Temperature Variation

The case of reservoir temperature variation was investigated in the range of 460K to 510K at intervals of 10K. The results are presented in Figure 4-29, Figure 4-30 and Figure 4-31.

Reduced reservoir temperature is shown to increase the mass flow rate for SCCO₂. Review of the test case data showed no direct correlation to a specific factor that would explain the increase other than more favourable fluid properties allowing the energy balance to occur at higher mass flow rate.

The reduced reservoir temperature reduces the mass flow rate of the water circuit due to the increase in density causing higher pressure drop.

The thermal efficiency of the systems shows negligible change. The net effect is that the reduction in net exergy for the SCCO₂ system is less than the reduction for water. This leads to an indication that SCCO₂ can offer an advantage in lower temperature reservoir.

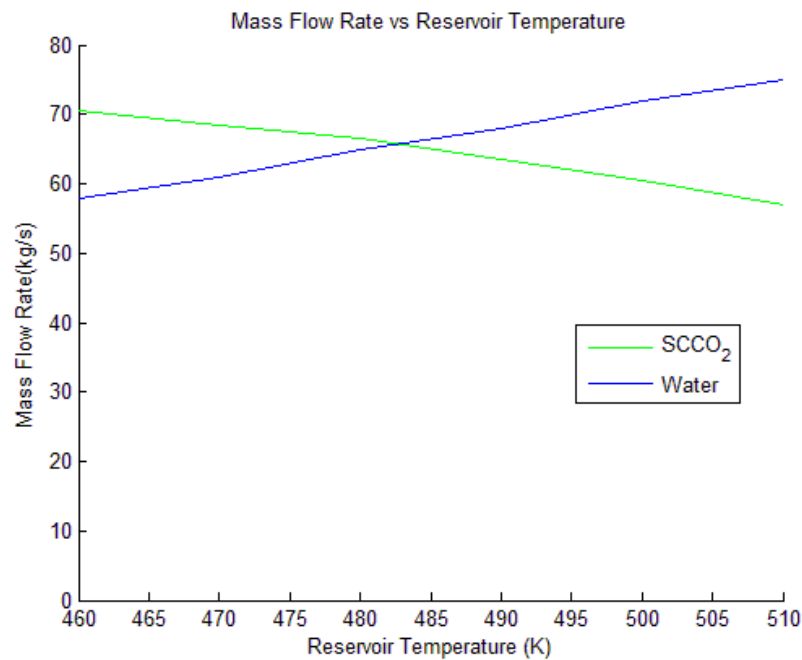


Figure 4-29 – Mass flow rate vs reservoir temperature for water and SCCO₂ systems

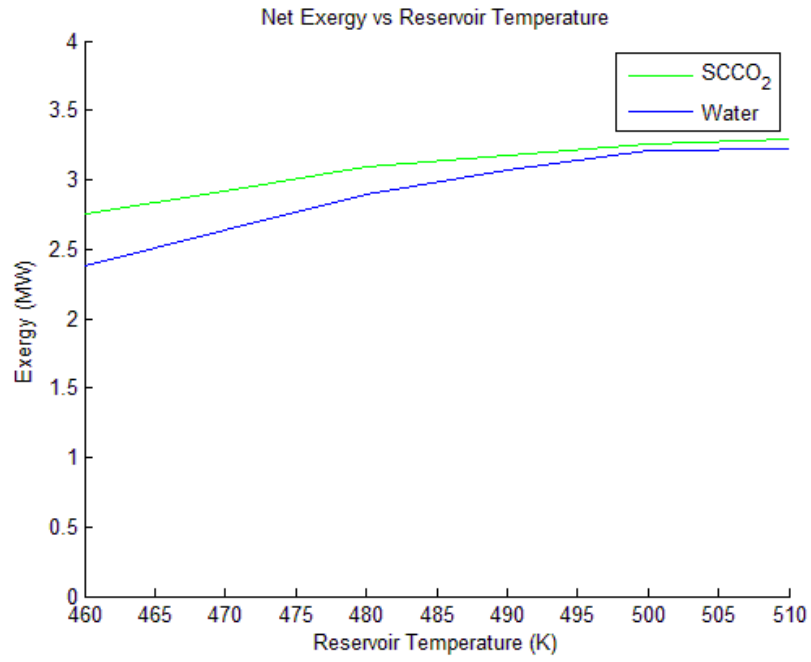


Figure 4-30 – Net exergy vs reservoir temperature for water and SCCO₂ systems

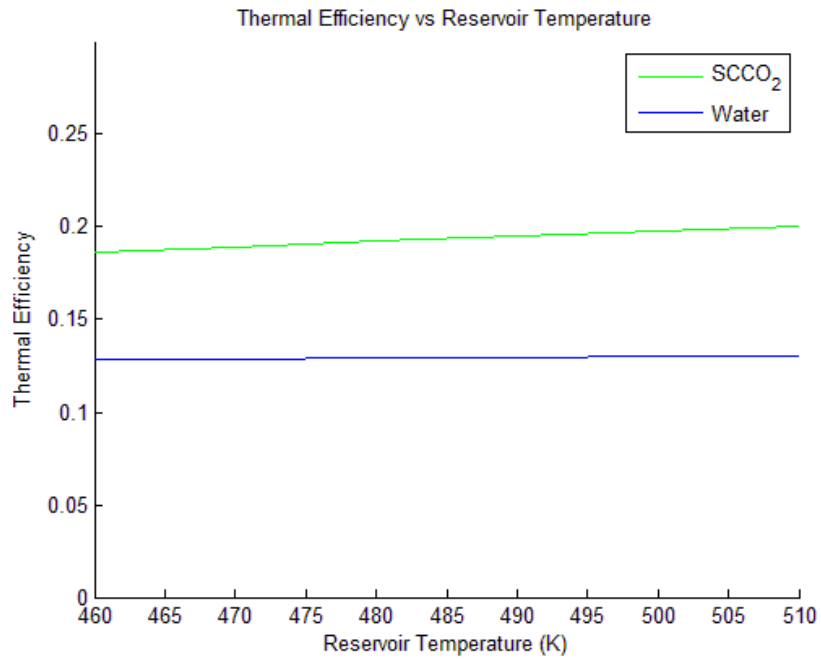


Figure 4-31 – Thermal efficiency vs reservoir temperature for water and SCCO₂ systems

5 CONCLUSIONS

5.1 Overall Findings

With reference to the objectives of the project, a mathematical model has been developed and used to test several parametric cases. The technical feasibility of using SCCO₂ as a geothermal heat mining fluid has been investigated in the context of these test cases. The CFD component of the project was not successful however this has not detracted significantly from the project outcomes.

5.1.1 Model Uncertainty

The parametric study has presented some interesting results, in some cases matching pre-conceptions and previous studies, in other cases not. It must be noted that it was found that some of the assumptions used may have affected the outcomes. Most specifically, the assumed efficiency factors may have a significant effect on the magnitude of the exergy results. A specific case study would require considerably more confidence in these factors. It was observed that the thermal efficiency of the water based system converged to, and was therefore wholly reliant on, the assumed factors in each test. The intent of this study was to investigate the trends resulting from the variation of the selected parameters; as such, the “shape” of the data will remain largely valid and a useful outcome.

Another region of uncertainty is the true effect of the of the fluid property changes on the system. The Matlab model shows significant departures from “normal” behaviour in the SCCO₂ model. The reference case found a narrow band of injection pressure for which the system is calculated to deliver peak exergy output. It was shown that changing other system variables in isolation can show unexpected trends. This would suggest the SCCO₂ system is sensitive and perhaps not as robust as the water based system. In practice, the chances of all variables matching a mathematical model are slim. It follows that the chances of the system failing to perform on the narrow curve that this study found as ideal, presents a considerable technical risk. It is the opinion of the author that these departures should be validated further.

5.1.2 Parametric Test Outcomes

Within the confines of the uncertainty in the model discussed above, the following conclusions were drawn for each test:

Significant gains can be made with larger diameter well bores in the SCCO₂ systems. The ability to make these well bores larger diameter would need to be investigated thoroughly in a cost/benefit study. In this case, doubling the diameter from 0.2 m to 0.4 m resulted in an almost 260% increase in exergy for the SCCO₂ system from 3.3 MW to 8.5 MW. The same change yielded a 146% increase the water system

from 3.2 MW to 4.7 MW. The well bore diameter had by far the largest effect on performance of any of the systems. Quantifying this gain compared to the increased cost of drilling is the next stage of investigation.

The water system outperformed the SCCO₂ system at shallower depths under the conditions of the reference case used. The water system saw an increase of exergy from 3.2 MW at 5000m depth to 3.6 MW at 3000m depth. The SCCO₂ system saw a decrease of exergy from 3.3MW at 5000m depth to 1.7 MW at 3000m depth. It is noted that the behaviour of the SCCO₂ system was the opposite of expectations and may vary if the system were optimised for each depth.

The SCCO₂ system shows measureable performance advantage in reservoirs of low permeability. For the parameters used in this study, the SCCO₂ system showed better performance for values of $kA < 2 \times 10^{-9} \text{ m}^4$. Controlled stimulation of the reservoir may mean that permeability can be targeted to suit the higher yield of a water based system.

The SCCO₂ system showed less sensitivity to lower reservoir temperature; i.e. the performance was reduced but not as dramatically as the water system. For a temperature range of 460 K to 510 K, the water system exergy dropped 25% from 3.2 MW to 2.4 MW. The SCCO₂ system exergy dropped 17% from 3.3 MW to 2.7 MW. The reduced sensitivity may help SCCO₂ to maintain better performance towards the end of a reservoir's life as its temperature degrades over time.

5.1.3 CFD Analysis Outcomes

The CFD component of this project was not successful. Despite a significant amount of time invested, the difficulty of getting useful results was beyond the capacity of the author in the timeframe available. Specifically, it was found that the combinations of factors indirectly lead to a lack of useful results:

- Underestimation of the task size completing a CFD analysis of a complex system with a supercritical fluid.
- Differences in geometry scale (0.2 m diameter pipe, 5000m long → frequent solver failure)
- Differences in velocity scale (fast in well bores, almost stationary in the reservoir → frequent solver failure and failure to converge)
- Compressible flow with heat transfer and porous regions being sensitive to boundary conditions (frequent solver failure)
- Under specified boundary conditions (needed mathematical model results as boundary conditions)

It was found that the model constructed would only run if the boundary conditions were specified by using output from the mathematical model which (in the opinion

of the author) defeats the purpose of the CFD analysis. Even then, the model could not be made to converge to a satisfactory level.

Ultimately, it was determined that the CFD analysis was intended to be a tool for the project outcomes, not the outcome itself. As such, the opinion of the author is that the objectives of the project have not been significantly diminished with the exclusion of that component and an opportunity for further work has been identified.

5.2 Further Work

The following areas have been identified as having value in further investigation.

- Validate non-linear behaviour in the SCCO₂ system. Investigate the real effect of C_p variation (at surface plant pressure and temperature) on the mass flow rate of the thermosiphon.
- Investigate and refine assumptions regarding surface plant efficiency with appropriate data and case studies. This may include expanding this model to allow phase change in the fluids and possibly investigate a pumped SCCO₂ system.
- Thermosiphon validation – validate the energy method used to determine the thermosiphon flow rate. This could take the form of a CFD investigation.
- Investigate cost/benefit of changes to the parameters that have been shown to favourable results.
- Refinement of the Matlab model to account for temperature change in SCCO₂ circuit in compressible flow (Joule Thompson effect).

APPENDIX A – PROJECT SPECIFICATION

University of Southern Queensland
FACULTY OF ENGINEERING AND SURVEYING

ENG4111 / 4112 RESEARCH PROJECT PROJECT SPECIFICATION

FOR: Patrick Taylor

TOPIC: Modelling and analysis of hot dry rock geothermal energy system using supercritical CO₂ in a single loop.

SUPERVISORS: Ruth Mossad

PROJECT AIM: Investigate the feasibility and operation of a theoretical geothermal plant which uses supercritical CO₂ (SCCO₂) as a working fluid. More specifically focussed on a single loop system where the geothermal fluid is also used as the power cycle fluid i.e. replaces the role of steam in a conventional binary power plant.

Investigate the parameters that affect its performance.

Conduct a CFD analysis to validate the impact of changing some of these parameters on efficiency and practicality of the system.

SPONSORSHIP: University of Southern Queensland

PROGRAMME: (Version 1, 16 March 2014)

1. Literature search of geothermal energy systems that use supercritical CO₂ (SCCO₂) as a working fluid, in particular:
 - a. Investigate potential advantages, drawbacks of basic concept. E.g. carbon sequestration potential etc. (Overview only)
 - b. Investigate the feasibility of the system from a more practical perspective i.e. sources of CO₂, probability and consequence of leakage and other aspects.
 - c. Investigate the parameters that affect the system operation and its performance.
 - d. Research and determine appropriate boundary conditions for a thermodynamic analysis of the system.
2. Conduct a CFD analysis of the system to:
 - a. Determine its theoretical efficiency.
 - b. Investigate the impact of changing some parameters on efficiency and practicality of the system.
3. Write the thesis.

If time permits:

4. Perform an energy/mass/pressure balance on an EGS system for the two concepts: binary and direct. Compare the efficiency to a conventional binary system.
(Binary system with SCCO₂ as the geothermal fluid and conventional steam turbine circuit)

Patrick Taylor
0019522109

Page 1 of 2

Version 1
16 March 2014

AGREED:

_____ (Student) _____ (Supervisors)
 / / / / / /
_____ _____ (Date)

APPENDIX B – REFERENCE CASE PARAMETER SOURCES

For all references to system locations, refer to Figure 2-1. Note that many other parameter values are used and referenced throughout this paper.

Table B-1 - System Parameter Values and Source Reference

Parameter	Value	Source
System output	5 MW	Assumed for initial estimates only
Turbine efficiency	0.8	Assumed
Pressure at point 1	8MPa	Reference point from Atrens, Gurgenci and Rudolph (2009). Selected as lowest system pressure and temperature point and set to be above critical pressure.
Temperature at point 1	315K	Reference point from Atrens, Gurgenci and Rudolph (2009). Selected as lowest system pressure and temperature point and set to be above critical temperature.
Well Depth	5000m	Assumed but typical of hot dry rock resource location.
Wellbore diameter	0.2m	Assumed but in range of typical well bore (Finger & Blankenship 2010)
Surface Roughness (e)	0.0004	Concrete (moody chart)
Gravity (g)	9.81 m/s ²	
Reservoir impedance (k.A)	2.2e-9 m ⁴	Reference point from Atrens, Gurgenci and Rudolph (2009). Noted that this value was “tuned” specifically to achieve pressure drop results close to tested values.
Reservoir length	1000m	Assumed
Reservoir temperature	510K	Assumed but close to similar studies typical HDR reservoir.

Reservoir effective cross-sectional area	10000m ²	Assumed for CFX model geometry
Fracture width in granite	0.02m	Assumed for Reynolds number approximation in reservoir.
Fluid state values other than calculated from Peng and Robinson (1976)	Multiple	Span and Wagner (1996) provide tabulated fluid properties from a large range of SCCO ₂ isotherms that cover the range of temperature and pressure. Where these values could not be practically calculated from the temperature and pressure condition, these tables were the primary reference.

APPENDIX C – MATLAB SCRIPT

Geothermal_Main

```
%% Geothermal_Main.m
% Main controlling script
% Author - Patrick Taylor, USQ, Student 0019522109 Oct 2014
% This script is intended to control the test cases
%
clear, clc, close all hidden

%% Known or assumed variables
eta=0.8; % Turbine efficiency for CO2 system(assumed)
eta2=0.136; % Secondary binary circuit efficiency for water
circuit (DiPippo 2008)
eta3=0.9; % Water pump efficiency (DiPippo 2008)

%% Wellbore
WellDep=5000; % metres - well depth
dz=10; % metres - differential element size
d_pipe=0.2; % metres - pipe diameter
e=0.0004; % meters - wellbore roughness
g=-9.81; % m/s^2 - gravity
qwall=2500; % = 250 W/m x 10m

%% Reservoir
KA=2.1e-9; % m^4 (Atrens et al)
WellLen=1000; % metres - well length
dL=10; % m - differential element size
Tres=510; % K - reservoir temperature
Ar=100*100; % m^2 reservoir cross sectional area ** CHECK
CrackWid=0.02; % Assumed crack width *** CHECK

%% Variables for iterative runs
% Manually set "for" loops to iterate through test cases as required
j=1;

for WellDep=3000:250:5000; % metres - well depth
%for Tres=460:10:510; % K - reservoir temperature
%for KA=1e-8:1e-9:8e-9; % m^4 (Atrens et al)
%for d_pipe=0.2:0.05:0.4
%for Pl=[8000000 10500000 14500000] % Used in reference case
investigation only

%% CO2 Section
% Point 1 - Injection State Properties
% Initial Pressure for single runs CO2
Pl=8000000; % Pa - pressure at point 1 *** Set this line to
comment during pressure iteration ***
T1=315; % K - temp at point 1
Ap=(pi*d_pipe^2)/4;

% Mass flow rate initial values
mdotCO2=5; % kg/s
dm=0.5 ; % change in mdot per loop. Set to lower value for
increased resolution.

% First iteration
```

```

    Geothermal_CO2
    i=1;

% Results matrix
% PowerResultCO2 records data for each iteration for inspection /
plotting etc

PowerResultCO2(i,1:12)=[mdotCO2,EBal,P1,T1,P2,T2,P3,T3,P4,T4,P5,T5];
    PowerResultCO2(i,13:23)=[-PoutTurb,InjHeat,-InjFric,ResHeat,-
ResFric,-ProdHeat,-ProdFric,-PoutCool,0,ThermEffCO2,XCO2];
    PowerResultCO2(i,25)=XCO2;% Net useful power after pumping power
is removed
    PowerResultCO2(i,24)=WellDep;% Insert tested parameter here for
plotting

% Loop to iterate through range of mass flow rates.
% desired condition for loop exit - either energy balace for
thermosiphon
% or as P4 approaches P5 for functional pumped system limit.

while PowerResultCO2(i,2)>=0    % Set to this condition for energy
balance
%while P4-P5>500000    % Set to this condition to investigate pumped
flow to the
                        % limit of well bore outlet pressure >=
injection pressure
    mdotCO2=mdotCO2+dm;
    Geothermal_CO2

    i=i+1;

PowerResultCO2(i,1:12)=[mdotCO2,EBal,P1,T1,P2,T2,P3,T3,P4,T4,P5,T5];
    PowerResultCO2(i,13:23)=[-PoutTurb,InjHeat,-InjFric,ResHeat,-
ResFric,-ProdHeat,-ProdFric,-PoutCool,0,ThermEffCO2,XCO2];
    PowerResultCO2(i,25)=XCO2;% Net useful power after pumping power
is removed (no pump power for thermosiphon)
    PowerResultCO2(i,24)=WellDep; % Insert tested parameter here for
plotting
end

% Final records the case data at the exit point
Final(j,:,1)=PowerResultCO2(i,:);

%% Water Section
% Point 1 - Injection State Properties
% Initial Pressure for single runs
    P1=10000000; % Pa - pressure at point 1
    T1=315; % K - temp at point 1
    Ap=(pi*d_pipe^2)/4;

% Mass flow rate initial values
    mdotWater=5; % kg/s
    dm=1 ;
    i=1;

% First iteration
    Geothermal_Water

```

```

% Results matrix setup
% PowerResultWater records data for each iteration for inspection /
plotting etc

PowerResultWater(i,1:12)=[mdotWater,EBal,P1,T1,P2,T2,P3,T3,P4,T4,P5,
T5];
    PowerResultWater(i,13:23)=[-PoutTurb,InjHeat,-InjFric,ResHeat,-
ResFric,-ProdHeat,-ProdFric,0,PinPump,ThermEffWater,XWater];
    PowerResultWater(i,25)=XWater-PinPump; % Net useful power after
pumping power is removed
    PowerResultWater(i,24)=WellDep;% Insert tested parameter here
for plotting

% Loop to iterate through range of mass flow rates. Loop stops when
P4
% approaches 5MPa (close to steam flashing point at 510 K)
while P4>=5000000
%while XWater<=XCO2
    mdotWater=mdotWater+dm;

    Geothermal_Water

    i=i+1;

PowerResultWater(i,1:12)=[mdotWater,EBal,P1,T1,P2,T2,P3,T3,P4,T4,P5,
T5];
    PowerResultWater(i,13:23)=[-PoutTurb,InjHeat,-InjFric,ResHeat,-
ResFric,-ProdHeat,-ProdFric,0,PinPump,ThermEffWater,XWater];
    PowerResultWater(i,25)=XWater-PinPump; % Net useful power after
pumping power is removed
    PowerResultWater(i,24)=WellDep;% Insert tested parameter here
for plotting

end

% Final records the case data at the exit point
Final(j,:,2)=PowerResultWater(i,:);

%% Index for next iteration
    j=j+1;

end %

Plot % Call separate plot file as required

```

Geothermal_CO2.m

```
% Geothermal_CO2.m - Program to calculate fluid properties at
differential
% points around the geothermal circuit
% Author - Patrick Taylor, USQ, Student 0019522109

%% Material initial property functions
    T=T1;
    P=P1;
    [density,h,s,cp,cv,mu,kf,Z] = CO2_Prop(T,P);

%% Injection Well Section
% Results matrix set-up
    m=(WellDep/dz)+1; % number of reference points in the vertical z
direction
    n=13;% Column count for property results matrix
    inj=zeros(m,n); % Create empty results matrix for the injection
well.

% Initial conditions
    inj(1,1)=0; % meters - height dz = 0 at ground level
    inj(1,2)=P1; % Pa - pressure at inject point
    inj(1,3)=T1; % K - temp at inject point
    inj(1,4)=density; % kg/m^3 - density at injection point -
calculated
    inj(1,5)=cv; % kJ/kg K - Specific heat constant volume - cv
    inj(1,6)=cp; % J/kg K - Specific heat constant pressure - cp
    inj(1,7)=s; % J/K - Entropy - s
    inj(1,8)=h; % J/kg - Enthalpy - h
    inj(1,9)=mdotCO2/inj(1,4)/Ap; % m/s^2 - Velocity - V
    inj(1,10)=mu; % MPa.s - Dynamic Viscosity
    inj(1,11)=inj(1,4)*inj(1,9)*d_pipe/inj(1,10); % Re - Reynolds
Number
    inj(1,12)=inj(1,6)*inj(1,10)/kf; % Pr - Prandlt Number
    inj(1,13)=kf; % Thermal conductivity

% Iterative Loop - Injection well
    % Create zero value variable for cumulative values in loop.
    InjHeat=0;
    InjFric=0;

for a = 1:m-1
    % Depth value for reference
        inj(a+1,1)=inj(a,1)+dz;

    % Pressure increase from gravity and decrease from friction
        % Friction
        D=d_pipe;
        Re=inj(a,11);
        f=(-1.8*log10((e/D/3.7)^1.11+(6.9/Re)))^-2;
        dPf=(f*dz/D*0.5*inj(a,4)*inj(a,9)^2);

        % Gravity
        dPg=(inj(a,4)*g*dz);

        % Velocity
        % Note - purpose of loop is to remove error at first
iteration
```

```

total      % where there is no (a-1) value to be read. Minor error over
           % length is regarded acceptable.
           if a>=2
               dPv=1/2*inj(a,4)*((inj(a,9)^2)-(inj(a-1,9)^2));
           else
               dPv=0;
           end

           inj(a+1,2)=inj(a,2)-dPg-dPf-dPv;

%Temp gradient in well bore

           % Pipe wall temp increases linearly with depth
           Tpipe=T1+((Tres-T1)*dz/WellDep*a);

           % Heat transfer
           % Fluid based (not used)
           %Awall=pi*d_pipe*dz;
           %hc=0.027*(inj(a,11)^0.8)*(inj(a,12)^0.4)*inj(a,13)/D;
           %qwall=hc*Awall*(Tpipe-inj(a,3));

           % Rock based estimate
           inj(a+1,3)=inj(a,3)+(qwall/mdotCO2/cp);

% Density calculation with temp and pressure
           P=inj(a+1,2);
           T=inj(a+1,3);
           [density,h,s,cp,cv,mu,kf,Z] = CO2_Prop(T,P);
           inj(a+1,4)=density;% kg/m^3

% Specific heat constant volume
           inj(a+1,5)=cv;% J/kg K

% Specific heat constant pressure
           inj(a+1,6)=cp;% J/kg K

% Entropy
           inj(a+1,7)=s;% J/kg K

% Enthalpy
           inj(a+1,8)=h;% J/kg

% Velocity
           inj(a+1,9)=mdotCO2/inj(a+1,4)/Ap;% m/s

% Dynamic Viscosity
           inj(a+1,10)=mu;% Pa.s

% Thermal Conductivity
           inj(a+1,13)=kf;% W/m.K

% Re - Reynolds Number
           inj(a+1,11)=inj(a+1,4)*inj(a+1,9)*d_pipe/inj(a+1,10);

% Pr - Prandlt Number
           inj(a+1,12)=inj(a+1,6)*inj(a+1,10)/inj(a+1,13);

```

```

    % Cumulative Heat Energy Input
    % InjHeat=InjHeat+(mdotCO2*cp*(inj(a+1,3)-inj(a,3))); %
Watts
    InjHeat=InjHeat+qwall; % Watts

    % Cumulative Energy Loss from Friction
    InjFric=InjFric+(mdotCO2/density*dPf); % Watts

    a=a+1;

end

%% Reservoir Heat Addition and Pressure change
% Reservoir Results matrix set-up
p=(WellLen/dL)+1; % number of reference points in the vertical z
direction
res=zeros(p,n);

% Initial conditions
res(1,1)=0; % meters - length dL = 0 at reservoir entrance
res(1,2)=inj(m,2); % Pa - pressure at inject point
res(1,3)=inj(m,3); % K - temp at inject point
res(1,4)=inj(m,4); % kg/m^3 - density at injection point -
calculated
res(1,5)=inj(m,5); % J/kg K - Specific heat constant volume - cv
res(1,6)=inj(m,6); % J/kg K - Specific heat constant pressure -
cp
res(1,7)=inj(m,7); % J/K - Entropy - s
res(1,8)=inj(m,8); % J/kg - Enthalpy - h
res(1,9)=mdotCO2/res(1,4)/Ar; % m/s - Velocity - V
res(1,10)=inj(m,10); % Pa.s - Dynamic Viscosity
res(1,11)=res(1,4)*res(1,9)*CrackWid/res(1,10); % Re - Reynolds
Number
res(1,12)=res(1,6)*res(1,10)/kf; % Pr - Prandlt Number
res(1,13)=inj(m,13); % Thermal conductivity

% Iterative Loop - Reservoir
% Create zero value variable for cumulative values in loop.
ResHeat=0;
ResFric=0;

b=1;

for b = 1:p-1
    % Length value for reference
    res(b+1,1)=res(b,1)+dL;

    % Pressure loss across reservoir
    dPf=mdotCO2*res(b,10)*dL/res(b,4)/KA;
    res(b+1,2)=res(b,2)-dPf;

    %Temp gradient assumed to be linear across reservoir
    dT=(Tres-res(1,3))/(p-1);
    res(b+1,3)=res(b,3)+dT;

    % Density calculation with temp and pressure
    P=res(b+1,2);
    T=res(b+1,3);
    [density,h,s,cp,cv,mu,kf,Z] = CO2_Prop(T,P);

```

```

        res(b+1,4)=density; % kg/m^3

% Specific heat constant volume
        res(b+1,5)=cv; % J/kg K

% Specific heat constant pressure
        res(b+1,6)=cp; % J/kg K

% Entropy
        res(b+1,7)=s; % J/kg K

% Enthalpy
        res(b+1,8)=h; % J/kg

% Velocity
        res(b+1,9)=mdotCO2/res(b+1,4)/Ar;% m/s

% Dynamic Viscosity
        res(b+1,10)=mu; % Pa.s

% Thermal Conductivity
        res(b+1,13)=kf; % W/m.K

% Re - Reynolds Number
        res(b+1,11)=res(b+1,4)*res(b+1,9)*CrackWid/res(b+1,10);

% Pr - Prandlt Number
        res(b+1,12)=res(b+1,6)*res(b+1,10)/res(b+1,13);

% Cumulative heat energy input
ResHeat=ResHeat+(mdotCO2*cp*(res(b+1,3)-res(b,3)));

% Cumulative Energy Loss from Friction
ResFric=ResFric+(mdotCO2/density*dPf);

b=b+1;

end

%% Production Well Results matrix set-up
prod=zeros(m,n);

% Initial conditions
prod(1,1)=WellDep; % meters - height dz = 0 at ground level
prod(1,2)=res(p,2); % Pa - pressure at point 3
prod(1,3)=res(p,3); % K - temp at point 3
prod(1,4)=res(p,4); % kg/m^3 - density at point 3
prod(1,5)=res(p,5); % J/kg K - Specific heat constant volume -
cv
prod(1,6)=res(p,6); % J/kg K - Specific heat constant pressure -
cp
prod(1,7)=-res(p,7); % J/kg K - Entropy - s
prod(1,8)=res(p,8); % J/kg - Enthalpy - h
prod(1,9)=mdotCO2/prod(1,4)/Ap; % m/s^2 - Velocity - V
prod(1,10)=res(p,10); % Pa.s - Dynamic Viscosity
prod(1,11)=prod(1,4)*prod(1,9)*d_pipe/prod(1,10); % Re -
Reynolds Number
prod(1,12)=prod(1,6)*prod(1,10)/res(p,13); % Pr - Prandlt Number

```

```

prod(1,13)=res(p,13); % W/m.K Thermal conductivity

% Iterative Loop - Production well
% Create zero value variable for cumulative values in loop.
ProdHeat=0;
ProdFric=0;

a=1;
for a = 1:m-1
% Depth value for reference
prod(a+1,1)=prod(a,1)-dz;

% Pressure increase from gravity and decrease from friction
% Friction
D=d_pipe;
Re=prod(a,11);
f=(-1.8*log10((e/D/3.7)^1.11+(6.9/Re)))^-2;
dPf=(f*dz/D*0.5*prod(a,4)*prod(a,9)^2);

% Gravity
dPg=(prod(a,4)*g*dz);

% Velocity
% Note - purpose of loop is to remove error at first
iteration
% where there is no (a-1) value to be read. Minor error over
total
% length is regarded acceptable.
if a>=2
dPv=1/2*prod(a,4)*((prod(a,9)^2)-(prod(a-1,9)^2));
else
dPv=0;
end

prod(a+1,2)=prod(a,2)+dPg-dPf-dPv;

%Temp gradient

% Pipe wall temp increases linearly with depth
Tpipe=Tres-((Tres-T1)*dz/WellDep*a);

% Heat transfer
% Fluid based (not used - limited by rock capacity)
%hc=0.027*(prod(a,11)^0.8)*(prod(a,12)^0.3)*prod(a,13)/D;
%qwall=hc*Awall*(Tpipe-prod(a,3));

% Rock based estimate (governs actual heat transfer)
prod(a+1,3)=prod(a,3)-(qwall/mdotCO2/cp);

% Density calculation with temp and pressure
P=prod(a+1,2);
T=prod(a+1,3);
[ density,h,s,cp,cv,mu,kf,Z] = CO2_Prop(T,P);
prod(a+1,4)=density; % kg/m^3

% Specific heat constant volume ***
prod(a+1,5)=cv; % J/kg K

```

```

% Specific heat constant pressure ***
    prod(a+1,6)=cp; % J/kg K

% Entropy
    prod(a+1,7)=s; % J/kg K

% Enthalpy
    prod(a+1,8)=h; % J/kg

% Velocity
    prod(a+1,9)=mdotCO2/prod(a+1,4)/Ap; % m/s

% Dynamic Viscosity
    prod(a+1,10)=mu;% Pa.s

% Thermal Conductivity
    prod(a+1,13)=kf;% W/m.k

% Re - Reynolds Number
    prod(a+1,11)=prod(a+1,4)*prod(a+1,9)*d_pipe/prod(a+1,10);

% Pr - Prandlt Number
    prod(a+1,12)=prod(a+1,6)*prod(a+1,10)/prod(a+1,13);

% Cumulative heat energy input
    % ProdHeat=ProdHeat+(mdotCO2*cp*(prod(a,3)-prod(a+1,3)));
    ProdHeat=ProdHeat+qwall;

% Cumulative Energy Loss from Friction
    ProdFric=ProdFric+(mdotCO2/density*dPf);

a=a+1;
end

%% Turbine Power Extraction - Isentropic
% Isentropic expansion, find equivalent entropy on the initial
% pressure isotherm (P1). This will tell you the temperature and
enable
% calculation of power output.
    T2=res(1,3);
    P2=res(1,2);
    T3=prod(1,3);
    P3=prod(1,2);
    s4=s;
    s5=s4;
    T4=T;
    P4=P;
    T5=T;
    P5=inj(1,2);
    cv4=cv;
    h4=h;

while s4<=s5
    T5=T5-1;
    [rho5,h5,s5,cp5,cv5,~,~] = CO2_Prop(T5,P5);

end

```

```

PoutTurb=mdotCO2*((cv4+cv5)/2)*(T4-T5);
%PoutTurb=mdotCO2*(h4-h5);

%% Cooling Tower Heat Extraction
% Isobaric heat loss

PoutCool=mdotCO2*((inj(1,6)+cp5)/2)*(T5-T1);

%% Energy balance

EBal=-PoutTurb+InjHeat-InjFric+ResHeat-ResFric-ProdHeat-ProdFric-
PoutCool;

%% Exergy
XCO2=eta*mdotCO2*((h-h5)-(298*(s-s5)));

%% Thermal Efficiency
% useful energy out / total energy in

ThermEffCO2=eta*PoutTurb/(InjHeat+ResHeat);

```

CO2_Prop.m

```
% CO2_Prop.m : Function file written by Patrick Taylor
% Undergraduate at University of Southern Queensland
%
% [density,h,s,cp,cv,mu,kf,Z] = CO2_Prop(T,P)
%
% Calculates the supercritical fluid state properties for Carbon
Dioxide
% with temperature and pressure inputs based on the Peng Robinson
equation
% of state (PR EOS).
% Thermodynamic properties are estimated using the Peng Robinson
% departure functions.
% Viscosity and thermal conductivity are estimated using the
correlation
% by Heidaryan et al. (2011).
%
% Input units required
%   T: Temperature [=] K
%   P: Pressure [=] Pa
%
% Output Units
%   density = kg/m^3
%   h   = J/kg
%   s   = J/kg.K
%   cp  = J/kg.K
%   cv  = J/kg.K
%   mu  = Pa.s
%   kf  = W/m.K

%% Main Script
function [density,h,s,cp,cv,mu,kf,Z]=CO2_Prop(T,P)

% CO2 specific constant parameters
global Tc Pc w MW R

Tref=298;      % Tref:  [=] K
Pref=101325;   % Pref: reference pressure [=] Pa
Tc=304.25;    % Tc: critical temperature [=] K
Pc=7382000;   % Pc: critical pressure [=] Pa
w=0.228;      % w:  eccentric factor
MW=0.04401;   % MW: molar weight [=] kg/mol
R = 8.314;    % gas constant [=] J/(mol K)

% Reference State Calculation
% h2 and s2 are enthalpy and entropy departures at the fluid
reference
% state.

[~,Z,~,~,~,B,k,alfa,Tr] = PengMain(Tref,Pref);
[h2,s2]=HSCalc(Z,B,k,alfa,Tr);% J/kg.K

% System Fluid State Calculation
% h3 and s3 are enthalpy and entropy departures at the systems fluid
state.
% hdep and sdep are enthalpy and entropy ideal gas values at the
systems
% fluid state.
```

```

% cp and cv are specific heat values including Peng Robinson
departures
% at the systems fluid state.

[density,Z,a,b,A,B,k,alfa,Tr] = PengMain(T,P);
[cp,cv,h3,s3]=HCapCalc(T,Tref,P,Pref,Z,a,b,A,B,k,alfa);% J/kg.K
[hdep,sdep]=HSCalc(Z,B,k,alfa,Tr);% J/kg.K
    h=-h2+h3+hdep; % J/kg.K
    s=-s2+s3+sdep; %% J/kg.K

% mu is the dynamic viscosity at the system fluid state
[mu]=VisCalc(T,P);

% kf is the thermal conductivity at the system reference state
[kf]=ThermCalc(T,P);

end

%% Main Peng-Robinson Calculation
function [density,Z,a,b,A,B,k,alfa,Tr] = PengMain(T,P)
global Tc Pc w R MW
% Peng Robinson EOS
% Reduced variables
    Tr = T/Tc ;
    Pr = P/Pc ;

% Parameters of the EOS for a pure component
    k = 0.37464 + 1.54226*w - 0.26992*w^2;
    alfa = (1 + k*(1 - sqrt(Tr)))^2;
    a = 0.45724*(R*Tc)^2/Pc*alfa;
    b = 0.0778*R*Tc/Pc;
    A = a*P/(R*T)^2;
    B = b*P/(R*T);

% Compressibility factor
    Z = roots([1 -(1-B) (A-3*B^2-2*B) -(A*B-B^2-B^3)]);

    ZR = [];
% Select only the real roots from Z
for i = 1:3
    if isreal(Z(i))
        ZR = [ZR Z(i)];
    end
end

% Select the minimum real root from Z
    Z = min(ZR);

% Fugacity coefficient
    fhi = exp(Z - 1 - log(Z-B) -
A/(2*B*sqrt(2))*log((Z+(1+sqrt(2))*B)/(Z+(1-sqrt(2))*B)));

% If Z is negative, phi is imaginary and there is no solution for Z
if isreal(fhi)
    density=P*MW/(Z*R*T);
else
    disp(sprintf('Error - No solution for Z'))
    disp(sprintf('At pressure = %g',P))
    disp(sprintf('At temperature = %g',T))
end

```

```

disp(sprintf('Z = %g',Z))
disp(sprintf('ZR = %g',ZR))
disp(sprintf('B = %g',B))
end
end

%% Specific Heat Capacity and Ideal Gas Enthalpy and Entropy
function [cp,cv,h3,s3]=HCapCalc(T,Tref,P,Pref,Z,a,b,A,B,k,alfa)

% Ideal Gas Heat Capacity
% Method used in "Properties of Liquids and Gases" Poling (2001)
% Intermediate unit = J/mol.K
global Tc MW R

a0=3.259;
a1=1.356*10^-3;
a2=1.502*10^-5;
a3=-2.374*10^-8;
a4=1.056*10^-11;
cpig=(a0+(a1*T)+(a2*T^2)+(a3*T^3)+(a4*T^4))*R; % J/mol.K = Ideal Gas
Heat Capacity

% Departure Function Heat Capacity - Peng Robinson
% http://kshmakov.org/fluid/note/3/
ac=a/alfa;
ai=k*ac*((k/Tc)-((1+k)/sqrt(T*Tc)));
aii=k*ac*(1+k)/2/(sqrt((T^3)*Tc));
M=(Z^2+(2*B*Z)-B^2)/(Z-B);
N=ai*B/b/R;
cpdep=(aii*(T/2/(sqrt(2*b)))*log((Z+(sqrt(2)+1)*B)/(Z-(sqrt(2)-
1)*B)))+(R*(M-N)^2)/(M^2-(2*A*(Z+B)))-R; % J/mol.K

% Combine ideal gas and departure function and covert from molar to
mass
% based units
cp=(cpig+cpdep)/MW; % J/kg.K
cv=((R*(M-N)^2)/((2*A*(Z+B))-M^2)+cpig+cpdep)/MW;% J/kg.K

% Entropy and Enthalpy
% Modified method from "Properties of Liquids and Gases" Poling
(2001)
% Converted from molar to mass based
h3=(a0*(T - Tref) + a1/2*(T^2 - Tref^2) + a2/3*(T^3 - Tref^3) +
a3/4*(T^4 - Tref^4)+a4/5*(T^5-Tref^5))*R/MW;% J/kg.K
s3=(a0*log(T/Tref) + a1*(T - Tref) + a2/2*(T^2 - Tref^2) + a3/3*(T^3
- Tref^3)+a4/4*(T^4-Tref^4) - log(P/Pref))*R/MW; % J/kg.K%

end

%% Departure functions enthalpy and entropy;
function [hdep,sdep]=HSCalc(Z,B,k,alfa,Tr)

global Tc MW R

% Departure Function Enthalpy
hdep=R*Tc*(Tr*(Z-1)-2.078*(1+k)*((alfa)^0.5)*log((Z+2.414*B)/(Z-
0.414*B)))/MW; % J/kg

```

```

% Departure Function Entropy
sdep=R*(log(Z-B)-(2.078*k*((1+k)/(Tr^0.5))-k)*log((Z+2.414*B)/(Z-
0.414*B)))/MW; % J/Kg.K

end

%% Viscosity Calculation
% Units = (Pa.s)
function [mu]=VisCalc(T,P)

A1=-1.146067e-01;
A2=6.978380e-07;
A3=3.976765e-10;
A4=6.336120e-02;
A5=-1.166119e-02;
A6=7.142596e-04;
A7=6.519333e-06;
A8=-3.567559e-01;
A9=3.180473e-02;

P=P*10^-5;

% Note input units - pressure = bar, Temp = Kelvin
mu=(A1+A2*P+A3*P^2+A4*log(T)+A5*(log(T))^2+A6*(log(T))^3)/(1+A7*P+A8
*log(T)+A9*(log(T))^2)/1000;

end

%% Thermal Conductivity
% Units = (W/m.K)

function [kf]=ThermCalc(T,P)

P=P/1000000;

A1=1.49288267457998e01;
A2=2.62541191235261e-03 ;
A3=8.77804659311418e-06;
A4=-5.11424687832727;
A5=4.37710973783525e-01;
A6=2.11405159581654e-05;
A7=-4.73035713531117e-01;
A8=7.36635804311043e-02;
A9=-3.76339975139314e-03;

% Note - equation accepts Pressure in MPa and Temp in Kelvin

kf=(A1+A2*P+A3*P^2+A4*log(T)+A5*log(T)^2)/(1+A6*P+A7*log(T)+A8*log(T)
)^2+A9*log(T)^3)/1000;

end

```

Geothermal_Water.m

```
% Geothermal_Water.m - Program to calculate fluid properties at
differential
% points around the geothermal circuit
% Author - Patrick Taylor, USQ, Student 0019522109

%% Injection Well Section
% Results matrix set-up
    m=(WellDep/dz)+1; % number of reference points in the vertical z
direction
    n=13;%
    inj=zeros(m,n);
    T=T1;
    P=P1;

% Initial conditions
    inj(1,1)=0; % meters - height dz = 0 at ground level
    inj(1,2)=P1; % Pa - pressure at inject point
    inj(1,3)=T1; % K - temp at inject point
    inj(1,4)=XSteam('rho_pT',P/100000,T-273); % kg/m^3 - density at
injection point - calculated
    inj(1,5)=XSteam('Cv_pT',P/100000,T-273)*1000; % J/kg K -
Specific heat constant volume - cv
    inj(1,6)=XSteam('Cp_pT',P/100000,T-273)*1000; % J/kg K -
Specific heat constant pressure - cp
    inj(1,7)=XSteam('s_pT',P/100000,T-273)*1000; % J/kg K - Entropy
- s
    inj(1,8)=XSteam('h_pT',P/100000,T-273)*1000; % J/kg - Enthalpy -
h
    inj(1,9)=mdotWater/inj(1,4)/Ap; % m/s^2 - Velocity - V
    inj(1,10)=XSteam('my_pT',P/100000,T-273); % Pa.s - Dynamic
Viscosity
    inj(1,11)=inj(1,4)*inj(1,9)*d_pipe/inj(1,10); % Re - Reynolds
Number
    inj(1,13)=XSteam('tc_pT',P/100000,T-273); % Thermal conductivity
    inj(1,12)=inj(1,6)*inj(1,10)/inj(1,13); % Pr - Prandlt Number

% Iterative Loop - Injection well
InjHeat=0;
InjFric=0;

for a = 1:m-1
    % Depth value for reference
    inj(a+1,1)=inj(a,1)+dz;

    % Pressure increase from gravity and decrease from friction
    % Friction
    D=d_pipe;
    Re=inj(a,11);
    f=(-1.8*log10((e/D/3.7)^1.11+(6.9/Re)))^-2;
    dPf=(f*dz/D*0.5*inj(a,4)*inj(a,9)^2);

    % Gravity
    dPg=(inj(a,4)*g*dz);

    % Velocity
    % Note - purpose of loop is to remove error at first
iteration
```

```

total      % where there is no (a-1) value to be read. Minor error over
           % length is regarded acceptable.
           if a>=2
               dPv=1/2*inj(a,4)*((inj(a,9)^2)-(inj(a-1,9)^2));
           else
               dPv=0;
           end

           inj(a+1,2)=inj(a,2)-dPg-dPf-dPv;

%Temp gradient in well bore

           % Pipe wall temp increases linearly with depth
           Tpipe=T1+((Tres-T1)*dz/WellDep*a);

           % Heat transfer
           cp=XSteam('Cp_pT',P/100000,T-273)*1000;
           % Fluid based (not used)
           %Awall=pi*d_pipe*dz;
           %hc=0.027*(inj(a,11)^0.8)*(inj(a,12)^0.4)*inj(a,13)/D;
           %qwall=hc*Awall*(Tpipe-inj(a,3));

           % Rock based estimate
           inj(a+1,3)=inj(a,3)+(qwall/mdotWater/cp);

% Density calculation with temp and pressure
           P=inj(a+1,2);
           T=inj(a+1,3);
           inj(a+1,4)=XSteam('rho_pT',P/100000,T-273); % kg/m^3

% Specific heat constant volume
           inj(a+1,5)=XSteam('Cv_pT',P/100000,T-273)*1000; % J/kg K

% Specific heat constant pressure
           inj(a+1,6)=cp; % J/kg K

% Entropy
           inj(a+1,7)=XSteam('s_pT',P/100000,T-273)*1000; % J/kg K

% Enthalpy
           inj(a+1,8)=XSteam('h_pT',P/100000,T-273)*1000; % J/kg

% Velocity
           inj(a+1,9)=mdotWater/inj(a+1,4)/Ap; % m/s

% Dynamic Viscosity
           inj(a+1,10)=XSteam('mu_pT',P/100000,T-273); % Pa.s

% Thermal Conductivity
           inj(a+1,13)=XSteam('tc_pT',P/100000,T-273); % W/m.K

% Re - Reynolds Number
           inj(a+1,11)=inj(a+1,4)*inj(a+1,9)*d_pipe/inj(a+1,10);

% Pr - Prandlt Number
           inj(a+1,12)=inj(a+1,6)*inj(a+1,10)/inj(a+1,13);

```

```

    % Cumulative Heat Energy Input
    % InjHeat=InjHeat+(mdotWater*cp*(inj(a+1,3)-inj(a,3))); %
Watts
    InjHeat=InjHeat+qwall; % Watts

    % Cumulative Energy Loss from Friction
    InjFric=InjFric+(mdotWater/inj(a+1,4)*dPf); % Watts

    a=a+1;

end

%% Reservoir Heat Addition and Pressure change
% Reservoir Results matrix set-up
p=(WellLen/dL)+1; % number of reference points in the vertical z
direction
res=zeros(p,n);

% Initial conditions
res(1,1)=0; % meters - length dL = 0 at reservoir entrance
res(1,2)=inj(m,2); % Pa - pressure at inject point
res(1,3)=inj(m,3); % K - temp at inject point
res(1,4)=inj(m,4); % kg/m^3 - density at injection point -
calculated
res(1,5)=inj(m,5); % J/kg K - Specific heat constant volume - cv
res(1,6)=inj(m,6); % J/kg K - Specific heat constant pressure -
cp
res(1,7)=inj(m,7); % J/kg K - Entropy - s
res(1,8)=inj(m,8); % J/kg - Enthalpy - h
res(1,9)=mdotWater/res(1,4)/Ar; % m/s - Velocity - V
res(1,10)=inj(m,10); % Pa.s - Dynamic Viscosity
res(1,11)=res(1,4)*res(1,9)*CrackWid/res(1,10); % Re - Reynolds
Number
res(1,12)=res(1,6)*res(1,10)/inj(m,13); % Pr - Prandtl Number
res(1,13)=inj(m,13); % Thermal conductivity

% Iterative Loop - Reservoir
% Create zero value variable for cumulative values in loop.
ResHeat=0;
ResFric=0;

b=1;

for b = 1:p-1
    % Length value for reference
    res(b+1,1)=res(b,1)+dL;

    % Pressure loss across reservoir
    dPf=mdotWater*res(b,10)*dL/res(b,4)/KA;
    res(b+1,2)=res(b,2)-dPf;

    %Temp gradient assumed to be linear across reservoir
    dT=(Tres-res(1,3))/(p-1);
    res(b+1,3)=res(b,3)+dT;

    % Density calculation with temp and pressure
    P=res(b+1,2);
    T=res(b+1,3);
    res(b+1,4)=XSteam('rho_pT',P/100000,T-273); % kg/m^3

```

```

% Specific heat constant volume
res(b+1,5)=XSteam('Cv_pT',P/100000,T-273)*1000; % J/kg K

% Specific heat constant pressure
res(b+1,6)=XSteam('Cp_pT',P/100000,T-273)*1000; % J/kg K
cp=res(b+1,6);

% Entropy
res(b+1,7)=XSteam('s_pT',P/100000,T-273)*1000; % J/kg K

% Enthalpy
res(b+1,8)=XSteam('h_pT',P/100000,T-273)*1000; % J/kg

% Velocity
res(b+1,9)=mdotWater/res(b+1,4)/Ar;% m/s

% Dynamic Viscosity
res(b+1,10)=XSteam('mu_pT',P/100000,T-273); % Pa.s

% Thermal Conductivity
res(b+1,13)=XSteam('tc_pT',P/100000,T-273); % W/m.K

% Re - Reynolds Number
res(b+1,11)=res(b+1,4)*res(b+1,9)*CrackWid/res(b+1,10);

% Pr - Prandlt Number
res(b+1,12)=res(b+1,6)*res(b+1,10)/res(b+1,13);

% Cumulative heat energy input
ResHeat=ResHeat+(mdotWater*cp*(res(b+1,3)-res(b,3)));

% Cumulative Energy Loss from Friction
ResFric=ResFric+(mdotWater/res(b+1,4)*dPf);

b=b+1;

end

%% Production Well Results matrix set-up
prod=zeros(m,n);

% Initial conditions
prod(1,1)=WellDep; % meters - height dz = 0 at ground level
prod(1,2)=res(p,2); % Pa - pressure at point 3
prod(1,3)=res(p,3); % K - temp at point 3
prod(1,4)=res(p,4); % kg/m^3 - density at point 3
prod(1,5)=res(p,5); % J/kg K - Specific heat constant volume -
cv
prod(1,6)=res(p,6); % J/kg K - Specific heat constant pressure -
cp
prod(1,7)=-res(p,7); % J/kg K - Entropy - s
prod(1,8)=res(p,8); % J/kg - Enthalpy - h
prod(1,9)=mdotWater/prod(1,4)/Ap; % m/s^2 - Velocity - V
prod(1,10)=res(p,10); % Pa.s - Dynamic Viscosity
prod(1,11)=prod(1,4)*prod(1,9)*d_pipe/prod(1,10); % Re -
Reynolds Number
prod(1,12)=prod(1,6)*prod(1,10)/res(p,13); % Pr - Prandlt Number

```

```

prod(1,13)=res(p,13); % W/m.K Thermal conductivity

% Iterative Loop - Production well
% Create zero value variable for cumulative values in loop.
ProdHeat=0;
ProdFric=0;

a=1;
for a = 1:m-1
% Depth value for reference
prod(a+1,1)=prod(a,1)-dz;

% Pressure increase from gravity and decrease from friction
% Friction
D=d_pipe;
Re=prod(a,11);
f=(-1.8*log10((e/D/3.7)^1.11+(6.9/Re)))^-2;
dPf=(f*dz/D*0.5*prod(a,4)*prod(a,9)^2);

% Gravity
dPg=(prod(a,4)*g*dz);

% Velocity
% Note - purpose of loop is to remove error at first
iteration
% where there is no (a-1) value to be read. Minor error over
total
% length is regarded acceptable.
if a>=2
dPv=1/2*inj(a,4)*((inj(a,9)^2)-(inj(a-1,9)^2));
else
dPv=0;
end

prod(a+1,2)=prod(a,2)+dPg-dPf-dPv;

%Temp gradient

% Pipe wall temp increases linearly with depth
Tpipe=Tres-((Tres-T1)*dz/WellDep*a);

% Heat transfer
cp=XSteam('Cp_pT',P/100000,T-273)*1000;
% Fluid based (not used - limited by rock capacity)
%hc=0.027*(prod(a,11)^0.8)*(prod(a,12)^0.3)*prod(a,13)/D;
%qw=hc*Aw*(Tpipe-prod(a,3));

% Rock based estimate (governs actual heat transfer)
prod(a+1,3)=prod(a,3)-(qw/mdotWater/cp);

% Density calculation with temp and pressure
P=prod(a+1,2);
T=prod(a+1,3);
prod(a+1,4)=XSteam('rho_pT',P/100000,T-273); % kg/m^3

% Specific heat constant volume
prod(a+1,5)=XSteam('Cv_pT',P/100000,T-273)*1000; % J/kg K

```

```

% Specific heat constant pressure
    prod(a+1,6)=cp; % J/kg K

% Entropy
    prod(a+1,7)=XSteam('s_pT',P/100000,T-273)*1000; % J/kg K

% Enthalpy
    prod(a+1,8)=XSteam('h_pT',P/100000,T-273)*1000; % J/kg

% Velocity
    prod(a+1,9)=mdotWater/prod(a+1,4)/Ap;% m/s

% Dynamic Viscosity
    prod(a+1,10)=XSteam('mu_pT',P/100000,T-273); % Pa.s

% Thermal Conductivity
    prod(a+1,13)=XSteam('tc_pT',P/100000,T-273); % W/m.k

% Re - Reynolds Number
    prod(a+1,11)=prod(a+1,4)*prod(a+1,9)*d_pipe/prod(a+1,10);

% Pr - Prandlt Number
    prod(a+1,12)=prod(a+1,6)*prod(a+1,10)/prod(a+1,13);

% Cumulative heat energy input
%ProdHeat=ProdHeat+(mdotWater*cv*(prod(a,3)-prod(a+1,3)));
ProdHeat=ProdHeat+qwall;

% Cumulative Energy Loss from Friction
ProdFric=ProdFric+(mdotWater/prod(a+1,4)*dPf);

a=a+1;
end

%% Additional properties
T2=res(1,3);
P2=res(1,2);
T3=prod(1,3);
P3=prod(1,2);
P4=P;
T4=T;
h4=prod(a,8);
s4=prod(a,7);
P5=P4;
T5=T1;
cp4=cp;
cp5=XSteam('Cp_pT',P5/100000,T5-273)*1000; % J/kg K
h5=XSteam('h_pT',P5/100000,T5-273)*1000; % J/kg
s5=XSteam('s_pT',P5/100000,T5-273)*1000; % J/kg K
rho5=XSteam('rho_pT',P5/100000,T5-273); % kg/m^3

%% Heat Exchanger Power Extraction for Turbine Circuit
% Isobaric heat extraction through heat exchanger

cpavg=(cp4+cp5)/2;
PoutTurb=cpavg*(T4-T5)*mdotWater;% Watts

%% Pumping Power Addition

```

```

% Isothermal pressure increase

rho=inj(1,4); %kg/m^3
%PinPump=mdotWater/rho*(P1-P5); % Watts
PinPump=(PoutTurb-InjHeat+InjFric-
ResHeat+ResFric+ProdHeat+ProdFric);

%% Energy balance

EBal=-PoutTurb+InjHeat-InjFric+ResHeat-ResFric-ProdHeat-
ProdFric+PinPump;

%% Exergy
XWater=eta2*mdotWater*((h4-h5)-(298*(s4-s5)));

%% Thermal Efficiency
% useful energy out / total energy in

ThermEffWater=(PoutTurb*eta2)/(PinPump/eta3+ResHeat+InjHeat);

```

XSteam.m

This Matlab function file was not written by the author of this paper. XSteam.m was written entirely by Holmgren (2007) and is used completely unchanged from the freely available open-source file. The reader is directed to contact the author of this file if inspection of the code and methodology is desired. The file is well annotated but unreasonably large to warrant inclusion of the full code into these Appendices.

REFERENCES

Atrens, A, Gurgenci, H & Rudolph, V 2009, 'Exergy Analysis of a CO₂ Thermosiphon', in *Thirty-Fourth Workshop on Geothermal Reservoir Engineering: proceedings of the Thirty-Fourth Workshop on Geothermal Reservoir Engineering* Stanford University, Stanford, California.

Atrens, AD, Gurgenci, H & Rudolph, V 2008, 'CO₂ Thermosiphon for Competitive Geothermal Power Generation', *Energy & Fuels*, vol. 23, no. 1, pp. 553-7.

Atrens, AD, Gurgenci, H & Rudolph, V 2010, 'Electricity generation using a carbon-dioxide thermosiphon', *Geothermics*, vol. 39, no. 2, pp. 161-9.

Bahadori, A, Zendehboudi, S & Zahedi, G 2013, 'A review of geothermal energy resources in Australia: Current status and prospects', *Renewable and Sustainable Energy Reviews*, vol. 21, pp. 29-34.

Bıyıkoğlu, A & Yalçınkaya, R 2013, 'Effects of different reservoir conditions on carbon-dioxide power cycle', *Energy Conversion and Management*, vol. 72, pp. 125-33.

Brown, DW 2000, 'A Hot Dry Rock Geothermal Energy Concept Using Supercritical CO₂ Instead of Water', in *Twenty-Fifth Workshop on Geothermal Reservoir Engineering: proceedings of the Twenty-Fifth Workshop on Geothermal Reservoir Engineering* Stanford University, Stanford, California.

DiPippo, R 2008, *Geothermal Power Plants: Principles, Applications, Case Studies and Environmental Impact*, Elsevier Science & Technology.

DiPippo, R 2012, *Geothermal Power Plants: Principles, Applications, Case Studies and Environmental Impact, Third Edition*, Elsevier Science.

Dorminey, B 2012, 'EGS Takes Geothermal Global', *Renewable Energy World*, viewed 17/05/2014, <<http://www.renewableenergyworld.com/rea/news/article/2012/05/egs-takes-geothermal-global>>

EPA 2013, <<http://www.epa.gov/climatestudents/solutions/technologies/geothermal.html>>.

Finger, J & Blankenship, D 2010, *Handbook of Best Practices for Geothermal Drilling*, Sandia National Laboratories, Albuquerque, New Mexico.

Fox, RW, Pritchard, PJ & McDonald, AT 2009, *Introduction to Fluid Mechanics, 7th Ed*, John Wiley & Sons, Inc.

GeoExchange 2011, *Home Heating With GeoExchange*, 24/03/2011, <<http://www.geoexchange.org/library/residential-illustrations#>>.

Geothermal Energy Association 2014, *Geothermal Energy Association - Geothermal Basics*, viewed 09/05/2014, <<http://geo-energy.org/basics.aspx>>.

Gurgenci, H 2011, *A typical geothermal well design*, <<http://www.geothermal.uq.edu.au/24-August-2011>>.

Gurgenci, H, Rudolph, V, Saha, T & Lu, M 2008, 'Challenges for Geothermal Energy Utilisation', in *Thirty-Third Workshop on Geothermal Reservoir Engineering: proceedings of the Thirty-Third Workshop on Geothermal Reservoir Engineering* Stanford University, Stanford, California.

Haghshenas Fard, M, Hooman, K & Chua, HT 2010, 'Numerical simulation of a supercritical CO₂ geothermosiphon', *International Communications in Heat and Mass Transfer*, vol. 37, no. 10, pp. 1447-51.

Heidaryan, E & Jarrahan, A 2013, 'Modified Redlich-Kwong equation of state for supercritical carbon dioxide', *The Journal of Supercritical Fluids*, vol. 81, no. 0, pp. 92-8.

Heidaryan, E, Hatami, T, Rahimi, M & Moghadasi, J 2011, 'Viscosity of pure carbon dioxide at supercritical region: Measurement and correlation approach', *The Journal of Supercritical Fluids*, vol. 56, no. 2, pp. 144-51.

Holmgren, M 2007, *XSteam, Thermodynamic properties of water and steam.*, Matlab Central, <<http://www.mathworks.com.au/matlabcentral/fileexchange/9817-x-steam--thermodynamic-properties-of-water-and-steam/content//XSteam.m>>.

IPCC 2014, *Intergovernmental Panel on Climate Change*, viewed 03/05/2014, <<http://www.ipcc.ch/index.htm>>.

Jarrahian, A & Heidaryan, E 2012, 'A novel correlation approach to estimate thermal conductivity of pure carbon dioxide in the supercritical region', *The Journal of Supercritical Fluids*, vol. 64, no. 0, pp. 39-45.

Kreith, F, Manglik, RM & Bohn, MS 2011, *Heat Transfer, 7th Edition, SI Version*, Cengage Learning, Stamford.

Peng, D-Y & Robinson, DB 1976, 'A New Two-Constant Equation of State', *Industrial & Engineering Chemistry Fundamentals*, vol. 15, no. 1, pp. 59-64, viewed 2014/05/19.

Perrot, P 1998, *A to Z of Thermodynamics*, Oxford University Press.

Poling, BE 2001, *The properties of gases and liquids*, 5th ed. edn, McGraw-Hill, New York.

Pruess, K 2006, 'Enhanced geothermal systems (EGS) using CO₂ as working fluid—A novel approach for generating renewable energy with simultaneous sequestration of carbon', *Geothermics*, vol. 35, no. 4, pp. 351-67.

Pruess, K 2007, *Enhanced Geothermal Systems (EGS) comparing water with CO₂ as heat transmission fluids*, <<http://www.escholarship.org/uc/item/1fr9q7q8>>.

Pruess, K 2008, *On the production behavior of enhanced geothermal systems with CO₂ as working fluid*, <<http://www.escholarship.org/uc/item/6xf1m956>>.

Pruess, K & Azaroual, M 2006, 'On the Feasibility of Using Supercritical CO₂ as Heat Transmission Fluid in an Engineered Hot Dry Rock Geothermal System', in *Thirty-First Workshop on Geothermal Reservoir Engineering: proceedings of the Thirty-First Workshop on Geothermal Reservoir Engineering* Stanford University, Stanford, California.

Renewable Energy World 2014, *Geothermal Energy*, viewed 06/04/2014, <<http://www.renewableenergyworld.com/rea/tech/geothermal-energy>>.

Shmakov, K 2012, *Peng Robinson equation*, viewed 14th September, <<http://kshmakov.org/fluid/note/3/>>.

Solarpraxis 2014, *Shallow Geothermal Energy*, <<http://work.renewables-made-in-germany.com/en/start/geothermal.html>>.

Span, R & Wagner, W 1996, 'A New Equation of State for Carbon Dioxide Covering the Fluid Region from the Triple-Point Temperature to 1100 K at Pressures up to 800 MPa', *Journal of Physical and Chemical Reference Data*, vol. 25, no. 6, pp. 1509-96.

U.S. Department of Energy Genomic Science 2008, *Carbon Cycling and Biosequestration: Integrating Biology and Climate Through Systems Science*, <<http://genomicscience.energy.gov>>.

Yusaf, T, Goh, S & Borserio, JA 2011, 'Potential of renewable energy alternatives in Australia', *Renewable and Sustainable Energy Reviews*, vol. 15, no. 5, pp. 2214-21.

Zhang, F-Z, Jiang, P-X & Xu, R-N 2013, 'System thermodynamic performance comparison of CO₂-EGS and water-EGS systems', *Applied Thermal Engineering*, vol. 61, no. 2, pp. 236-44.